

THEORETICAL INVESTIGATIONS OF THE BIGINELLI REACTION
AND THE GLUCOSE TRANSFORMATION TO 5-HYDROXYMETHYLFURFURAL

Miss Maneeporn Puripat



บทคัดย่อและแฟ้มข้อมูลฉบับเต็มของวิทยานิพนธ์ตั้งแต่ปีการศึกษา 2554 ที่ให้บริการในคลังปัญญาจุฬาฯ (CUIR)
เป็นแฟ้มข้อมูลของนิสิตเจ้าของวิทยานิพนธ์ ที่ส่งผ่านทางบัณฑิตวิทยาลัย

The abstract and full text of theses from the academic year 2011 in Chulalongkorn University Intellectual Repository (CUIR)
are the thesis authors' files submitted through the University Graduate School.

A Dissertation Submitted in Partial Fulfillment of the Requirements
for the Degree of Doctor of Philosophy Program in Nanoscience and Technology
(Interdisciplinary Program)
Graduate School
Chulalongkorn University
Academic Year 2015

Copyright of Chulalongkorn University

การศึกษาเชิงทฤษฎีของปฏิกิริยาบิกิเนลลี
และปฏิกิริยาการแปลงกลูโคสเป็น 5-ไฮดรอกซีเมทิลเฟอร์ฟูรัล



วิทยานิพนธ์นี้เป็นส่วนหนึ่งของการศึกษาตามหลักสูตรปริญญาวิทยาศาสตรดุษฎีบัณฑิต
สาขาวิชาวิทยาศาสตร์นาโนและเทคโนโลยี (สหสาขาวิชา)
บัณฑิตวิทยาลัย จุฬาลงกรณ์มหาวิทยาลัย
ปีการศึกษา 2558
ลิขสิทธิ์ของจุฬาลงกรณ์มหาวิทยาลัย

Thesis Title	THEORETICAL INVESTIGATIONS OF THE BIGINELLI REACTION AND THE GLUCOSE TRANSFORMATION TO 5-HYDROXYMETHYLFURFURAL
By	Miss Maneeporn Puripat
Field of Study	Nanoscience and Technology
Thesis Advisor	Associate Professor Vudhichai Parasuk, Ph.D.

Accepted by the Graduate School, Chulalongkorn University in Partial
Fulfillment of the Requirements for the Doctoral Degree

.....Dean of the Graduate School
(Associate Professor Sunait Chutintaranond, Ph.D.)

THESIS COMMITTEE

.....Chairman
(Assistant Professor Sukkaneste Tungasmita, Ph.D.)

.....Thesis Advisor
(Associate Professor Vudhichai Parasuk, Ph.D.)

.....Examiner
(Sakulsuk Unarunotai, Ph.D.)

.....Examiner
(Ratthapol Rangkupan, Ph.D.)

.....External Examiner
(Assistant Professor Narin Lawan, Ph.D.)

.....External Examiner
(Associate Professor Waraporn Parasuk, Ph.D.)

มณีภรณ์ ภูริพัฒน์ : การศึกษาเชิงทฤษฎีของปฏิกิริยาบิกิเนลลี และปฏิกิริยาการแปลงกลูโคสเป็น 5-ไฮดรอกซีเมทิลเฟอร์ฟูรัล (THEORETICAL INVESTIGATIONS OF THE BIGINELLI REACTION AND THE GLUCOSE TRANSFORMATION TO 5-HYDROXYMETHYLFURFURAL) อ.ที่ปรึกษาวิทยานิพนธ์หลัก: รศ. ดร. วุฒิชัย พาราสุข, 123 หน้า.

ในวิทยานิพนธ์ฉบับนี้ได้ทำการศึกษาเชิงทฤษฎีของปฏิกิริยาอินทรีย์ 2 ปฏิกิริยา คือ ปฏิกิริยาบิกิเนลลี และปฏิกิริยาการแปลงกลูโคสเป็น 5-ไฮดรอกซีเมทิลเฟอร์ฟูรัล ทั้งนี้ ได้มีการทำนายกลไกปฏิกิริยา และอิทธิพลของตัวทำละลายที่ผลต่อปฏิกิริยาดังกล่าว ในการศึกษาปฏิกิริยาบิกิเนลลี ผู้จัดทำได้นำระเบียบวิธีแรงเทียมเหนียวมาปฏิกิริยามาใช้เพื่อหาวิถีของปฏิกิริยาทั้งหมดที่เป็นไปได้ของปฏิกิริยาหลายองค์ประกอบชนิดนี้อย่างเป็นระบบ จากการศึกษา พบว่า วิถีปฏิกิริยาที่เป็นไปได้มากที่สุด คือ การเริ่มต้นจากการก่อเกิดพันธะระหว่างธาตุคาร์บอนและธาตุไนโตรเจนของยูเรีย และเบนซัลดีไฮด์ จากนั้นจึงเกิดปฏิกิริยาการเติมนิวคลีโอฟิลิกของสารเอทิล แอซีโตอะซิเตท อันเป็นที่น่าสนใจอย่างยิ่งที่โมเลกุลของยูเรียที่ถูกเพิ่มเข้าไปนั้นสามารถเร่งปฏิกิริยาบิกิเนลลีเกือบทุกขั้นตอน ดังนั้น เราจึงกล่าวได้ว่า ปฏิกิริยาบิกิเนลลีเป็นปฏิกิริยาหลายองค์ประกอบที่ถูกเร่งโดยโมเลกุลยูเรีย นอกจากนี้ ปฏิกิริยาบิกิเนลลีที่เกิดในเอทานอล และโทลูอีนก็ให้ผลลัพธ์ไปในทางเดียวกัน สำหรับการศึกษาปฏิกิริยาการแปลงกลูโคสเป็น 5-ไฮดรอกซีเมทิลเฟอร์ฟูรัลที่เกิดขึ้นในของเหลวไอออนิกและในน้ำนั้นได้ใช้ระเบียบวิธีริซึม เอสซีเอฟ เอสอีดีดี ควบคู่กับทฤษฎีแอบ อินิซิโอ โครงสร้างอิเล็กทรอนิกส์ ที่มีชื่อว่า ซีซีเอสดี(ที) พบว่า ปฏิกิริยาไอโซเมโรเซชันของกลูโคสที่เกิดในน้ำจะชอบเกิดกลไกปฏิกิริยาแบบวง ในขณะที่ปฏิกิริยาที่เกิดในของเหลวไอออนิกจะชอบเกิดกลไกปฏิกิริยาแบบโซ่เปิด นอกจากนี้ พบว่าวิถีปฏิกิริยาที่สมเหตุสมผลสำหรับปฏิกิริยาการแปลงฟรักโทสเป็น 5-ไฮดรอกซีเมทิลเฟอร์ฟูรัลที่เกิดในน้ำและของเหลวไอออนิก คือ กลไกปฏิกิริยาแบบวง ทั้งนี้ ในการศึกษาอิทธิพลตัวทำละลายของของเหลวไอออนิกนั้นได้ใช้ระเบียบวิธีริซึม เอสซีเอฟ เอสอีดีดี เพื่อแจกแจงพลังงานอิสระและและฟังก์ชันการกระจายเชิงรัศมีของตัวถูกละลายและตัวทำละลาย

สาขาวิชา วิทยาศาสตร์นาโนและเทคโนโลยี ลายมือชื่อนิสิต

ปีการศึกษา 2558 ลายมือชื่อ อ.ที่ปรึกษาหลัก

5487845120 : MAJOR NANOSCIENCE AND TECHNOLOGY

KEYWORDS: DFT / AFIR METHOD / BIGINELLI REACTION / RISM-SCF-SEDD / 5-HYDROXYMETHYLFURFURAL

MANEEPORN PURIPAT: THEORETICAL INVESTIGATIONS OF THE BIGINELLI REACTION AND THE GLUCOSE TRANSFORMATION TO 5-HYDROXYMETHYLFURFURAL. ADVISOR: ASSOC. PROF. VUDHICHA PARASUK, Ph.D., 123 pp.

In this thesis, the new insights of the Biginelli reaction, and the glucose transformation to 5-hydroxymethylfurfural have been provided. The obtained most favorable pathways have been purposed without prejudice. Also, the solvent effect in each reaction has been considered. The artificial force induced reaction (AFIR) method was applied to investigate systematically all possible multi-component pathways for the Biginelli reaction mechanism. Among all possible pathways, the most favorable one starts from the C-N bond formation between urea and benzaldehyde molecules, and follows by the nucleophilic addition of ethyl acetoacetate molecule. Surprisingly, an extra urea molecule is catalyzing the reaction nearly every step. Therefore, the Biginelli reaction is a urea-catalyzed multicomponent reaction. The reaction was found identical in ethanol and toluene. For glucose transformation to 5-hydroxymethylfurfural (HMF), RISM-SCF-SEDD method coupled with ab initio electronic structure theory, namely coupled cluster single, double, and perturbative triple excitation (CCSD(T)) has been employed to consider the reaction in both ionic liquid (IL) and water. We found that glucose isomerization in water favored the cyclic mechanism, while open chain mechanism is more favorable in ILs. Besides, the reasonable pathway of the transformation of fructose into HMF is the cyclic mechanism in both IL and water. The decomposition of free energies and radial distribution functions (RDFs) of solute-solvent that are operated by RISM-SCF-SEDD was utilized to clarify the solvent effects of IL.

Field of Study: Nanoscience and
Technology

Student's Signature

Advisor's Signature

Academic Year: 2015

ACKNOWLEDGEMENTS

First of all, I am grateful to thank my advisor, Assoc. Prof. Dr. Vudhichai Parasuk, who gives me a great opportunity to participate in many conferences and do research in the field of Physical Chemistry in Thailand and abroad. His kindness, guidance, help and support inspire me to accomplish my Ph.D. program. I would like to give all gratitude affectionately to him and his wife, Assoc. Prof. Dr. Waraporn Parasuk, for all their love and encouragement during the whole period of my Ph.D. study.

I would like to express my deepest appreciation and especially thank to Prof. Dr. Keiji Morokuma, Assist. Prof. Dr. Miho Hatanaka and Dr. Romain Ramozzi for their patronizing suggestions and valuable experiences during my long-term research in Fukui Institute for Fundamental Chemistry (FIFC), Kyoto University, Kyoto, Japan. Besides, I would like to thank Prof. Dr. Satoshi Maeda of Hokkaido University for the GRRM code. I also would express my sincere gratitude to Prof. Dr. Stephan Irle, Assoc. Prof. Dr. Daisuke Yokogawa, and Arifin for their help and kind advicement during my long-term research in Quantum Chemistry (QC) Group, Institute for Advanced Research, Department of Chemistry, Nagoya University, Nagoya, Japan.

Moreover, I would like to thank Assist. Prof. Dr. Narin Lawan for his kindness and helpful suggestion during my short-term research in Department of Chemistry, Chiang Mai University. This work was supported by the Development and Promotion of Science and Technology Talents Project (DPST) (Royal Government of Thailand scholarship) of Thailand. The Computer resources at the Institute for Information Management and Communication (IIMC) of Kyoto University and Computational Chemistry Unit Cell (CCUC), Chulalongkorn University. The authors also acknowledge National e-Science Infrastructure Consortium for providing computing resources that have contributed to the results reported within this thesis.

CONTENTS

	Page
THAI ABSTRACT	iv
ENGLISH ABSTRACT	v
ACKNOWLEDGEMENTS	vi
CONTENTS	vii
List of Figures.....	9
List of Schemes.....	14
List of Tables	15
CHAPTER I INTRODUCTION	16
CHAPTER II THEORETICAL BACKGROUND.....	25
2.1 Quantum Mechanical Calculations.....	25
2.1.1 Molecular quantum mechanics and Hartree-Fock Approximation.....	26
2.1.2 Electron correlation and coupled-cluster method	29
2.1.3 Reaction pathway search: Artificial Force Induced Reaction (AFIR).....	32
2.1.4 Solvation models	36
CHAPTER III COMPUTATIONAL DETAILS	41
3.1 Biginelli reaction	41
3.2 Glucose to 5-Hydroxymethylfurfural transformation.....	42
CHAPTER IV RESULTS AND DISCUSSIONS	45
4.1 Biginelli reaction	45
4.1.1 Route A: Iminium Route.....	45
4.1.2 Route B: Enamine Route.....	56
4.1.3 Route C: Knoevenagel Route.....	58

	Page
4.1.4 Comparison among all routes	60
4.1.5 Solvent effects	61
4.2 Glucose to 5-Hydroxymethylfurfural transformation.....	62
4.2.1 Glucose isomerization into Fructose	62
4.2.2 Fructose dehydration into HMF	67
4.2.3 Energy decomposition analysis	70
CHAPTER V CONCLUSION.....	73
REFERENCES	75
APPENDIX.....	94
VITA.....	123



List of Figures

Figure 1.1 Three main routes for the Biginelli reaction ^[41]	18
Figure 1.2 The structure of cellulose.....	19
Figure 1.3 Conversion of cellulose to biofuel ^[76]	19
Figure 1.4 The proposed mechanisms of glucose transformation to HMF.....	20
Figure 1.5 Examples of Ionic Liquids.....	21
Figure 2.1 Domain of dynamical equations ^[129]	25
Figure 2.2 The potential energy surface plotted against the reaction coordinate. ^[135]	33
Figure 2.3 F(Q) in (Eq. 2.20): (a) with $\alpha = 0$, (b) with small α and (c) with large α ^[143]	35
Figure 4.1 Intermediates and transition states between protonated urea and benzaldehyde (Step I in Route A). Gibbs free energies (1 atm, 298.15 K) (electronic energies with ZPE correction in parentheses), in kcal mol ⁻¹ relative to the isolated reactant molecules, were obtained at the M06-2X/6-31+G(d) level in PCM ethanol..	46
Figure 4.2 Two-, three- and four-component Step I (C-N bond formation) for Route A . See Figure 4.1 for computational details.	49
Figure 4.3 The most favorable pathways of Step II (Route A). See Figure 4.1 for computational details. The straight dashed line shows intermediates that are not connected by IRC.	51
Figure 4.4 Diketo-enol tautomerization of an ethyl acetoacetate.	52
Figure 4.5 The most favorable pathways of Step III and IV (Route A) starting from A1UE-7 to DHP. See Figure 4.1 for computational details. The straight dashed line shows intermediates that are not connected by IRC.	52
Figure 4.6 C-N bond formation leading to diurea derivative (A1-6). See Figure 4.1 for computational details.....	53

Figure 4.7 The best overall pathway for Route A . See Figure 4.1 for computational details.	55
Figure 4.8 The best pathway for Route B . See Figure 4.1 for computational details.....	57
Figure 4.9 The best pathway for Route C (Step I-IV) leading to A1UE-11 . See Figure 4.1 for computational details.....	60
Figure 4.10 Optimized geometries of the intermediates during the glucose isomerization into fructose via cyclic mechanism in [MMIM]Cl (1 atm, 353.15 K). The selected bond lengths and angles are given in unit of Angstrom and degree respectively. The labels for carbon and oxygen atoms are given for glucose and the important sites for each intermediate.	63
Figure 4.11 Optimized geometries of the intermediates during the glucose isomerization into fructose via open chain mechanism in [MMIM]Cl (1 atm, 353.15 K). The selected bond lengths are given in unit of Angstrom.	65
Figure 4.12 Free energy profile of glucose isomerization to fructose via (a) cyclic and (b) open chain mechanisms. Orange line shows the free energy changes in [MMIM]Cl at (1 atm, 353.15 K) condition. Blue line shows the free energy changes in water at (10 MPa, 473.15 K) condition. All values are reported in kcal mol ⁻¹	66
Figure 4.13 Geometry changes during the fructose transformation into HMF via cyclic mechanism in [MMIM]Cl at 1 atm, 353.15 K. It is started from TS_{Cy6-Fh1} . The selected bond lengths are given in unit of Angstrom.	68
Figure 4.14 Free energy profile of fructose transformation into HMF. Orange line shows the free energy changes in [MMIM]Cl at (1 atm, 353.15 K) condition. Blue line shows the free energy changes in water at (10 MPa, 473.15 K) condition. All values are reported in kcal mol ⁻¹	69
Figure 4.15 Definition of atomic labels (Main, H, Cl) for the contribution to the solvation free energy. The regions surrounded by the red line are represented as 'Main'.	71

Figure 4.16 (a) RDFs between Cl sites in HCl and $\text{TS}_{\text{Op5-Op6}}$. Inset on shows the interactions of the solute sites with Cl_v and CR_v sites. (b) Schematic figure of cations and anions around free HCl and $\text{TS}_{\text{Op5-Op6}}$	72
Figure S1 Proton Affinity (Gibbs free energy in kcal mol^{-1}) in PCM ethanol with respect to H_3O^+ at the M06-2X/6-31+G(d) level.....	95
Figure S2 Detailed mechanism with a second urea (in red circle) to the intermediate A2-3 and leading to product A1-3 . Gibbs free energies ($P=1$ atm, $T=298.15$ K) (energies with ZPE correction in parentheses), in kcal mol^{-1} relative to individual reactants, were obtained at the M06-2X/6-31+G(d) level in PCM (ethanol).	95
Figure S3 The obtained three-component pathways for Step I (C-N bond formation) with an extra urea and benzaldehyde for Route A . See Figure S2 for computational details.	96
Figure S4 The obtained three-component pathways for Step I (C-N bond formation) with an extra ethyl acetoacetate for Route A . See Figure S2 for computational details.	97
Figure S5 Pathways for Step I (C-N bond formation) with four components for Route A . See Figure S2 for computational details.	98
Figure S6 Detailed mechanism of Step II (Dehydration) of Route A with different catalysts. See Figure S2 for computational details.	99
Figure S7 Pathways for Step III (Bond formation with ethyl acetoacetate) with three and four components for Route A . See Figure S2 for computational details. .	100
Figure S8 Detailed mechanism for Step III (C-C bond formation) passing through a diurea derivative (A1-6) leading to product A1E-11 . See Figure S2 for computational details.	101
Figure S9 Gibbs Free energy profiles for Step IV (Route A) in ethanol. See Figure S2 for computational details.	101

Figure S10 Additional concerted pathway of cyclization step for Route A from A1UE-11' to A1UE-15' which does not go through A1UE-13 . See Figure S2 for computational details.	102
Figure S11 All obtained initial association pathways for Route B . See Figure S2 for computational details.	103
Figure S12 Detailed mechanism with an additional urea (in red circle) and benzaldehyde (BA) (in blue circle) to the intermediate B2-3 and leading to product B1-3 . See Figure S2 for computational details.	104
Figure S13 Detailed mechanism for Step II (Dehydration) of Route B with different catalysts. See Figure S2 for computational details.	105
Figure S14 Pathways for Step III (Bond formation with benzaldehyde) with three and four components for Route B . See Figure S2 for computational details.	106
Figure S15 Gibbs Free energy profiles for Step IV (Route B) in ethanol. See Figure S2 for computational details.	107
Figure S16 All obtained initial association pathways for Route C . See Figure S2 for computational details.	108
Figure S17 Detailed mechanism of adding a second urea (in red circle) to the intermediate C2-3 leading to product C1-3 . See Figure S2 for computational details.	109
Figure S18 Detailed mechanism of Step II (Dehydration) of Route C with different catalysts. See Figure S2 for computational details.	110
Figure S19 Additional concerted pathway of dehydration step for Route C from C1UU-5' to C1UU-9' which does not go through C1UU-7 . See Figure S2 for computational details.	111
Figure S20 Pathways for Step III (Bond formation with urea) with three and four components for Route C . See Figure S2 for computational details.	112

Figure S21 Free energy profiles of three main routes: Route A in blue, Route B in pink and Route C in green See Figure S2 for computational details.	112
Figure S22 Free energy profiles of overall reaction for route A with four components at the M06-2x/6-31+G(d) level. Reactions in EtOH and toluene were demonstrated in blue line and orange line, respectively.	113
Figure S23 Free energy profiles of the most favorable pathways of step I-II (Route A) in toluene. Three- and four components step were demonstrated in pink line and blue line, respectively. See Figure S2 for computational details.	114
Figure S24 Free energy profiles of the most favorable pathways of step III-IV (Route A) in toluene. Three- and four components step were demonstrated in pink line and blue line, respectively. See Figure S2 for computational details.....	115
Figure S25 Geometry changes during the glucose-fructose isomerization via cyclic mechanism in water at 10 MPa, 473.15 K. The selected bond lengths are given in unit of Angstrom.	116
Figure S26 Geometry changes during the glucose-fructose isomerization via open chain mechanism in water at 10 MPa, 473.15 K. The selected bond lengths are given in unit of Angstrom.	117
Figure S27 Geometry changes Op4 and Op6 stabilized by Cl^- ion (Op4' and Op6' , respectively) in open mechanism in [MMIM]Cl at 1 atm, 373.15 K. The selected bond lengths are given in unit of Angstrom.	118
Figure S28 Geometry changes during the fructose transformation into HMF via cyclic mechanism in water at 10 MPa, 473.15 K. The selected bond lengths are given in unit of Angstrom.	118

List of Schemes

Scheme 1.1 The Biginelli reaction ^[41]	17
Scheme 4.1 Proposed catalytic process with a second urea (in red circle).....	47



List of Tables

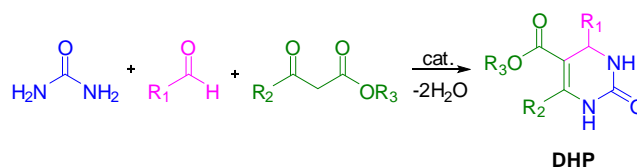
Table 2.1 Type of CC methods and their T operator expansion	32
Table 3.1 Lennard-Jones parameters of solutes	44
Table 4.1 The energies (in kcal mol ⁻¹) of the transition states of.....	61
Table 4.2 The change of solvation free energy on each site.	71
Table S1 Activation energy difference of Step II (Dehydration) of Route A with different catalysts at the M06-2X/6-31+G(d) level. All energies are relative to the activation energy of reaction using urea+ ethyl acetoacetate (EAA) as catalysts.....	100
Table S2 The energies (in kcal mol ⁻¹) of the transition states of the rate-determining step for the different routes with para-substitution on aryl ring of benzaldehyde, were obtained at the M06-2X/6-31+G(d) level in PCM ethanol.....	102
Table S3 Activation energy difference for Step II (Dehydration) of Route B with different catalysts at the M06-2X/6-31+G(d) level. All energies are relative to the activation energy of reaction using urea as a catalyst.....	106
Table S4 Activation energy difference of Step II (Dehydration) of Route C with different catalysts at M06-2X/6-31+G(d) level. All energies are relative to the activation energy of reaction using urea as a catalyst.....	111
Table S5 The energies (in kcal mol ⁻¹) of the transition states of the rate-determining step for the different routes, were obtained at the M06-2X/6-31+G(d) level in PCM toluene.....	115
Table S6 Lennard-Jones parameters of solvents	115
Table S7 Energy difference of Op4' and Op6' stabilized by chloride anion in [MMIM]Cl.....	117

CHAPTER I INTRODUCTION

Previous studies of some organocatalytic reactions might have some missing pathways. It is likely because of intricacy to speculate real transition state (TS) structures in several conceivable pathways; hence most pathways were based on chemical intuition. There are two remarkable organocatalytic reactions: 1) the Biginelli reaction and 2) the glucose transformation to 5-HMF, which are essential for pharmacology, and alternative energy, respectively. The first reaction, namely Biginelli reaction, has had great impact in organic synthesis due to its higher atom and energy economy compared to linear synthesis.^[1] Also, it is noteworthy that a class of compounds exhibits pharmacological activity.^[2-4] The second reaction is the glucose transformation to 5-hydroxymethylfurfural. It starts from plants and leaves debris, which mostly comprised of cellulose^[5], followed by conversion to biofuel. These would provide results of merit to agricultural country like Thailand. Thus, both reactions are much worthy to understand with the deeper insights, since the knowledge can be used to design more efficient processes, or even to design new catalysts with enhanced efficiency.

Multicomponent reactions (MCRs) are the chemical reaction which involves three or more reagents in one pot.^[6-15] MCRs have many advantages in organic synthesis due to atom-economy fashion, and less waste generation compared to stepwise linear synthesis.^[1] Actually, there are many types of MCRs such as Passerini^[16-19], Ugi coupling,^[20-22] Biginelli,^[23, 24] and Hantzsch reactions.^[25, 26]

The Biginelli reaction is an important multicomponents reaction.^[2, 27, 28] It was used to synthesize many bioactive compounds,^[2-4] such as antihypertensive agents,^[29] potassium channel antagonists,^[30] anti-HIV agents,^[31] and so forth.^[32-40] Firstly discovered in 1893,^[23, 24] this reaction brings about three-component coupling: urea, aldehyde, and β -keto ester, in one pot to form 4-aryl-3,4-dihydropyrimidin-2(1H)-one (DHP) as demonstrated in **Scheme 1.1**.



Scheme 1.1 The Biginelli reaction^[41]

The variations of the experimental conditions were proposed to enhance the efficiency of process.^[27] Brönsted acids^[42-46], Lewis acids,^[15, 47-50] ionic liquids,^[51-56] or even excess of one reactant^[47, 51, 57-60] have been used as catalysts. After its discovery, various mechanisms were proposed (see **Figure 1.1**). The first one, namely iminium route,^[57] considers the condensation of the benzaldehyde and urea to form the iminium followed by a nucleophilic addition of the third partner (Route **A** in **Figure 1.1**). The second mechanism, the so-called enamine route^[14] (Route **B** in **Figure 1.1**), starts from the coupling between urea and ethyl acetoacetate to give the enamine followed by the reaction of the carbonyl compound. Finally, the third mechanism is a Knoevenagel type reaction^[13] between the aldehyde and the β -keto ester followed by a C-N bond formation with the urea (Route **C** in **Figure 1.1**).

Various experimental and theoretical studies have been conducted to verify its reaction mechanism.^[8, 15, 47, 51, 52, 59-63] De Souza *et al.*^[64] have identified intermediates by direct infusion electrospray ionization mass spectrometry (ESI-MS). They found different intermediates involving all three routes. The study was then supported by theoretical calculations for C-C and C-N bonds formation steps and summarized that the iminium route was most favorable routes. The C-C bond formation corresponding to the nucleophilic addition of the β -ketoester on the iminium was found as the rate-determining step of the process. Recently, Clark *et al.*^[65] proved that the solvent ability to promote the tautomeric equilibrium for the β -ketoester impacts on the process efficiency. They showed that the proticity of the solvent is not critical for the efficiency of the process, as the yields were found similar in both protic and aprotic solvents.

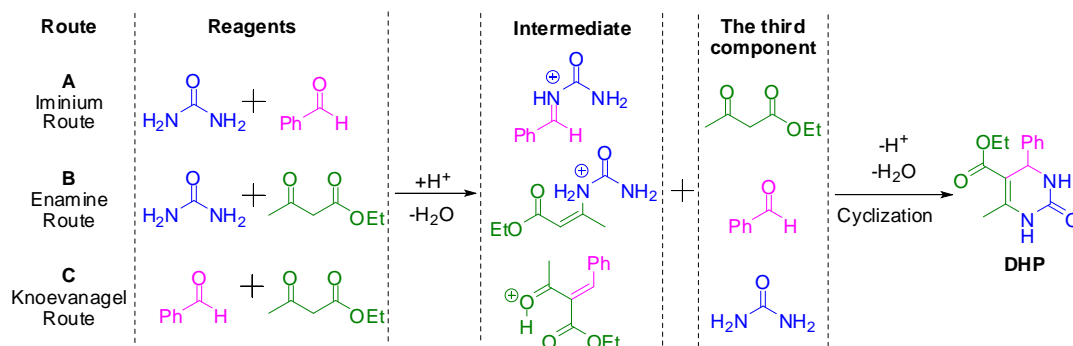


Figure 1.1 Three main routes for the Biginelli reaction^[41]

The absence of theoretical investigations on Biginelli reaction, such as the cyclization and dehydration steps, as well as the absence of a systematic study, are driving us to reconsider the preferred reaction pathway for deep insights of these essential reactions. Are there only three routes demonstrated which possibly lead to the **DHP**? Are the reactions in protic and aprotic solvents exactly identical? Are the proticity and polarity of the solvent critical? Does one of reactants act as a catalyst?

The next organocatalytic reaction is the glucose transformation to 5-HMF. This reaction is now the hot issue since human beings are concerned about the depletion of petroleum resources. Thus, renewable power and alternative energies have been focused by vast numbers of researchers. One of the areas of interest is the conversion of cellulose from plant's waste to biofuel because of its superabundance, renewability, and worldwide branching.^[66]

Cellulose is a polysaccharide which consists of several thousand glucose units linking together with a linear chain β (1 \rightarrow 4) glycosidic linkage as shown in **Figure 1.2**.^[67] Regularly, cellulose is insoluble in water and most organic solvents, but its glucose units can be chemically broken down with concentrated acids at high temperature.^[68-72] However, it was found that cellulose can be dissociated in ionic liquids (ILs) and then converted to biofuel.^[73] Consequently, cellulose could be used as a renewable energy resource.

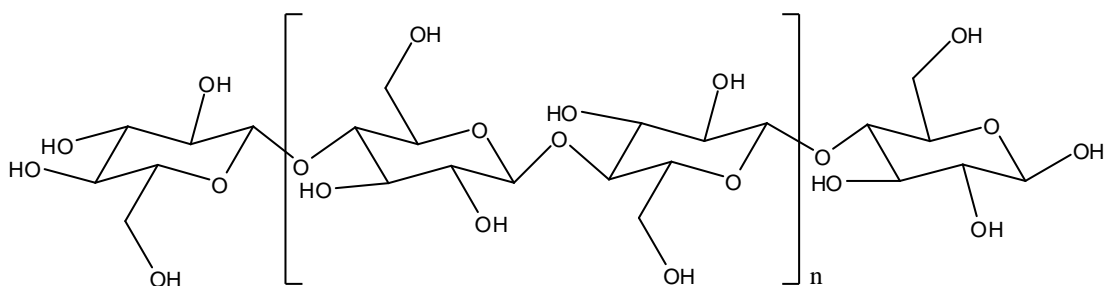


Figure 1.2 The structure of cellulose

Ordinarily, major component of plants and leaves debris is lignocellulose which is composed of cellulose, hemicellulose and lignin.^[5] Cellulose can be separated from lignin for using in the process of biofuel production. The processes of degradation and transformation biomass to biofuel consist of various steps.^[68, 74] as shown in **Figure 1.3**, and many green chemicals are produced. Firstly, polymer chains of cellulose are hydrolyzed into low molecular weight fragments by hydrolysis process. Then, the glucose units are isomerized into fructose units. After that, fructose is transformed to 5-hydroxymethylfurfural (HMF) which can be converted to many useful chemicals, such as 2,5-dimethylfuran (DMF), levulinic acid (LA) and so forth.^[75]

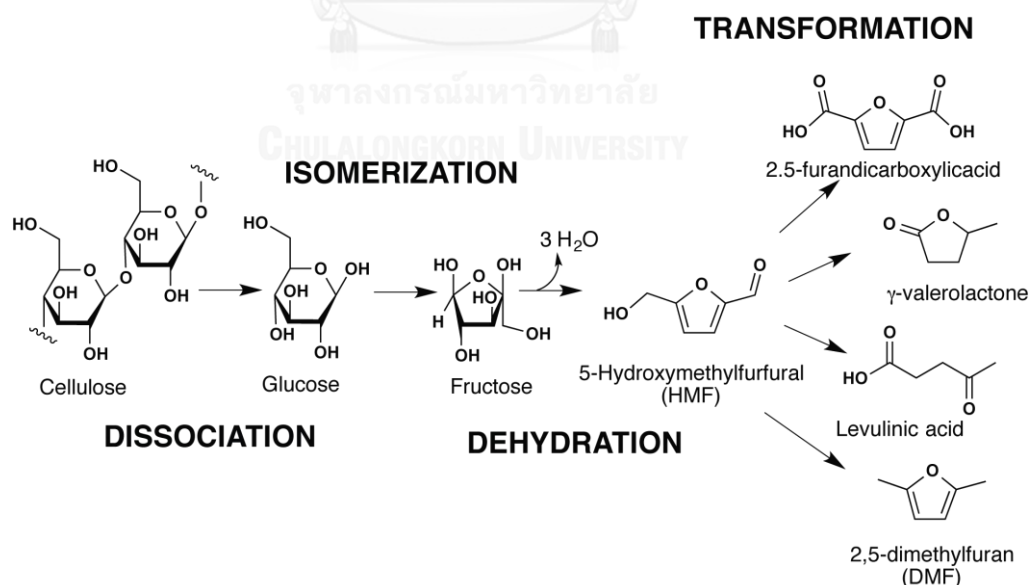


Figure 1.3 Conversion of cellulose to biofuel^[76]

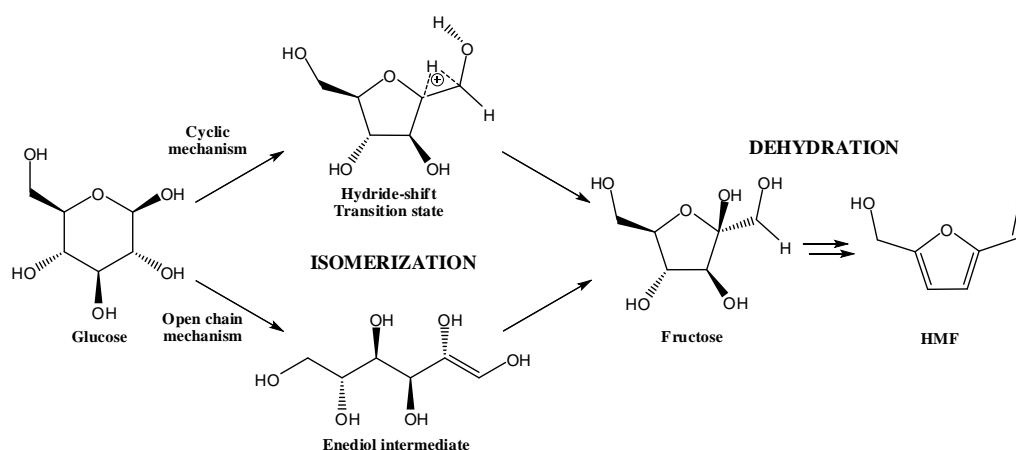


Figure 1.4 The proposed mechanisms of glucose transformation to HMF

Several mechanisms of glucose transformation to HMF have been investigated.^[77] Recently, the two mechanisms of hexose isomerization of pyranose into furanose and a subsequent transformation to furfural have been suggested: cyclic^[78-85] and open chain mechanisms^[80, 86-91] (See **Figure 1.4**). The open chain mechanism initially begins with an open chain aldose isomerization to the ketose structure. After that, two water molecules are dehydrated from an open chain ketose via acid-catalyzed dehydration followed by the chain closing and furfural forming. On the other hand, Antal *et al.*^[78, 79] suggested a cyclic mechanism for the transformation of fructose into HMF without the ring opening. Also, his guidance was relied on the experimental evidences.

In 1934,^[92] Graenasher first suggested that cellulose could be dissolved by molten N-ethylpyridinium chloride, in the presence of nitrogen-containing bases. From these reasons, many kinds of ILs were used as the novel solvent for dissolving cellulose and other biopolymers.^[93-102]

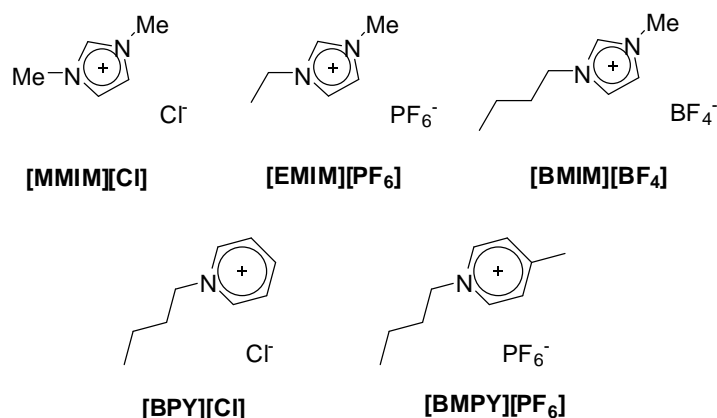


Figure 1.5 Examples of Ionic Liquids

ILs are molten salt at room temperature because of its low melting point (below 100°C). Normally, it composed of an organic heterocyclic cation mostly containing nitrogen or phosphorus and an inorganic anion. Anions significantly affect the miscibility with water and other solvents, whereas, cations markedly affect the melting point, viscosity, and electrochemical stability.^[103-106] Due to its low toxicity, high ionic conductivity, non-volatility, non-flammability, wide electrochemical window, high thermal stability and recyclability,^[107, 108] ILs are demanded as interesting green solvents and effective solvent for cellulose dissolution. Examples of ionic liquids are displayed in **Figure 1.5**.

Recently, cellulose dissociation into glucose units in ILs and acidic aqueous solutions have been theoretically considered by Nishimura and co-workers.^[109] Moreover, Zhao *et al.*^[110] showed that the glucose conversion to HMF occurred from an isomerization of pyranose to furanose and followed by dehydration to HMF. However, the conversion of biomass to biofuel in form of HMF is a new process and its notions are not entirely comprehended, especially mechanisms.^[86, 111] This knowledge is advantageous to the design of more effective processes. In this work, we will focus only the mechanism of glucose transformation to 5-hydroxymethylfurfural.

To provide more insights and understanding, the theoretical approaches, such as molecular dynamics simulations and *ab initio* quantum mechanics, have been

employed to study the reaction mechanisms. In previous studies, the implicit solvation model such as PCM, COSMO, SMD, and G4MP2 level of theory have been utilized to examine the transformation of glucose and fructose to HMF.^[80, 81, 85, 106, 112-115] The details of the overall pathways of glucose dehydration and conversion have been provided from these studies. Besides, the reaction in 1-ethyl-3-methylimidazolium chloride ([EMIM]Cl), has been theoretically studied using the B3LYP functional. As it is hard to look for the exact dielectric constant of [EMIM]Cl, its physical data was still inadequate.^[116] Additionally, the implicit solvation models still be devoided of the properties of full accounting of microscopic. Soon after its discovery, a microscopic enlightenment of solute-solvent circumstances during the process has been demonstrated by Qian *et al.*^[83, 84, 111, 117, 118] The progression of studies carried out by Car-Parrinello molecular dynamics and metadynamics simulations (CPMD-MTD) have been published to show the free energy surfaces of isomerization, mutarotation, and dehydration of glucose to HMF in aqueous solutions.

Although the molecular dynamics can confirm the equilibrium state, the thermodynamic properties can be also considered by statistical mechanics model. The important point of view is that these molecular simulations provide the amount of particles in radial distance demonstrated by the radial distribution functions (RDFs).^[119] However, an outstanding alternative method, which offers reasonable computational time due to no need to define the 'simulation box' is 'Reference Interaction Site Model' (RISM), which will be further employed and discussed in section 4.2.

The breakthrough of green technologies for renewable energy from biomass is much more important to develop sustainable economy. HMF and its derivatives are dramatic because their energy capacities are higher than that of ethanol and almost equivalent to that of gasoline. DMF, gasoline and ethanol can provide around 31.5 MJ L⁻¹, 35 MJ L⁻¹ and 23 MJ L⁻¹, respectively.^[120, 121] Thus, it is a promising alternative fuel for transportation. Moreover, the transformation biomass to HMF and its derivatives is uncomplicated and can be completed in one step. Thus, this process is

remarkable to biofuel production which is much suitable to Thailand, which is an agricultural country.

As the reaction in ILs can take place at milder conditions (100-140°C) and the chemicals are less harmful to environments, we can say that this reaction is green. Nevertheless, the kinetic studies of this reaction are still in its infancy, especially mechanisms, thus its perceptions might not be completely understood. This reaction is a new process composed of multiple reaction pathways, several of ring and open chain isomers of sugars, and solvation effects.^[86] Based on the requirement of engineering applications for biomass, it is essential to investigate these reaction pathways.

Theoretical studies on chemical reactions give hints to resolving the reaction mechanism. Experimentally, a reaction mechanism could be suggested from found intermediates. This is in some ways an almost impossible task, since many species are very reactive thus having short-life. However, accurate estimations of reactive intermediates as well as transition state complexes can be achieved by means of quantum chemical calculations. In the reaction mechanism study, finding transition state (TS) structures is essential missions to analyze and predict how the reaction proceeds.^[122] This knowledge has advantages for the design of more effective processes. However, it is still a difficult task in theoretical study of complicated reaction mechanisms.^[123-128]

Herein, the author will study systematically a quantum chemical study of all possible pathways among three reactant molecules of the Lewis acid-catalyzed Biginelli reaction using a new theoretical approach for finding transition states (TSs), namely AFIR method with DFT calculation. The most favorable pathway without bias and prejudice will be proposed. Moreover, the glucose and fructose transformation to HMF in ILs and acidic aqueous solutions will be considered with DFT calculation and coupled-cluster electronic structures, as well as RISM-SCF-SEDD solvation theory. Additionally, solvent effect will be considered.

Therefore, in this thesis, the author will provide new insights for Biginelli reaction, and the glucose transformation to 5-hydroxymethylfurfural. The most favorable pathways will be proposal without preconception. The different pathways in each reaction will be discussed. The author hopes that the proposed reaction mechanisms and the roles of solvation will give the deeper insights on those reaction processes.



CHAPTER II THEORETICAL BACKGROUND

2.1 Quantum Mechanical Calculations

Quantum mechanical calculations have been widely applied in chemistry. In practice, they were employed to determine transition states, ground and excited states of atoms and molecules, and predicting physical and chemical properties of chemical compounds. The dynamical equation of particles can be distributed into four regions as shown in **Figure 2.1** concerning to velocity and mass.

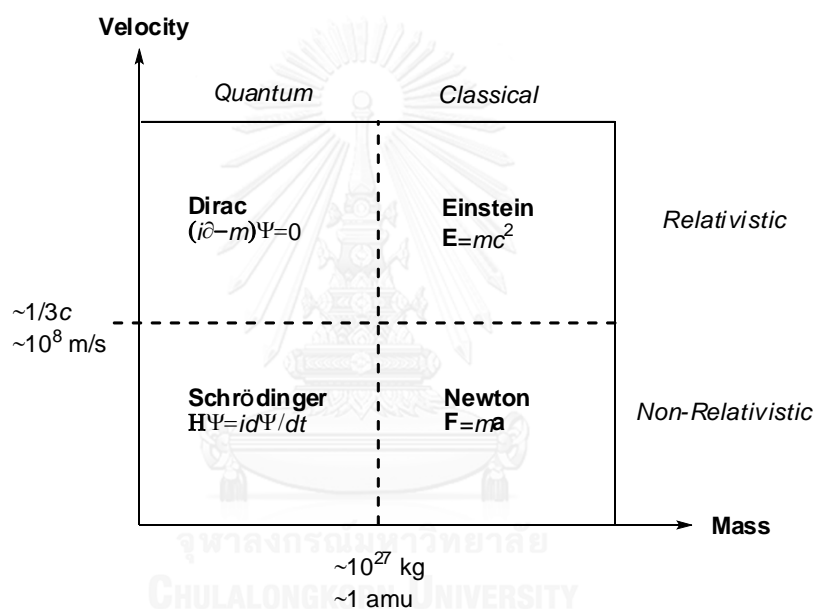


Figure 2.1 Domain of dynamical equations^[129]

The Newton's second law, $F=ma$, is mostly employed to heavy particles with quite slow motion. However, the relativistic effect becomes crucial when the particle's velocity is close to the speed of light. The quantum mechanics was used to explain the light particle including electrons, which acts both particle and wave characteristics. The difference between classical mechanics and quantum mechanics is that quantum mechanics displays the probability, which can locate the position of particle over time. On the other hand, classical mechanics demonstrates the determining, which just provides the probability of the particle being at the absolute position and at the exact time.^[129] In the following section, quantum mechanical

calculations will be explained in brief and in the following order 1) Molecular quantum mechanics and Hartree-Fock Approximation, 2) Electron correlation and coupled-cluster method, 3) Reaction pathway search method: Artificial Force Induced Reaction (AFIR), and 4) Solvation models.

2.1.1 Molecular quantum mechanics and Hartree-Fock Approximation

Determining energies and properties of molecules is the major goal of quantum mechanical calculations. Normally, they can be obtained by solving the fundamental equation, so-called Schrödinger equation.^[129-131]

$$\hat{H}\Psi = E\Psi \quad (\text{Eq. 2.1})$$

where Ψ is the wavefunction, \hat{H} is the Hamiltonian operator, and E is the energy of the state. The probability distribution of finding the particle can be defined by the absolute square of the wavefunction ($|\Psi|^2$).

Generally, the Hamiltonian operator of all particles is the combination of potential (\hat{V}) and kinetic (\hat{T}) operators for N particles.

$$\hat{H} = \hat{V} + \hat{T} \quad (\text{Eq. 2.2})$$

However, with $3N$ degree of freedom the Schrödinger equation is too complicated to be solved. Considering the fact that the mass of nuclei is much larger than that of electron, nucleus should shift more torpidly. This makes electron adapt their distribution to quickly alter the location of nuclei. This suggested that the distribution of electrons is not based on their velocities, but the position of nucleus.^[132] Realizing this fact, the complicity of solving Schrödinger equation for a molecular system is then reduced to solving series of the electronic Schrödinger

equation in the field of fixed nuclei. This is the underline of the Born-Oppenheimer approximation.

The electronic Schrödinger equation is given as

$$\hat{H}^{elec}\Psi^{elec}(\mathbf{r}, \mathbf{R}) = E^{eff}(\mathbf{R})\Psi^{elec}(\mathbf{r}, \mathbf{R}) \quad (\text{Eq. 2.3})$$

where $E^{eff}(\mathbf{R})$ is an effective electronic energy, Ψ^{elec} is the electronic wave function relied on the coordinate (\mathbf{r}) and nuclear coordinate (\mathbf{R}), \hat{H}^{elec} is defined as the combination of the kinetic energy of electrons, the attractive interaction of electron to nuclei, and the repulsive interaction between electrons as follows (in atomic unit)

$$\hat{H}^{elec} = -\sum_{i=1}^N \frac{1}{2} \nabla_i^2 - \sum_{i=1}^N \sum_{A=1}^N \frac{Z_A}{r_{iA}} + \sum_{i=1}^N \sum_{j>i}^N \frac{1}{r_{ij}} \quad (\text{Eq. 2.4})$$

The constant repulsion energy of nuclei is combined to the total energy in case of fixed nuclei (ϵ) as follows

$$\epsilon = E^{eff} + \sum_{A=1}^M \sum_{B>A}^M \frac{Z_A Z_B}{R_{AB}} \quad (\text{Eq. 2.5})$$

Normally, the Born-Oppenheimer approximation provided only the error of 10^{-4} a.u. for hydrogen atom and also becomes better for the system of heavier nuclei.

The exact solution of the electronic Schrödinger equation of (Eq. 2.3) cannot be obtained for system containing more than one electron. Thus, an approximate solution must be sought. One of the simplest approaches is the Hartree-Fock (HF)

approximation which employed the variational principle. Therefore, the determinant of one-electron wavefunctions for orbitals χ_i was defined as

$$|\Psi_0\rangle = \frac{1}{\sqrt{N!}} \begin{vmatrix} \chi_1(x_1)\chi_2(x_1) \cdots \chi_N(x_1) \\ \chi_1(x_2)\chi_2(x_2) \cdots \chi_N(x_2) \\ \vdots \\ \chi_1(x_N)\chi_2(x_N) \cdots \chi_N(x_N) \end{vmatrix} \quad (\text{Eq. 2.6})$$

In HF approximation, electronic energy is defined as

$$E_0 = \langle \Psi_0 | \hat{H} | \Psi_0 \rangle \quad (\text{Eq. 2.7})$$

where \hat{H} represent full electronic Hamiltonian. Substituting Ψ_0 in (Eq. 2.6), the Hartree-Fock energy can be determined from

$$E_0 = \sum_{a=1}^N \varepsilon_a \frac{1}{2} \sum_{a=1}^N \sum_{b=1}^N \left[\int \chi_a^*(x_1)\chi_a(x_1)r_{12}^{-1}\chi_b^*(x_2)\chi_b(x_2)dx_1dx_2 - \int \chi_a^*(x_1)\chi_b(x_1)r_{12}^{-1}\chi_b^*(x_2)\chi_a(x_2)dx_1dx_2 \right] \quad (\text{Eq. 2.8})$$

The orbital χ_i can be obtained from the canonical Hartree-Fock equation

$$f_i\chi_a(x_i) = \varepsilon_a\chi_a(x_i) \quad (\text{Eq. 2.9})$$

where f_i is Fock operator, which demonstrates effective operator for each electron and ε_a is the orbital energy. The Hartree-Fock energy (E_0) and the orbital energy (ε_a) are defined as follow

$$E_0 = \sum_{a=1}^N \varepsilon_a \frac{1}{2} \sum_{a=1}^N \sum_{b=1}^N \left[\iint \chi_a^*(x_1) \chi_a(x_1) r_{12}^{-1} \chi_b^*(x_2) \chi_b(x_2) dx_1 dx_2 \right. \\ \left. - \iint \chi_a^*(x_1) \chi_b(x_1) r_{12}^{-1} \chi_b^*(x_2) \chi_a(x_2) dx_1 dx_2 \right]$$

(Eq. 2. 10)

$$\varepsilon_a = \int \chi_a^* h \chi_a dx_1 \\ + \sum_{b=1}^N \left[\iint \chi_a^*(x_1) \chi_a(x_1) r_{12}^{-1} \chi_b^*(x_2) \chi_b(x_2) dx_1 dx_2 \right. \\ \left. - \iint \chi_a^*(x_1) \chi_b(x_1) r_{12}^{-1} \chi_b^*(x_2) \chi_a(x_2) dx_1 dx_2 \right]$$

(Eq. 2.11)

The Hartree-Fock equation in (Eq. 2.9) is not linear and must be iteratively solved by self-consistent field (SCF) method.

2.1.2 Electron correlation and coupled-cluster method

Weak interactions of few kcal mol⁻¹ play important roles in chemistry. Thus, to predict weak interactions quantum mechanical calculations should yield accuracy within 1 kcal mol⁻¹. By treating electron-electron interaction in an approximate way, the Hartree-Fock method cannot provide the exact total energy. The deficiency of Hartree-Fock method can be termed (lack of) “electron correlation”. One of the wavefunction-based approaches which taking into account of electron correlation is coupled-cluster (CC) method.^[119, 133]

One of the deficiencies of HF method is one-electron wavefunction or orbital obtained from HF equation. This is somehow can be circumvented by introducing many-determinant wavefunction instead of single-determinant one. The idea of coupled-cluster method is to generate many-determinant wavefunction by using excitation operator T .^[129, 134]

$$T = T_1 + T_2 + T_3 + \cdots + T_N \quad (\text{Eq. 2.12})$$

where T_i is cluster operator, i is defined as the cluster order. The T_N results to the N-table excitation determinants. For instance,

$$T_1|\Psi_0\rangle = \sum_a^{N_{occ}} \sum_r^{N_{virt}} t_a^r |\Psi_a^r\rangle \quad (\text{Eq. 2.13})$$

$$T_2|\Psi_0\rangle = \sum_{ab}^{N_{occ}} \sum_{rs}^{N_{virt}} t_{ab}^{rs} |\Psi_{ab}^{rs}\rangle \quad (\text{Eq. 2.14})$$

⋮

and

$$T_N|\Psi_0\rangle = \sum_{ab\cdots}^{N_{occ}} \sum_{rs\cdots}^{N_{virt}} t_{ab\cdots}^{rs\cdots} |\Psi_{ab\cdots}^{rs\cdots}\rangle \quad (\text{Eq. 2.15})$$

where t_a^r , t_{ab}^{rs} , ... , are cluster amplitudes. $|\Psi_a^r\rangle$, $|\Psi_{ab}^{rs}\rangle$, ... , are single, double, ... , excitation determinants, respectively. N_{occ} and N_{virt} represent number of occupied and virtual orbitals, respectively.

The coupled cluster (CC) wavefunction is then defined as^[119]

$$|\phi\rangle = e^T |\Psi_0\rangle \quad (\text{Eq. 2.16})$$

Since $e^T = 1 + T + \frac{T^2}{2!} + \frac{T^3}{3!} + \cdots$, then

$$\begin{aligned}
|\phi\rangle &= \left(1 + T + \frac{T^2}{2!} + \frac{T^3}{3!} + \dots\right) |\Psi_0\rangle \\
&= |\Psi_0\rangle + (T_1 + T_2 + \dots + T_N) |\Psi_0\rangle \\
&\quad + \frac{1}{2} (T_1^2 + T_2^2 + T_3^2 + \dots + 2T_1T_2 + \dots) |\Psi_0\rangle + \dots \\
&= |\Psi_0\rangle + T_1 |\Psi_0\rangle + \left(T_2 + \frac{1}{2} T_1^2\right) |\Psi_0\rangle \\
&\quad + \left(T_3 + T_2T_1 + \frac{1}{6} T_1^3\right) |\Psi_0\rangle \\
&\quad + \left(T_4 + T_3T_1 + \frac{1}{2} T_2^2T_1^2 + \frac{1}{24} T_1^4\right) |\Psi_0\rangle + \dots
\end{aligned}$$

(Eq. 2.17)

The Hartree-Fock state was denoted in (Eq. 2.17). The single, double, triple, and quadruple, ... , excitation determinants are represented in the second, the third, and the fourth term, ... , respectively. If only T_1 and T_2 are maintained, the method was called ‘coupled cluster singles doubles’ (CCSD). The CCSD wave function can be defined as follows

$$|\phi\rangle = e^{(T_1+T_2)} |\Psi_0\rangle$$

(Eq. 2.18)

$$\begin{aligned}
|\phi\rangle &= |\Psi_0\rangle + T_1 |\Psi_0\rangle + \left(T_2 + \frac{1}{2} T_1^2\right) |\Psi_0\rangle + \left(T_2T_1 + \frac{1}{6} T_1^3\right) |\Psi_0\rangle \\
&\quad + \left(\frac{1}{2} T_2^2 + \frac{1}{2} T_2T_1^2 + \frac{1}{24} T_1^4\right) |\Psi_0\rangle + \dots
\end{aligned}$$

(Eq. 2.19)

Table 2.1 Type of CC methods and their T operator expansion

Methods	T expansion
CCD	$T = T_2$
CCSD	$T = T_1 + T_2$
CCSDT	$T = T_1 + T_2 + T_3$
CCSDTQ	$T = T_1 + T_2 + T_3 + T_4$

The first term is Hartree-Fock state. The single, double, triple, quadruple,... excitation determinants are defined in the second, the third, the fourth and the fifth,... respectively. This shows that coupled-cluster methods are both size-extensive and size-consistent as this method contains full expansion of excitation types, but the identical number of excitation determinants will not be restored. **Table 2.1** demonstrates several types of coupled-cluster methods and their T operator expansions.

However, the accuracy of calculation is based on the contribution of the direct triple excitation ($T_3|\Psi_0\rangle$). The CCSD(T), which stands for coupled-cluster with single, double, and approximate triple excitations method is now widely used as the gold standard for theoretical studies. However, CCSD(T) consumes large computer resources since it is scaled to N^7 .

2.1.3 Reaction pathway search: Artificial Force Induced Reaction (AFIR)

In theoretical study of chemical reaction, finding transition state (TS) structures is an essential mission for analyzing and predicting reaction mechanisms. This knowledge is advantageous for the design of a more effective process. TS is not the stable state. It locates at the saddle point on potential energy surface. Nevertheless, searching for TS is a difficult task, since it is not easy to locate the most

suitable one owing to its large numbers of degrees of freedom. Hence, several TSs can be found for each reaction pathway. The “reaction coordinate” can be used to determine whether a particular TS is belong to a specific reaction pathway.^[119]

Activation energy, denoted by E_a , is the height of the reaction barrier which distinguishes two local minima (reactants and products) of the potential energy surface. (See **Figure 2.2**)^[129]

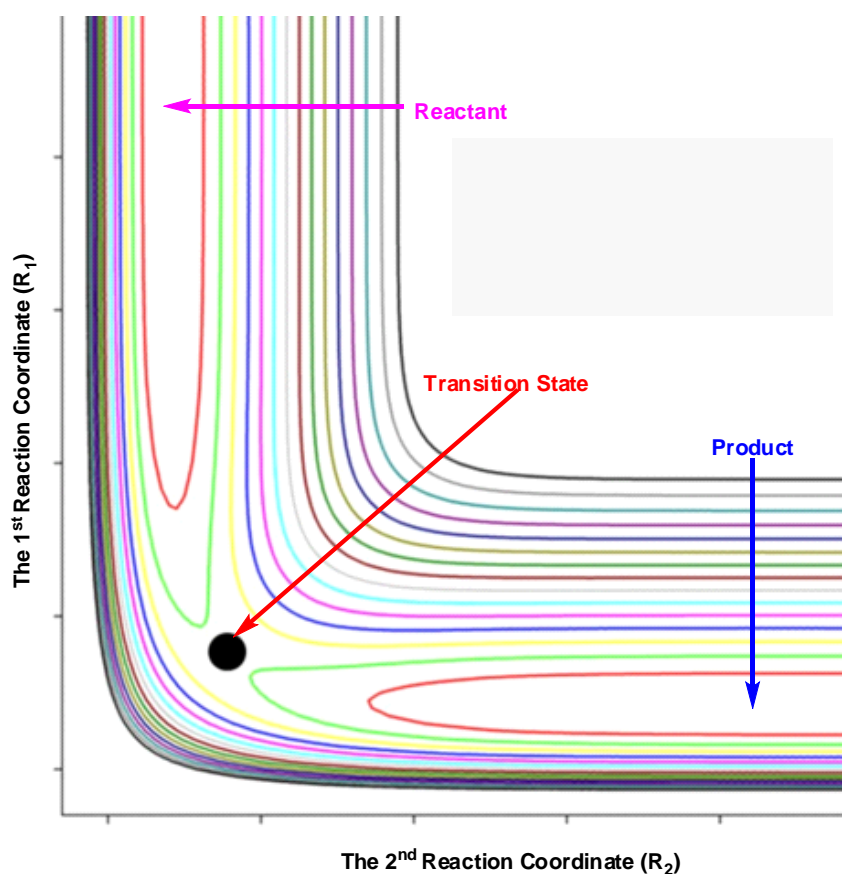


Figure 2.2 The potential energy surface plotted against the reaction coordinate.^[135]

It is a non-trivial task to find TS structures manually. Most TSs arrive from the chemical intuition (which means bias). Presently, there are numerous methods, which were developed for searching minimum energy reaction path automatically, such as the single coordinate driving (SCD),^[136-138] the metadynamics method,^[139, 140] the fast marching method^[141] and so forth. One of them, which was developed in 2010 by Morokuma and Maeda' group is the artificial force induced reaction (AFIR) method.^[142, 143] The AFIR explores all probable reaction pathways including unexpected reaction paths automatically and systematically without any arbitrariness. The concept of AFIR method is to impose the constant artificial force between two or more initial reagents randomly. All possible pathways could be found with various orientations of reactants molecules. This could avoid missing some important paths form a reaction, which may have several reaction pathways. Additionally, AFIR method was applied to various organic multi-components reactions. Several essential and unprecedented reaction pathways could be encountered automatically and efficiently

AFIR method^[142, 143] is ideally befitted for unbiased and systematic studies. All possible reaction mechanisms need to be carried on to resolve these crucial issues. Sometimes, they might involve to same molecules two or more times, and even concern to the reactant molecules in different order. For the simplest case in which A and B are single atoms, the constant artificial force can be employed as a linear function as shown in (Eq. 2.20)

$$F(r_{AB}) = E(r_{AB}) + \alpha r_{AB} \quad (\text{Eq. 2.20})$$

where the parameter α is the strength of the artificial force. **Figure 2.3** demonstrates the function of (Eq. 2.20) with several amounts of α . In case (a), there is no α added to the reaction. The reaction barrier obstructs the product X and the reagent region A + B. When the weak force is added as in case (b), a tight complex takes place before

the reaction barrier. However, the barrier will be vanished when a strong force is added as shown in case (c). The product X can be found by geometry minimization.

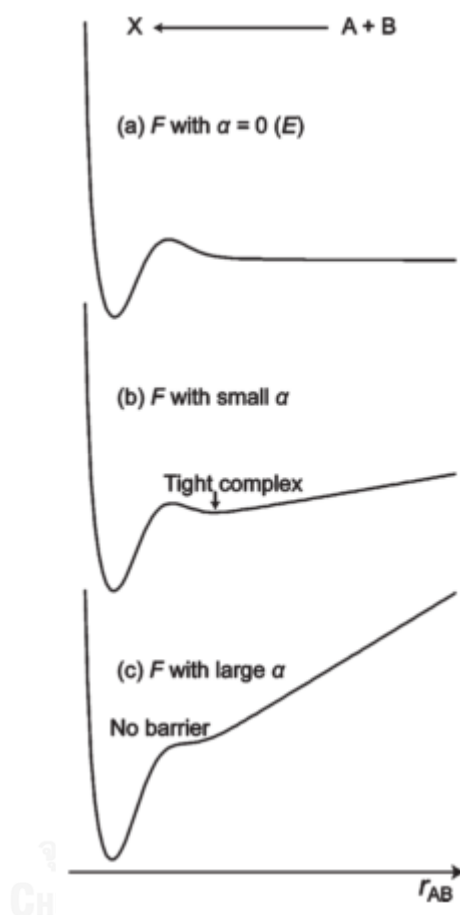


Figure 2.3 $F(Q)$ in (Eq. 2.20): (a) with $\alpha = 0$, (b) with small α and (c) with large α ^[143]

For general force term of AFIR function, a system with multiple degrees of freedom was designed. The best function was suggested to sum of isotropic functions centered at each atom. Thus, AFIR function was proposed as follows:

$$F(Q) = E(Q) + \alpha \frac{\sum_{i \in A} \sum_{j \in B} [(R_i + R_j)/r_{ij}]^p r_{ij}}{\sum_{i \in A} \sum_{j \in B} [(R_i + R_j)/r_{ij}]^p}$$

(Eq. 2.21)

where $E(Q)$ is the potential energy surface which concerned to atomic coordinates Q . The parameter p is weighting parameter, which was set to 6 for standard value.^[144] The r_{ij} is a distance between i^{th} and j^{th} atom of reagents.

The parameter α is given as follows:

$$\alpha = \frac{\gamma}{\left[2^{-\frac{1}{6}} - \left(1 + \sqrt{1 + \frac{\gamma}{\varepsilon}} \right)^{-\frac{1}{6}} \right] R_0}$$

(Eq. 2. 22)

Hence, γ represents model collision energy between any coupled molecules. In this thesis, the author will utilize γ instead of α . Furthermore, R_0 and ε will be set as the same as the argon cluster, which are 3.8164 Å and 1.0061 kJ mol⁻¹, respectively.^[145]

Then, all approximate transition states (TSs) and intermediates (local minima, LMs) of low-energy reaction pathways will be automatically searched. To obtain true TSs and LMs, these approximate stationary points will later be optimized without artificial force. Maeda *et al*^[145] has investigated the Passerini coupling approach and proposed that the reaction take place from the condensation between an aldehyde, an isocyanides and a carboxylic acid to form an α -acyloxy amide. This is in contrast to the common believed, which suggested that an additional carboxylic acid molecule is directly involved in the reaction and catalyzes the reaction.^[18, 19]

2.1.4 Solvation models

Most chemical reactions normally occur in solution. The normal practice to theoretically investigate the chemical reaction in solution phase is by the quantum mechanical calculations in combination with solvation effect. There are several theories for address solvent effects. The solvent effect could be classified as short-range and long-range. The short-range effect demonstrates that solvent molecules

have strong interaction, such as hydrogen bonding. The long-range effect is caused with the solutes by solvent polarization. To accommodate the solvent effect, two models, explicit and implicit, are imposed. In the explicit model, solvent molecules were added to the system. Normally, only those in the first solvation shell are added to save the computer time. However, this is only justified the short-range effect. To accommodate both short-range and long-range effects, more solvent molecules must be included and, hence, results in long computation time. Whereas, solvent is only viewed as dielectric media in the implicit solvent model. It is thus called the “continuum model”, where only the long-range effect or solvent polarization can be accounted for. In this section, only two solvation models, that was employed in this thesis i.e. Polarized-Continuum Model (PCM)^[119] and Reference Interaction Site Models (RISM)^[146] will be discussed.

2.1.4.1 Polarized Continuum Model (PCM)

Polarized Continuum Model (PCM) is one of the continuum models. The macroscopic media combined with fixed dielectric constant will be used instead of real solvent molecules. The electronic structure, which encircled by the dielectric medium, will be resolved in burrow of vacuum. The interaction of solvent polarization, reaction field, and solute molecules are stabilized. The solvation free energy is defined as follows.^[119, 146]

$$\Delta G_{solvation} = \Delta G_{cavity} + \Delta G_{dispersion} + \Delta G_{electrostatic}$$

(Eq. 2.23)

where $\Delta G_{solvation}$ is the solvation free energy, ΔG_{cavity} is the destabilization causing by cavity creation, $\Delta G_{dispersion}$ is the solute-solvent interaction, and $\Delta G_{electrostatic}$ is the electrostatic interaction of polarized medium and solute.

The surface potential V_{σ} is included to the Hamiltonian to incorporate the reaction field of solute-solvent interaction

$$H = H_0 + V_{\sigma} \quad (\text{Eq. 2.24})$$

where H_0 represents the vacuum state Hamiltonian.

The PCM can be used only for the system in which the interplay between solute and solvent is not very important, such as the reaction in aprotic solvents, for instance. Thus, it is not suitable to consider the reaction that has the short-range interaction.^[119]

2.1.4.2 Reference Interaction Site Model (RISM)

The reference interaction site model (RISM),^[147, 148] which is based on a theory in statistical mechanics for molecular liquid developed by Chandler *et al.*^[147], is an alternative for molecular dynamics simulation. In this theory, the radial distribution functions (rdfs) can be calculated analytically. This makes the statistical ensemble achievable at a proper computational cost. From the previous studies, the anomeric equilibrium of glucose and its derivative have been studied by RISM in aqueous solution.^[149, 150] Moreover, the Diels-Alder,^[151] S_N2 -type reaction,^[152] and S_N1 -type hydrolysis of cellobiose into two glucose in ILs^[109] have been successfully investigated by reference interaction site model self-consistent field model spatial electron density distribution (RISM-SCF-SEDD), which is the self-consistent combination of RISM and molecular orbital (MO) theory.

RISM can be summarized based on its advantages and manners as follows: 1) RISM concerns to an infinite number of solvent molecules. There is no need to define the 'simulation box' and it is free from statistical error. Also, thermodynamic ensemble provided is enough. 2) The computational cost is remarkably decreased

contrasted to method of standard molecular dynamics simulation, since an analytic expression for the solvent free energy is existed, 3) The inputs and outputs of the simulations are consistent with those computations.^[152, 153]

The new version of RISM, namely reference interaction site model self-consistent field model spatial electron density distribution (RISM-SCF-SEDD) was used in this dissertation since it is much more powerful in the interplay of molecular orbital and RISM calculation than the original RISM-SCF. In RISM-SCF-SEDD, the spatial electron density distribution was treated and the set of grid points are not demanded as these artificial parameters can be ignored.^[154]

In RISM-SCF-SEDD, the total energy of a system (ΔG) is defined as follows,^[154-156]

$$\Delta G = E_u + G_{\text{coor}} + \Delta\mu \quad (\text{Eq. 2.25})$$

E_u is the energy of the solute molecule from ab initio MO theory. G_{coor} is the thermal correction to the free energy. $\Delta\mu$ is solvation free energy given by^[156]

$$\Delta\mu = -\frac{\rho}{\beta} \sum_{\alpha s} \int d\mathbf{r} \left[c_{\alpha s}(r) - \frac{1}{2} h_{\alpha s}^2(r) \theta(-h_{\alpha s}(r)) + \frac{1}{2} h_{\alpha s}(r) c_{\alpha s}(r) \right] \quad (\text{Eq. 2.26})$$

where ρ is the number density and $\beta = 1/k_B T$. θ is the Heaviside step function. k_B is Boltzmann constant. T is the temperature in Kelvin. $h_{\alpha s}(r)$ and $c_{\alpha s}(r)$ are total and direct correlation functions, respectively between site α (in solute) and s (in solvent).^[157]

In case of hydrogen, for transition states of hydride transfer between carbon and oxygen, the Lennard-Jones distance parameter σ_{com}^H and well depth ϵ_{com}^H , were set as the arithmetic and geometric which related to CH and OH parameters,

$$\sigma_{com}^H = \frac{\sigma_{CH}^H + \sigma_{OH}^H}{2}$$

(Eq. 2.27)

$$\epsilon_{com}^H = \sqrt{\epsilon_{CH}^H \epsilon_{OH}^H}$$

(Eq. 2.28)

From the previous study^[109], the free energies (in water) are estimated by

$$\Delta G_{react}^{Solv} = \Delta G_{calc}^{Solv} \pm RT \ln[H_2O]$$

(Eq. 2.29)

where ΔG_{react}^{Solv} is free energy of the reaction. ΔG_{calc}^{Solv} is calculated free energy. R is the gas constant. $[H_2O]$ is the molar concentration of pure water. The symbol bases on the type of reaction which concerns to the molecules of water. For dehydration reaction the symbol is positive, while the symbol is negative for the hydration reaction.

CHAPTER III COMPUTATIONAL DETAILS

Methodologies and computational details for investigations of the Biginelli reaction and the glucose to 5-hydroxymethylfurfural transformation will be discussed in this chapter.

3.1 Biginelli reaction

Urea, benzaldehyde (BA), and ethyl acetoacetate (EAA) were used to model the three reactants in this study. The detailed multi component (MC)-AFIR calculation scheme is as follows. First, approximate local minimums (LMs) and transition states (TSs) for the first step between two components were explored extensively by the MC-AFIR method^[142, 143, 158] for all approached orientation and directions. In this case, $N_{\max} = 10$ and M06-2X/3-21G level of theory was used. Then, all the approximate LMs and TSs obtained by the initial MC-AFIR search were reoptimized at M06-2X/6-31+G(d) level without the AF. The AFIR functions were minimized with $\gamma = 200 \text{ kJ mol}^{-1}$ (suggests that pathways with a barrier of more than 50 kcal mol^{-1} will not be searched) starting from initial structures whose orientations and approach directions of two reactants were determined randomly. To examine the effect of the stabilization by other reactants, one or two reactants were coordinated to the reactive parts in the obtained TSs, and their structures were reoptimized at M06-2X/6-31+G(d).

Moreover, the AF was initially added to directly dehydrate the obtained bimolecular intermediates in step II: Dehydration step. Also, molecule of H_2O , EtOH, $\text{EtOH}+\text{EtOH}^+$ and urea were included as the catalyst. Herein, we manually added molecule of catalyst to the bimolecular intermediate in several ways for finding the complex with the lowest energy. To reduce the computational cost, we applied the AF ($\gamma = 200 \text{ kJ mol}^{-1}$) to the active part between an intermediate and catalyst to remove water molecule at M06-2X/6-31+G(d) level. After that, the approximate LMs and TSs were reoptimized at M06-2X/6-31+G(d) level without the AF. In this case,

simultaneous bond forming and breaking in the concerted processes are also examined. The AF was employed attractively (positive value of γ) between the atoms where a bond is intended to be formed and repulsively between the atoms where a bond is intended to be broken. These principles will be employed for the further steps as well.

In all the calculations, the solvation free energy was included by the polarized continuum model (PCM)^[146, 159, 160] with a dielectric constant of 24.852 for ethanol. In section 4.1.5, the obtained LMs and TSs along the most favorable pathway were reoptimized using the PCM with a dielectric constant of 2.3741 (toluene). Moreover, the effect of solvent proticity was also discussed by considering the explicit solvent molecule(s) in ethanol in case of the proton transfer steps. We reported the Gibbs free energy and the electronic energy with zero-point correction (ZPE, in parentheses) at 1 atm and 298.15 K. Here in, we would like to compare the different potential energy profiles with the same number of reagent molecules. Thus, we mainly use the Gibbs free energy.

After optimization of a TS, the intrinsic reaction coordinate (IRC)^[161, 162] was calculated from the TS to two LMs to confirm the reaction pathway. All these AFIR, reoptimization, and IRC calculations were performed by the Global Reaction Route Mapping (GRRM)^[163, 164] program using energies, first, and second energy derivatives computed by the Gaussian09^[165] program.

3.2 Glucose to 5-Hydroxymethylfurfural transformation

β -D-glucose molecule is used to model the starting pyranose structure of this study. For glucose isomerization step, two mechanisms, cyclic^[78-85] and open chain mechanism^[80, 86-91] were investigated. (See **Figure 1.4**). For the transformation of fructose into HMF, only cyclic mechanism were considered since Antal *et al.*^[78, 79] suggested that this process can take place without the ring opening. To find each TS, the interesting reaction coordinate is selected and varied as the energy profile. Each reaction coordinate will direct along the emphasized reaction step; hydration,

dehydration, protonation, and deprotonation. The highest point will be used to optimize for finding real TS. Geometries of LMs and TSs were optimized at B3LYP/6-31+G(d) level. The single-point CCSD(T)/aug-cc-pVDZ was carried out to re-evaluate those energies.

In all calculations, the solvation Gibbs free energy was included by RISM-SCF-SEDD. The Kovalenco-Hirata closure^[157] was used to solve the equation of RISM integral. The reactions were studied both in water (at 10 MPa, 473.15)^[166-168] and IL, the so-called 1-methyl-3-methylimidazolium ([MMIM]Cl) (at 1 atm, 373.15 K). The initial TS search was calculated at B3LYP/6-31+G(d) level in water. Then, all TSs and LMs obtained in water were re-optimized at B3LYP/6-31+G(d) in [MMIM]Cl. In water, values of 473.15 K, 10 MPa, 0.029114 molecules Å⁻³ were set for temperature (*T*), pressure (*P*), and number density (*ρ*), respectively. Likewise, values of 373.15 K, 1 atm, 0.005291 molecules Å⁻³ were set for *T*, *P* and *ρ* in [MMIM]Cl, respectively. Besides, the molar concentration of pure water is set to 55.5 M. **Table 3.1** shows the Lennard-Jones parameters of the solute.^[151, 169, 170] While, the Lennard-Jones parameters of the solvents, such as SPC-like water and [MMIM]Cl, are shown in Appendix. In this case, the diffuse functions of auxiliary basis functions for all atoms were removed so that the RISM-SCF-SEDD can rapidly converge during calculations of single point energy.^[171]

After optimization of TSs, the hessian was calculated to confirm the optimized TS whether it has only one imaginary frequency. All calculations were performed by a modified GAMESS program package.^[172]

Table 3.1 Lennard-Jones parameters of solutes

Site	$\sigma/\text{\AA}$	$\epsilon/\text{kcal mol}^{-1}$	References
C	3.500	0.066	[169]
O in C-O-C	2.900	0.140	[169]
H on C	2.500	0.030	[169]
H on O	1.000	0.056	[170]
H in O-H	3.166	0.155	[170]
H in C-H--O	1.750	0.041	See (Eq. 2.27) and (Eq. 2.28)
Cl in HCl	4.417	0.118	[151]
H in HCl	1.000	0.056	[170]

CHAPTER IV RESULTS AND DISCUSSIONS

In the following section, computational results of the Biginelli reaction and the glucose to 5-hydroxymethylfurfural transformation were discussed individually. In each reaction, all possible mechanisms were followed and then the most favorable mechanism was suggested. Moreover, the solvent effect and the involvement of additional reagents or solvent molecule were as well carefully examined.

4.1 Biginelli reaction

In this section, the three main routes will be considered separately: Route **A** begins with the reaction between the protonated urea and BA, Route **B** starts the reaction with the protonated urea and EAA, and Route **C** with the protonated EAA and BA. The reaction is composed of 4 steps; bond formation, and transformation.

4.1.1 Route A: Iminium Route

4.1.1.1 Step I: Initial bond formation

Firstly, the proton affinity of the reactants has been calculated. The initial protonation always arises on urea due to its highest proton affinity over the other reagents. (see **Figure S1** in Appendix).

The first step of the Route **A** is the reaction between protonated urea and BA. Three pathways (**A1-A3**) were obtained from the MC-AFIR calculations as shown in **Figure 4.1**. Among them, the C-O bond formation (**A2**) has the lowest activation Gibbs energy of $20.2 \text{ kcal mol}^{-1}$. The reactant complex (**A2-1**) obtained from IRC from **TS A2-2** is higher in energy than the complex (**A1-1**) despite of a lower proton affinity of BA than urea as proton affinity of BA and urea are 22.2 and 7.9, respectively. The second lowest pathway is the C-N bond formation (**A1**) whose activation free energy is only $0.6 \text{ kcal mol}^{-1}$ (**TS A1-2**) higher than that of **TS A2-2**. In pathway **A1**, IRC calculation demonstrated that the proton transfer from the urea

oxygen to the BA oxygen concertedly arises with the C-N bond formation between the BA carbonyl carbon and the urea amine group. The pathway **A3** is much higher in energy so it can be neglected.

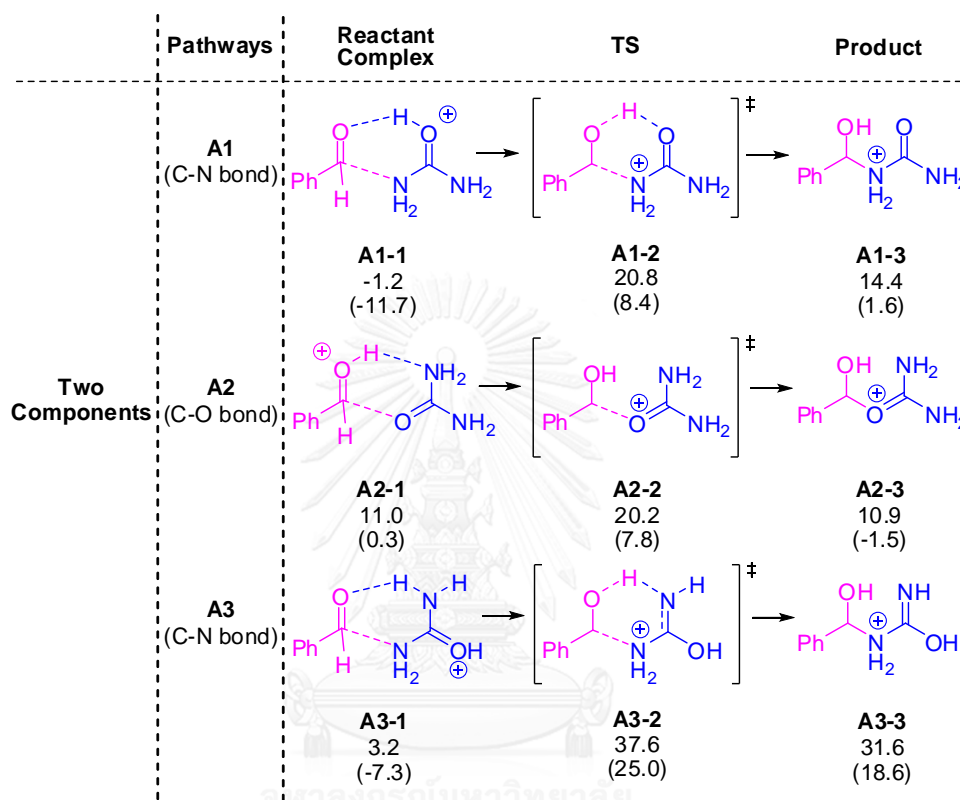
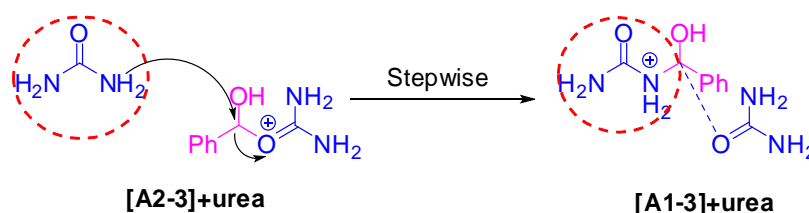


Figure 4.1 Intermediates and transition states between protonated urea and benzaldehyde (Step I in Route **A**). Gibbs free energies (1 atm, 298.15 K) (electronic energies with ZPE correction in parentheses), in kcal mol⁻¹ relative to the isolated reactant molecules, were obtained at the M06-2X/6-31+G(d) level in PCM ethanol.

However, to obtain the final product **DHP**, the C-N bond must be formed. Thus, the second urea addition to **A2-3** (the product of **A2-3**) was considered for the C-N bond formation pathway. (See **Scheme 4.1**) The AFIR search could not find the concerted process for the C-N bond formation of **A2-3** and the second urea. The reaction proceeds in stepwise process, where the C-O bond dissociation between the first urea and the BA initially occurred. It is followed by the C-N bond formation between the second urea and the BA. The lowest TS for this pathway is around 5.5

kcal mol⁻¹ higher than the TS of the direct C-N bond formation (**A1-2**). Therefore, the most reasonable reaction pathway for the first step of the Route **A** is the direct C-N bond formation (**A1**) from the resting stage (**A1-1**) of the reactant complex, even though the TS of the C-O bond formation has the lower energy.



Scheme 4.1 Proposed catalytic process with a second urea (in red circle)

In addition, three- and four-component step were also examined to investigate the possible involvement of additional components in this reaction. **Figure 4.2** shows the most stable conformations for each pathway. Other less stable conformations are shown in **Figure S3** and **Figure S4** in the Appendix. For three components step, an extra urea, a BA, and an EAA were added to the LMs and TS in the pathway **A1** denoted pathway **A1U**, **A1Z** and **A1E**, respectively. With the BA or EAA as a third partner (**A1Z** and **A1E**), the resulting TS structures are significantly similar to the ones without an extra component as it just stabilizes the acidic proton on the BA. Remarkably, the activation energy for the C-N bond formation is lowered by the extra urea as displayed in pathway **A1U**. The barrier difference between **A1** and **A1U** is 5.3 kcal mol⁻¹. In **A1U** pathway, the additional urea is protonated and it donates a proton to BA, whereas a proton is donated from the reactant (protonated urea) directly in **A1**. This increases the nucleophilicity of the urea and electrophilicity of the BA involved in the C-N bond formation. The main difference between pathway **A1** and pathway **A1U** is the position of the proton. the proton was bonded to the reacting urea in **A1**, but it moved to reside at the additional urea in the **A1U**. This make C-N bond formation becomes more nucleophilic compared to pathway **A1**. Also, the hydrogen-bonding with the extra protonated urea stabilizes the system and can explain the stabilization of the TS. In other three component reaction pathways

A1Z and **A1E**, the additional protonated BA and EAA stabilize the proton on the reactant BA, respectively. Thus, we can say that an extra urea catalyzes this step of Biginelli reaction. This is in good agreement with the observation that the excess urea was often used for this reaction.^[173, 174]

To consider other stabilization effects, the four-component step (**A1UE**) was also investigated. This was done by adding an EAA to the LMs and TS in pathway **A1U**, because EAA would react with the C-N bond formed product in the following step. We found that the barriers of **A1U** and **A1UE** are similar because the EAA just stabilizes a proton on nitrogen and does not involve in the reaction. In addition, adding a third urea (**A1UU**) and a second BA (**A1UZ**) in the four-component step were also considered. Their role is similar to the additional of EAA in **A1UE**. The barrier difference for **A1U** is very small. Therefore, we can summarize that the fourth component does not directly involve in the reaction.

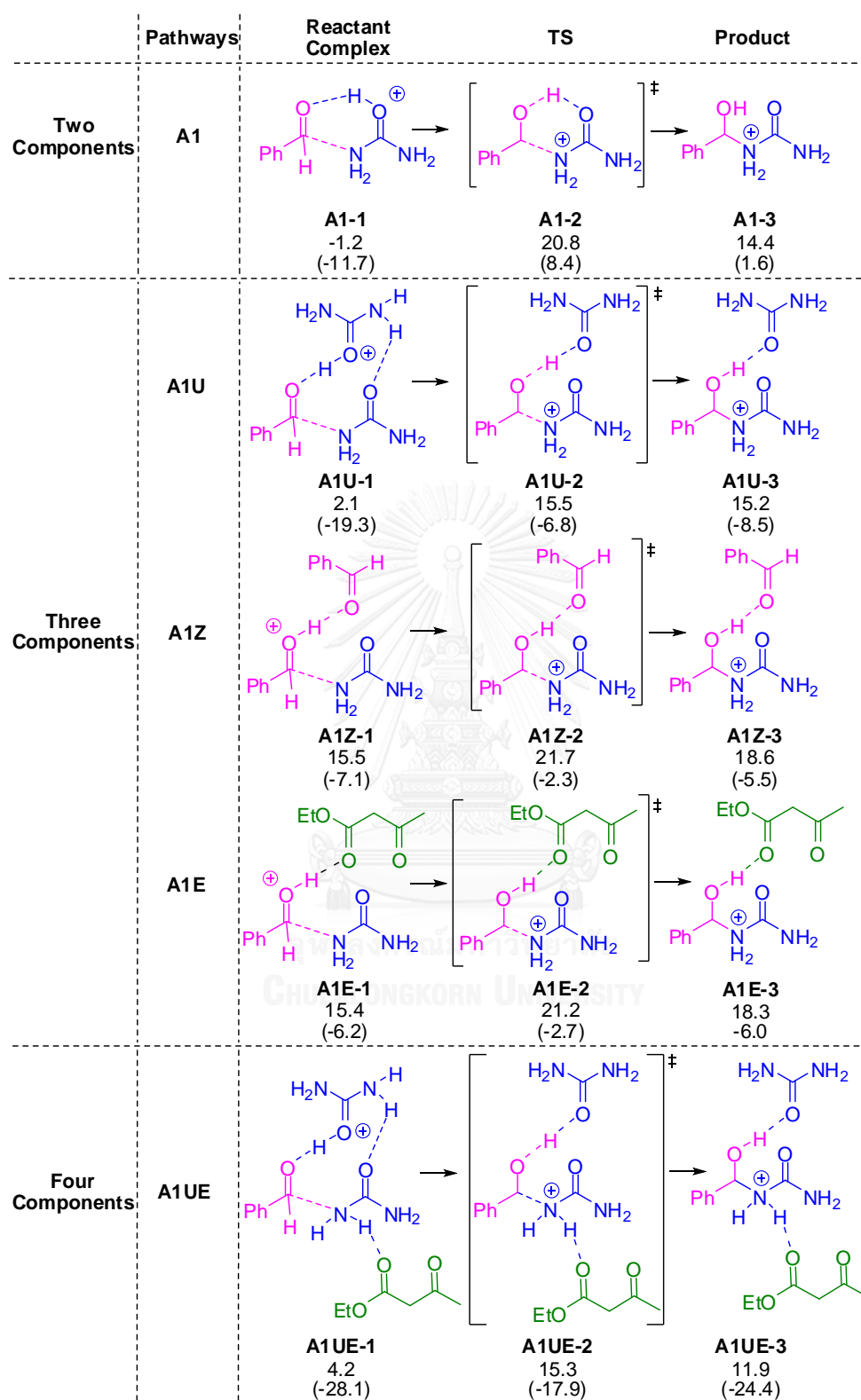


Figure 4.2 Two-, three- and four-component Step I (C-N bond formation) for Route A. See Figure 4.1 for computational details.

4.1.1.2 Step II: Dehydration

Since the iminium **A1-3** has been observed in ESI-MS.^[64] The following dehydration step will begin with an intermediate **A1-3**. The AFIR search showed that the dehydration step of **A1-3** cannot arise without any catalysts. Thus, to dehydrate an intermediate **A1-3**, several possible catalysts (in case of protic molecules) such as water, one and two ethanol molecules were studied. The detail mechanisms in each case were proposed and the activation energy differences for utilizing each catalyst were also calculated. Using water and EtOH as catalysts the reaction requires respectively 6.5, 4.1 and 3.9 kcal mol⁻¹ of activation energy higher than using urea. We found that the urea-catalyzed pathway is the most favorable pathways as shown in the Step IIA-IIB (**Figure 4.3**). The extra urea could catalyze this pathway by acting as a proton agent and the reaction is stepwise. An EAA was added to this pathway for making it consistent to the whole reaction. Despite the only mission it of is solvent, the barrier with and without an EAA were not significantly different. In this step, the reaction starts from the **A1UE-3'**, which is the most stable conformer of the intermediate from Step I. The proton was transferred from the tertiary nitrogen of the reacted urea to the extra urea carbonyl oxygen (Step IIA). A very low barrier was required for the intermediate **A1UE-5**. The reaction goes over the TS **A1UE-6** leading to the iminium ion **A1UE-7** (Step IIB) which coordinated with the water, EAA and urea products. Therefore, the extra urea catalyzes the dehydration step as well as Step I.

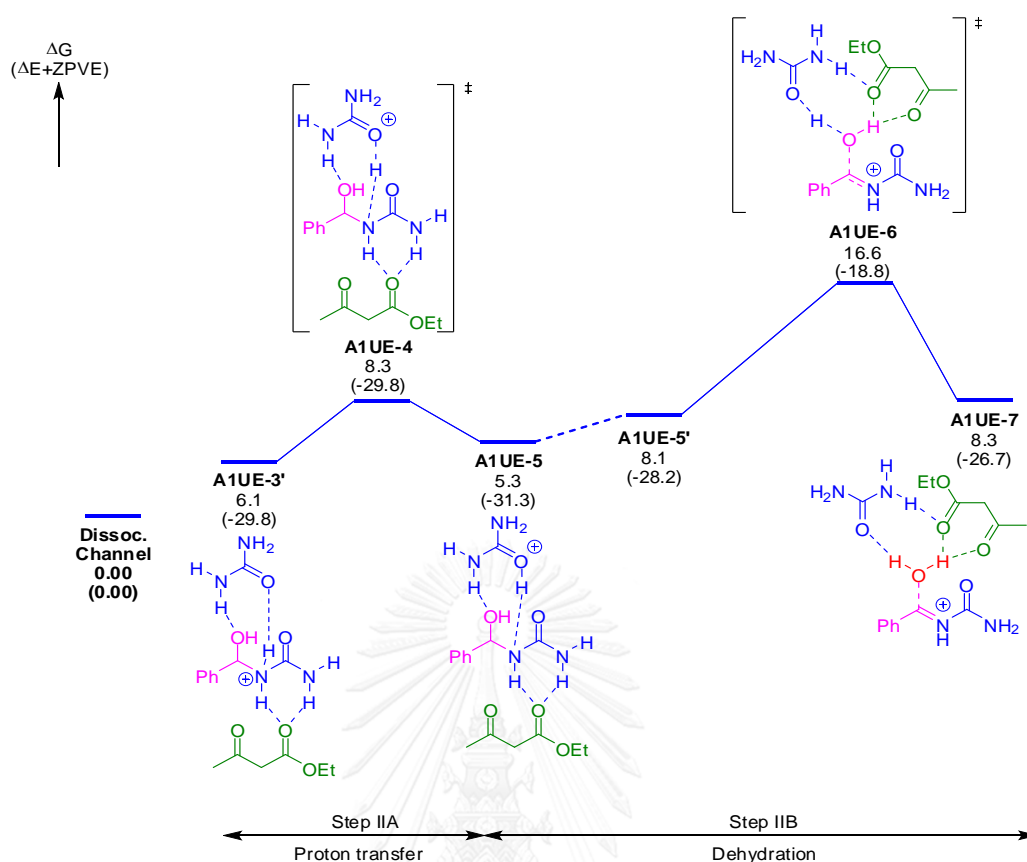


Figure 4.3 The most favorable pathways of Step II (Route A). See **Figure 4.1** for computational details. The straight dashed line shows intermediates that are not connected by IRC.

4.1.1.3 Step III: Condensation

Following the dehydration step, the condensation of the intermediate **A1-4** (**Figure S6**) and EAA was investigated. Regularly, an EAA can tautomerize between diketo and enol form in solution as displayed in **Figure 4.4**. In spite of the fact that the enol form of EAA molecule is less stable than the diketo form in equilibrium (~ 4 kcal mol⁻¹), the reaction is eventually preceded by an enolic EAA which forming a C-C bond with **A1-4** to yield an intermediate **A1UE-9** leading to **A1UE-11** (**Figure 4.5**). This is in good agreement with the experiment. Since the reaction efficiency is proportional to the diketo-enol tautomerization equilibrium constant (K_T).^[65]

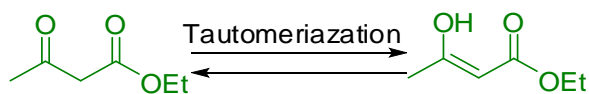


Figure 4.4 Diketo-enol tautomerization of an ethyl acetoacetate.

Furthermore, we found that urea also involved as a proton mediator in the mechanism of this step. Pathways for step III (Condensation with the third partner) with and without the extra urea were shown in **Figure S7** in Appendix. The initial barrier of $19.9 \text{ kcal mol}^{-1}$ (**A1E-10**) is taken down by $18.0 \text{ kcal mol}^{-1}$ owing to the affiliation of the extra urea in four components step (**A1UE10**). Even though, this would be only $1.9 \text{ kcal mol}^{-1}$ lower than the TS without an additional urea, the product of this step is stabilized by the extra urea. To sum up, while the second urea is not directly involved in the condensation step, it stabilizes the resulting intermediate by $12.5 \text{ kcal mol}^{-1}$ because it acts as a strong proton acceptor from the EAA fragment.

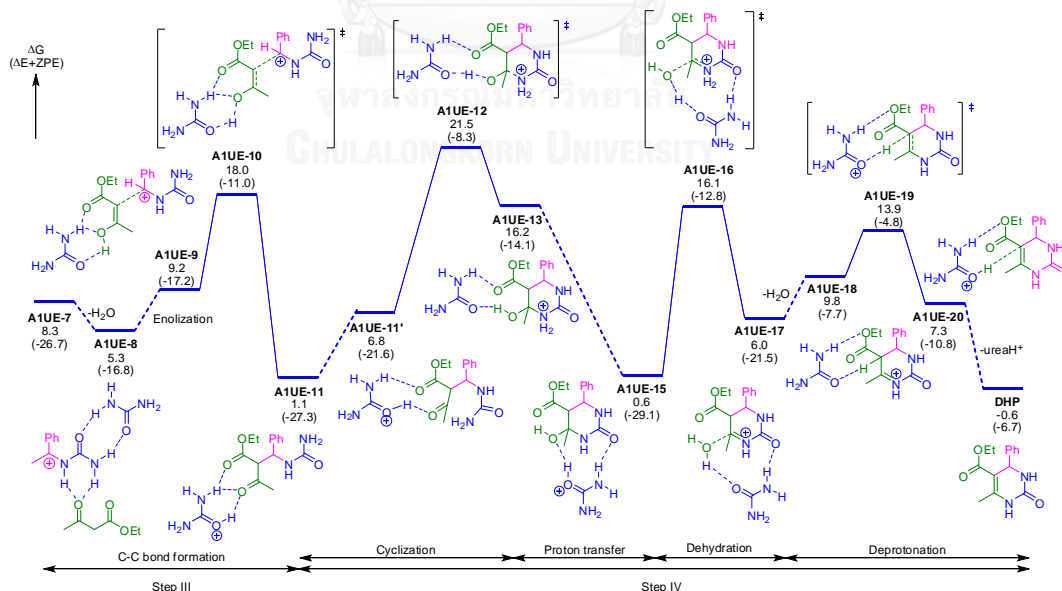


Figure 4.5 The most favorable pathways of Step III and IV (Route A) starting from **A1UE-7** to **DHP**. See **Figure 4.1** for computational details. The straight dashed line shows intermediates that are not connected by IRC.

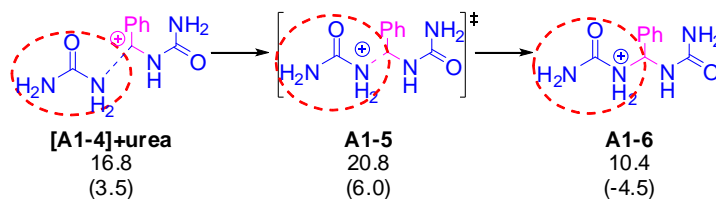


Figure 4.6 C-N bond formation leading to diurea derivative (**A1-6**). See **Figure 4.1** for computational details.

Based on the fact that most experiments often used excess urea and the reactions seem to depend on the use of urea.^[14, 15, 60, 61, 173-175] An optional reaction pathway including the second urea was considered. The authors also investigated the biureide-based reaction pathway leading to **A1E-11**. According to ESI-MS analyses,^[64] a diurea derivative **A1-6**, which results in a BA and two urea molecules has been monitored. We found that a biureide intermediate **A1-6** itself and its formation TS (**A1-5**) were not too high in term of free energy (10.4 and 20.8 kcal mol⁻¹, respectively). Consequently, it was not astonished that ESI-MS could observe this intermediate. Nevertheless, to form **A1E-11**, the reaction required huge energy around 36.7 kcal mol⁻¹ in term of free energy to overcome the barrier. This is too high when compared to **A1UE-10**, which demonstrated that the biureide-based pathway is not satisfactory. Therefore, the final product **DHP** cannot be formed from **A1-6**, even though the formation of an intermediate **A1-6** is ergodically possible. This suggests that the reaction that passing through a diurea derivative (**A1-6**) cannot transform to the final product **DHP** without going back to **A1-4**. Thus, the more preferable pathway is the direct condensation between the dehydrated intermediate to the enolic form of EAA promoted by an extra urea (**A1UE-10**).

4.1.1.4 Step IV: Transformation into **DHP**

The transformation into **DHP** starting from **A1UE-11** consists of many substeps as shown in **Figure 4.5**. Cyclization firstly takes place that is followed by proton transfer from the second urea to the enol part. Then, the dehydration and deprotonation by the extra urea bring about the final product **DHP**. The rate determining step (RDS) of

Route **A** is the cyclization step (**A1UE-12**), since it has the highest barrier is the 21.5 kcal mol⁻¹. The RDS of this route is different from the previous study which proposed that the RDS is the condensation step.^[64] Until recently, there is no study that finely determined every steps of the reaction in details including the cyclization step for the three main routes. Most of the reports just only focused on C-N (step I) and C-C (step III) bond formation.

Besides, the pathway of step IV with EtOH as a catalyst was investigated. The RDS is also the cyclization step (**[A1E-12]+EtOH**) but its barrier of 28.2 kcal mol⁻¹ can be lowered by 23.7 kcal mol⁻¹ when removing EtOH. Therefore, step IV which using EtOH is not pleasing. In this case, the extra urea can reduce the barrier heights dramatically in every substeps of this pathway. For the cyclization step, without any catalyst the barrier is changed from 28.2 kcal mol⁻¹ and 23.7 kcal mol⁻¹, respectively, to only 21.5 kcal mol⁻¹. This demonstrates that the cyclization step, **A1UE-12** is modestly stabilized by an additional urea (**Figure 4.5**), as the cyclization TS with the second urea, **A1UE-12**, is 2.2 kcal mol⁻¹ lower than that of **A1E-12**. Likewise, the second urea is utilized to accomplish the proton transfer and dehydration steps. Moreover, the concerted pathway starting from **A1UE-12'** leading to **A1UE-15** has been examined during AFIR search but it requires a 1.7 kcal mol⁻¹ higher than the stepwise pathway. As already mentioned, an extra urea can act as better proton donor during proton transfer and dehydration steps than water and ethanol. The TS for dehydration with ethanol molecule (**A1E-16+EtOH**) is 4.7 kcal mol⁻¹ less stable than that with an extra urea (**A1UE-16**). As the results, we can ascribe that the additional urea catalyzes Step IV.

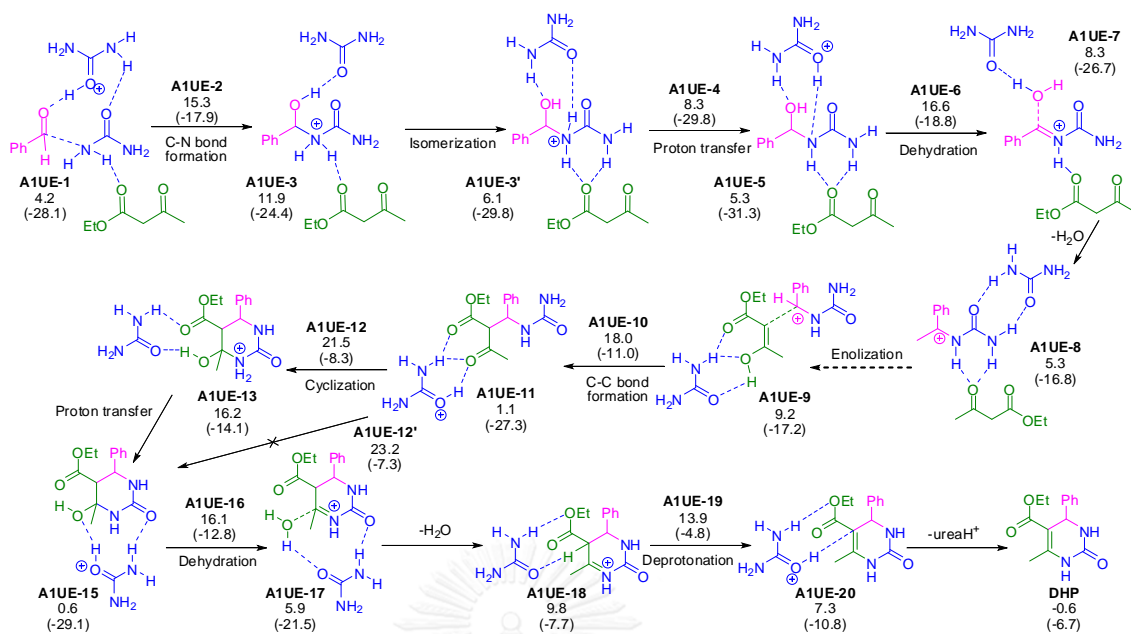


Figure 4.7 The best overall pathway for Route A. See **Figure 4.1** for computational details.

4.1.1.5 Overall pathway in Route A

Nearly all the steps along the Route A were catalyzed by an extra urea. This can explain why an excess of urea is often used experimentally.^[14, 15, 60, 61, 173-175] Urea directly involves in this reaction as an proficient organocatalyst. The result agrees with the experiment that the proticity and polarity of the solvent are not critical.^[65] Furthermore, the RDS of this route is the cyclization step. Because the final product (DHP) is not soluble, ΔG_r becomes very small for the reaction. Consequently, the reaction will be discussed as irreversible. Also, the higher TS structure (A1UE-12) is investigated as the rate-determining step. Nevertheless, the tautomerization of the β -keto ester into the enol needs to occur before this step, which is followed by the C-C bond formation. This pathway is consistent with experimental fact that an enolization of the β -keto ester has impact to the efficiency of this reaction.^[65]

To investigate the electronic effects of the aryl group of the aldehyde, an electron withdrawing group (EWG, -NO₂) or an electron donating group (EDG, -OMe) in

para position of the benzaldehyde have been added in all three pathways (See **Table S2** in Appendix). The RDS barriers are similar regardless of the substituents. Therefore, the influence of the aryl ring substitution of the aldehyde is very small. This is also consistent with the experimental results.^[65]

4.1.2 Route B: Enamine Route

For Route **B**, an urea and an EAA were employed for initial condensation and each reagent was protonated alternatively. MC-AFIR was utilized to search all possible pathways of bimolecular system. At each step of the reaction, the additional reagents have been determined to insure the obtained best pathway. All AFIR pathways are shown in **Figure S11-Figure S14** and **Table S3** in Appendix. The most favorable pathway in terms of the free energy of the transition state is C-O bond formation between these two reagents (**B2**). However, C-N bond was required to produce **DHP**. The urea and BA were added to **B1-3** to form C-N bond based on enamine- and iminium-like reaction. (**Figure S11**) Like those of Route **A**, they cannot occur with the lower barrier than that of pathway **B1**. The reaction preceded stepwise. Consequently, the most reasonable pathway obtained by MC-AFIR search is eventually pathway **B1**.

The best pathway with four components for Route **B** at the M06-2x/6-31+G(d) level was demonstrated in **Figure 4.8**. To be consistent with the whole reaction, the extra urea and BA were added to pathway **B1**. We found that the extra urea similarly involved in the reactions as a proton donor and proton acceptor, while a BA has only solvent role similar to route A. An extra urea and BA were utilized to stabilize the lowest pathway for the initial C-N bond formation, whose energy of the TS, **B1UZ-2**, is $14.8 \text{ kcal mol}^{-1}$. Then, the intermediate **B1UZ-3** is dehydrated in a two-steps process which promoted by the second urea as well.

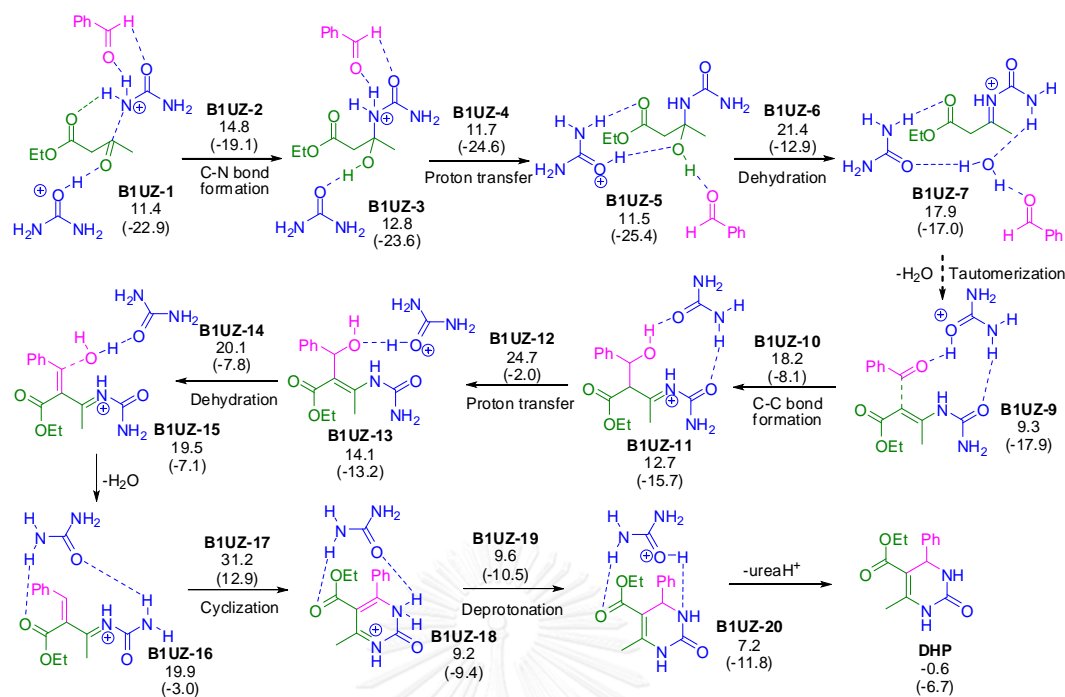


Figure 4.8 The best pathway for Route B. See **Figure 4.1** for computational details.

As shown in **Figure S13** and **Table S3** in Appendix, the energy of the TS (21.4 kcal mol⁻¹) is lower than the same step that catalyzed by other components. For dehydration step, several catalysts H₂O, EtOH, EtOH+EtOHH⁺ and urea, have been considered. The barrier differences for utilizing each catalyst were also calculated. We found that the dehydration assisted by urea is the most favorable pathway due to the entropy effect, the barrier of the dehydration assisted by urea and BA is 1.7 kcal mol⁻¹ higher than that using only urea in term of free energy but lower by 7.6 kcal mol⁻¹ for energies with ZPE correction. As the results, the dehydration step with four components is considered since it is consistent and facile when compare the whole reaction.

Pathways for step III (Condensed with the third partner) with and without the extra urea were displayed in **Figure S14**. To precede this step, an intermediate **B1-4** must be tautomerized into enolic form. The initial barrier of 26.9 kcal mol⁻¹ (**B1Z-10**) was lowered by 18.2 kcal mol⁻¹ with the participation of the extra urea in the four components step (**B1UZ-10**). After that, this resulting intermediate is tautomerized to

the enamine **B1UZ-9**, followed by the C-C bond formation, which takes place with $18.2 \text{ kcal mol}^{-1}$ activation barrier leading to **B1UZ-11**. Transformation into **DHP** starting from **B1UZ-11** initially commenced with proton transfer followed by dehydration, cyclization and deprotonation, respectively. (**Figure 4.8**) The second urea activates the BA during this process. The activation energy without the extra urea is $8.7 \text{ kcal mol}^{-1}$ higher. The successive dehydration step is supported by an extra urea to form **B1UZ-16**. Like those in Route **A**, the RDS of Route **B** is the cyclization step (**B1UZ-17**) with the barrier of $31.2 \text{ kcal mol}^{-1}$. To promote the cyclization step, several catalysts and conformations were examined. The lowest transition state structure concerned to an extra urea was shown in **Figure 4.8**. To provide **B1UZ-18**, the nucleophilicity of the nitrogen involved in the C-N bond formation was increased by an additional urea. Lastly, the anticipated product, **DHP** can be acquired.

Moreover, the pathway of step IV using EtOH as a catalyst was examined. (**Figure S15**) The RDS is also at cyclization steps (**[B1Z-17]+EtOH**). Its barrier of $38.2 \text{ kcal mol}^{-1}$ can be decreased by $33.4 \text{ kcal mol}^{-1}$ by removing EtOH. Thus, step IV with using EtOH was not satisfactory. Herein, the extra urea can also change the barrier heights dramatically, for cyclization process with and without catalyst, i.e. from 38.2 and $33.4 \text{ kcal mol}^{-1}$, respectively, to only $31.2 \text{ kcal mol}^{-1}$.

4.1.3 Route C: Knoevenagel Route

For Route **C**, a BA and an EAA were handled for the first condensation. All possible pathways of bimolecular system were searched by MC-AFIR and summarized in Appendix. In the same way to Route **A** and **B**, the most favorable pathways in terms of the free energy of the transition state was C-O bond formation (**C2**). In this case, C-C bond must be form to produce the product **DHP** but the barrier of C-C bond formation (**C1-2**) is much higher than C-N bond formation in Route **A** (**A1-2**) and Route **B** (**B1-2**). Despite the C-C bond formation between BA and an EAA was not satisfactory, the urea was added to **C2-3** based on enamine- and

iminium-like reaction. The obtained barrier is much higher than that of pathway **A1** and **B1**. However, we already knew that the extra urea can act as proton donor and acceptor and it was added to pathway **C1**. With a similar approach to the one used in route **A** and **B**, the best path with four components for Route **C** at the M06-2x/6-31+G(d) level was demonstrated in **Figure 4.9**. To be consistent with the whole reaction, two molecules of urea were added to pathway **C1**. We found that the first urea can catalyze pathway **C1** while the second urea only act as a solvent. The two molecules of urea can change the barrier heights dramatically, i.e. from 27.3 to only 23.4 kcal mol⁻¹. This suggests that the most favorable four-component pathway directing to the C-C bond formation step is passing through TS **C1UU-2**, with a 23.4 kcal mol⁻¹ activation barrier. As results, Route **C** is still challenged.

For dehydration step, several catalysts such as H₂O, EtOH, EtOH+EtOHH⁺ and urea have been considered. Activation energy differences for utilizing each catalyst were also discussed. We found the dehydration assisting by urea is the most favorable pathways among others. The energy of the reaction is raised when the solvent molecules (EtOH) or two urea molecules are employed. The barrier of dehydration assisting by two molecules of urea is 2.4 kcal mol⁻¹ higher than that by only one urea for free energy but is lower by 10.8 kcal mol⁻¹ for energy with ZPE correction. This is due to entropy effects similar to Route **B**. Herein; the dehydration step with four components is showed.

Based on whole mechanism of Route **C**, the RDS is the dehydration of step II (**C1UU-6**) with barrier height around 28.0 kcal mol⁻¹. The RDS of this route is totally different from that of Route **A** and Route **B**. (See **Figure 4.9**) In this case, a concerted pathway starting from **C1UU-5** to **C1UU-9**, which is through TS **C1UU-6'** was investigated, but the higher barrier (32.8 kcal mol⁻¹) was observed.

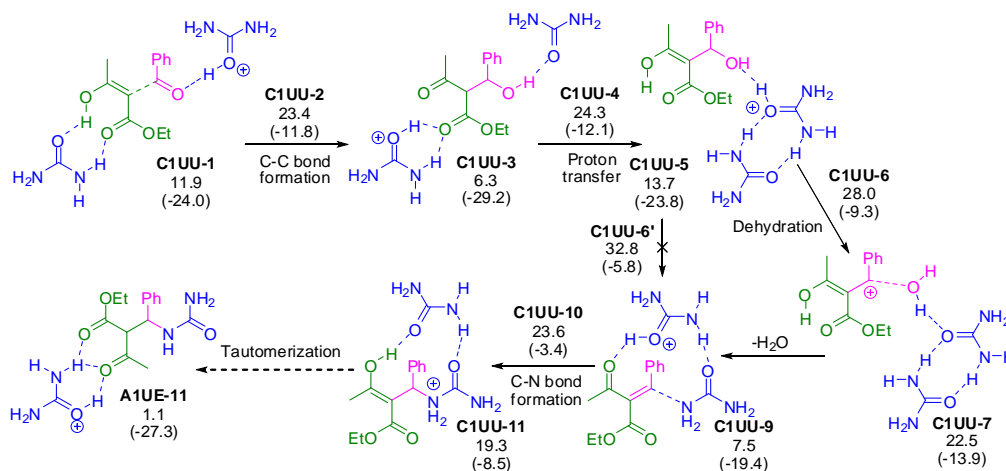


Figure 4.9 The best pathway for Route C (Step I-IV) leading to A1UE-11. See Figure 4.1 for computational details.

Pathways for step III (Condensation with the third partner) with and without the extra urea were displayed in Figure S20 in Appendix. The barrier of $31.8 \text{ kcal mol}^{-1}$ (C1U-10) was lowered by $23.6 \text{ kcal mol}^{-1}$ by the participation of the extra urea in four-component step (C1UU-10). We found that the resulting intermediate C1UU-11 can tautomerize to A1UE-11. It is a common intermediate with Route A, thus the following step, the cyclization and dehydration steps, were already regarded in section 4.1.1.

4.1.4 Comparison among all routes

The AFIR method has been applied to investigate reaction mechanism of Biginelli reaction based on three previously proposed mechanisms (routes): Route A (Iminium Route), Route B (Enamine Route), and Route C (Knoevenagel Route). No new route was discovered. However, the association of the extra urea was found to be the key to lower the activation barriers for nearly all the steps. The most favorable four-component pathways for Routes A, B, and C were demonstrated in Figure 4.7, Figure 4.8, and Figure 4.9, respectively. Also, they all are united and compared systematically in Figure S21 in the Appendix. As the two first steps, Route A and B are competitive. One can remark that the dehydration step of an

intermediate **B1UZ-3** is much higher than that in Route **A**, while Route **B** has the lowest TS in term of free energy for this first step. The RDS, which is the highest point on the reaction mechanism, was recapitulated in **Table 4.1**. For Route **B** and Route **C**, the reaction barrier is 6.5 and 9.7 kcal mol⁻¹ higher than that of Route **A**, respectively. It is noteworthy to mention that the RDSs are different from those proposed in the previous studies. In this research, we can mention that the lowest reactant complex is conjoint for all the routes **A**, **B**, and **C**. Consequently, we can consider about the rate relied on ΔG^\ddagger of the TSs.

Table 4.1 The energies (in kcal mol⁻¹) of the transition states of the rate-determining step for the different routes.

Route: Rate-Determining Step	ΔG^\ddagger
Route A : Cyclization/C-N bond formation (A1UE-12)	21.5
Route B : Cyclization/C-N bond formation (B1UZ-17)	31.2
Route C : Dehydration step/C-O bond breaking (C1UU-6)	28.0

4.1.5 Solvent effects

As already referred to the previous studied, the protic and aprotic solvents provided the similar yield, disrespect to their different polarity and proticity.^[65] As discussed in the previous section, while the solvent molecule such as EtOH does not directly involved in the reaction, urea is more significant for overall proton transfers. The optimized pathways from all three main routes were re-optimized in toluene to ensure that the similar mechanism can proceed in both protic and aprotic solvent. (See **Figure S22-Figure S24** and **Table S5**). The intermediates and TS structures obtained in ethanol are similar to the ones obtained in toluene. In this case, we can also considered about the rate determining step based on ΔG^\ddagger of the TSs, since the lowest reactant is the same for all the Routes **A**, **B**, and **C**. Route **A** is the best pathway. Route **B** and **C** is 9.6 and 1.8 kcal mol⁻¹ higher in energy than Route **A**,

respectively. Although, different from proposed in solvent ethanol C-N bond formation (step III) becomes the RDS of Route **C**, the RDSs still related to the cyclization step for Routes **A** and **B**. Thus, the conclusion remains the same. Therefore, reaction behaves in protic and aprotic solvent in the same way. Since the minimum energetic pathway (especially in the dehydration steps) does not concerned to the proticity of the solvent. The barrier of 21.5 kcal mol⁻¹ calculated in ethanol for Route **A**, is close to 22.0 kcal mol⁻¹ calculated in toluene. This result is in good agreement with the experimental results^[65] and it can be summarized that a similar mechanism is followed in protic and aprotic solvent.

4.2 Glucose to 5-Hydroxymethylfurfural transformation

First, the isomerization of glucose (**Glu**) to fructose (**Fruc**) through the cyclic and open chain mechanism was studied. Then, the fructose dehydration leading to HMF was investigated. The whole mechanisms of glucose transformation leading to HMF including essential transition states and intermediates were shown in **Figure 1.3**.

4.2.1 Glucose isomerization into Fructose

4.2.1.1 Cyclic mechanism

The intramolecular hydrogen bonding of **GLU** was found to be dominant in gas phase. The bond distances between atoms in water are almost the same with those in IL phase, but the orientation of some groups are different. **Figure 4.10** displayed optimized geometries of acid-catalyzed glucose isomerization in ILs, the so-called 1-methyl-3-methylimidazolium ([MMIM]Cl), following cyclic mechanism. The cyclic mechanism is started by protonation on the O2 site of **Glu** to form **Cy1**. After protonation, the hydroxyl group becomes a good leaving group, which leads the bond formation between C2 and ether oxygen atom, producing furanose ring and a water molecule. The bond distance between C2-O2 is elongated from 1.421 Å to 1.506 Å. Interestingly, the bond distance between C2 and an ether oxygen atom O5 is decreased (1.771 Å), while C2-O2 bond is increased (2.319 Å). As a result, the bond

between C2 and ether oxygen atom (O5) was formed. Due to the sp^2 character of structure **Cy2**, high energies were demanded for the direct rotations along the C1-OH. Thus, this drives to form structure **Cy3** by deprotonation at O1-H group.^[118] The torsion angle (O5-C2-C1-O1) of **Cy3** changes from 123.73 to 7.89 (for **Cy4**) due to rotation of the molecule, followed by protonation at O1 site leading to **Cy5**. Then, $TS_{Cy5-Cy6}$ confirms the hydride-shift (**Cy5**→**Cy6**) between carbocation C2 and C1. The bond distances between H atom, C1 and C2 become C1-H=1.38 Å and C2-H=1.34 Å. To form **Cy7**, carbocation C2 of **Cy6** is added a water molecule, followed by deprotonation of protonated fructose **Cy7** at O2 site to produce **Fruc**.

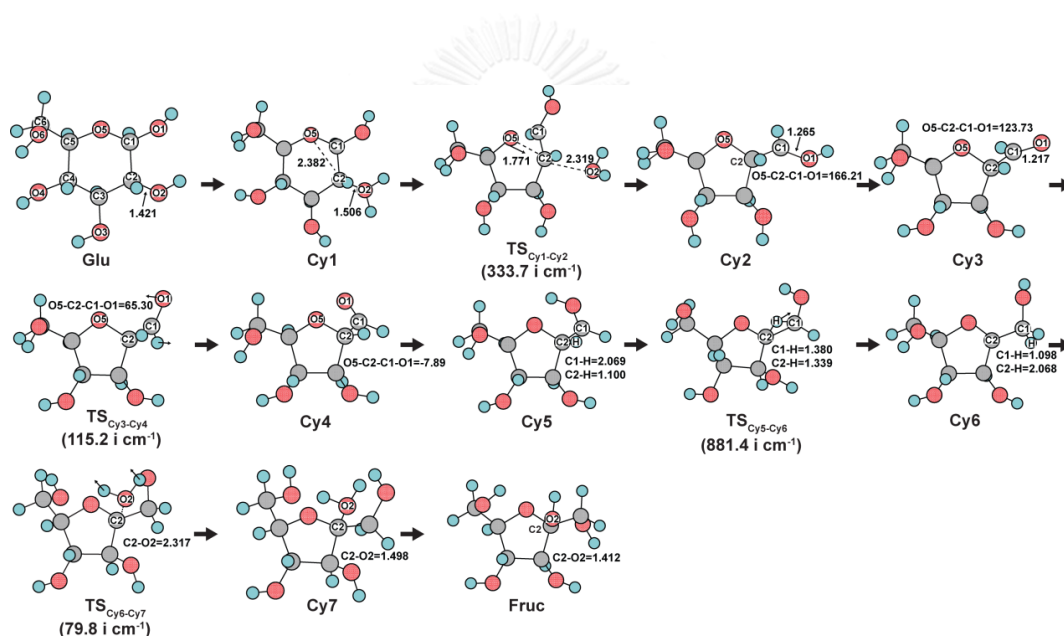


Figure 4.10 Optimized geometries of the intermediates during the glucose isomerization into fructose via cyclic mechanism in [MMIM]Cl (1 atm, 353.15 K.). The selected bond lengths and angles are given in unit of Angstrom and degree respectively. The labels for carbon and oxygen atoms are given for glucose and the important sites for each intermediate.

4.2.1.2 Open chain mechanism

The optimized geometries structures of acid-catalyzed glucose isomerization in [MMIM]Cl following open chain mechanism were shown in **Figure 4.11**. We found that the intramolecular hydrogen bonding is dominant in gas phase. The distance between atom almost same but the orientation of some groups are different. Likewise, the reaction mechanisms via open-chain mechanism was similar in water and [MMIM]Cl. Even so, the acid and base of reaction in water are H_3O^+ and H_2O , but HCl and Cl anion in [MMIM]Cl. The protonation of the ether oxygen atom in **Glu** was firstly initiated, followed by deprotonation at the O1 group, leading to the aldose form of glucose (**Op2**). Since the direct bond breaking between C1 and O5 requires high energy around 25 kcal mol^{-1} to overcome barrier,^[117] deprotonation reaction needs to occur. The bond distance of C1-O5 in **Op1** and **Op2** enlarges from 1.602 \AA to 2.618 \AA . **Op2** can lead to **Op3** by some rotations along C-C bonds, which totally looks like a chain. Due to these rotations, the bond between O5 and C1 is elongated to 5.351 \AA . **Op4'** results in the complex between **Op3** and HCl in [MMIM]Cl with the O1-H distance is 1.622 \AA . The structure **Op4'** is sequentially deprotonated and protonated leading to **Op5** and **Op6'**. In this case, C2 in **Op4'** is deprotonated by the chloride anion. Then, the double bond between C1 and C2 in **Op5** is formed with 1.338 \AA bond distance. The complex **Op6'**, with the distance between H and Cl of 1.704 \AA , is generated from **TS_{Op5-Op6}**, which is the reaction of proton transfer between the HCl and C1. Additionally, to close the chain, the bond distance between C2 and O5 in **Op8** becomes shorter to 3.07 \AA . To obtain **Op9**, which is fructose protonated at oxygen atoms of ether linkage, the carbonyl group of the ketone (O2) is protonated. Eventually, O5 site of **Op9** is deprotonate to manufacture **Fruc**.

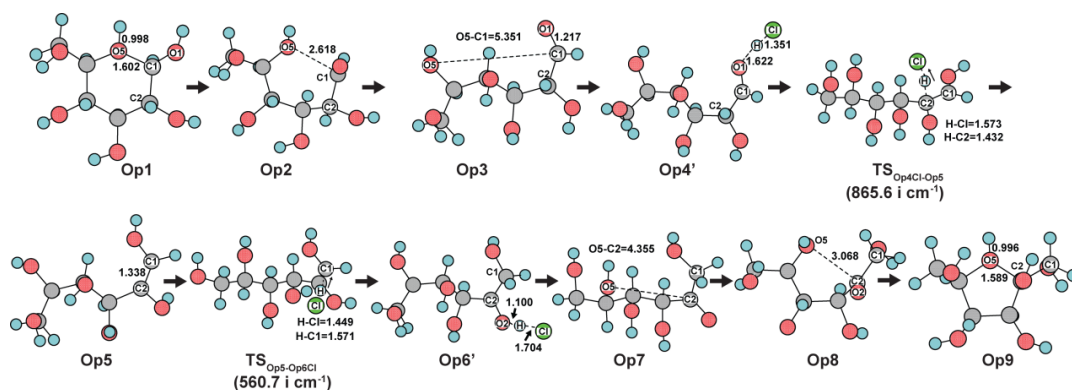


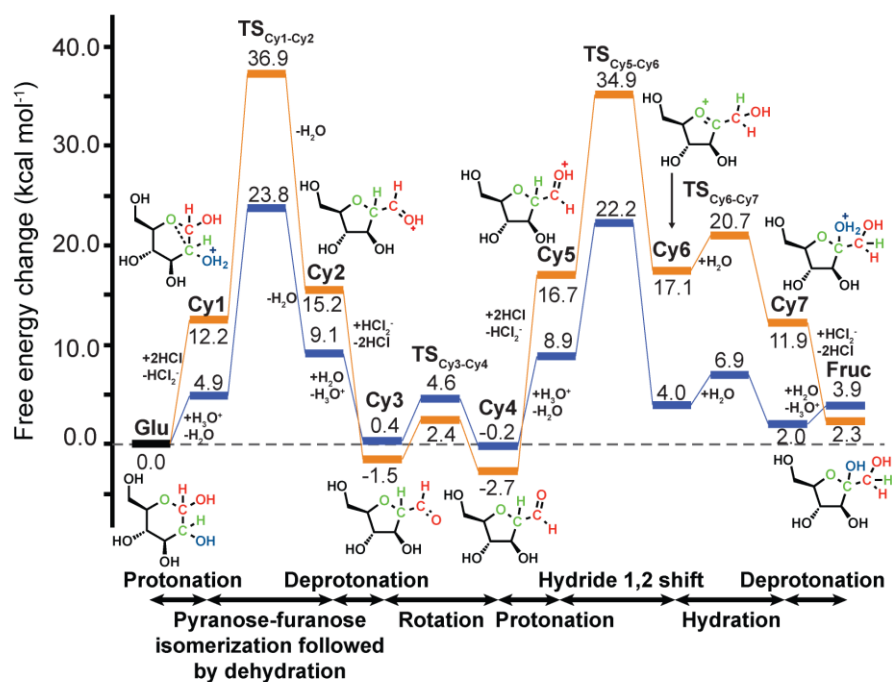
Figure 4.11 Optimized geometries of the intermediates during the glucose isomerization into fructose via open chain mechanism in [MMIM]Cl (1 atm, 353.15 K). The selected bond lengths are given in unit of Angstrom.

4.2.1.3 Comparison

The geometries structure of acid-catalyzed glucose isomerization optimized in water for acid-catalyzed isomerization of **Glu** to **Fruc** following the cyclic and the open chain mechanisms were demonstrated in (Figure S25 and Figure S26)Figure S28. We found that the TS structures in each step both in water and [MMIM]Cl are similar, despite the difference in the form of acid-base, which are $\text{H}_3\text{O}^+ - \text{H}_2\text{O}$ and $\text{HCl} - \text{HCl}_2^-$ for water and [MMIM]Cl, respectively. The spontaneous formation of HCl_2^- from HCl and Cl in ILs can take place.^[176-181] The formation of HCl_2^- from HCl and Cl was found to be an exothermic reaction by $6.3 \text{ kcal mol}^{-1}$.

The free energy profile of isomerization between glucose and fructose in [MMIM]Cl and water following the cyclic mechanism are shown in Figure 4.12 (a). The activation barrier of this process (**Cy1**→**TS_{Cy1-Cy2}**) are $36.9 \text{ kcal mol}^{-1}$ and $23.8 \text{ kcal mol}^{-1}$ for reaction in [MMIM]Cl and water, respectively. The rotation barrier between C1-C2 bond (**Cy3**→**Cy4**) are 2.4 and $4.6 \text{ kcal mol}^{-1}$ in [MMIM]Cl and water, respectively. Moreover, barriers for hydride shift (**Cy5**→**Cy6**) are 34.9 and $22.2 \text{ kcal mol}^{-1}$ in [MMIM]Cl and water, respectively.

(a) Cyclic mechanism



(b) Open chain mechanism

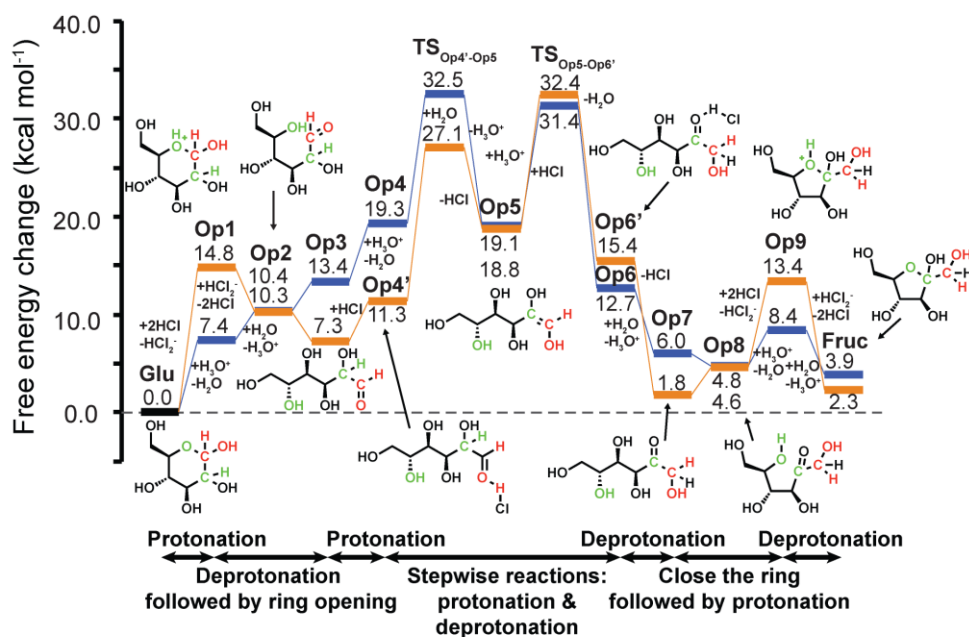


Figure 4.12 Free energy profile of glucose isomerization to fructose via (a) cyclic and (b) open chain mechanisms. Orange line shows the free energy changes in [MMIM]Cl at (1 atm, 353.15 K) condition. Blue line shows the free energy changes in water at (10 MPa, 473.15 K) condition. All values are reported in kcal mol⁻¹.

The free energy profile of glucose isomerization to fructose in [MMIM]Cl and water following the open chain mechanism are demonstrated in Figure 4.12 (b). Protonation of **Glu** to **Cy1** in [MMIM]Cl and water demands lower energies around $2.5 \text{ kcal mol}^{-1}$ than to **Op1**. However, intermediates with cyclic forms, e.g. **Op2**, **Op3**, **Op5**, **Op7**, and **Op8**, are more stable in [MMIM]Cl rather than in water. In addition, **Op4** and **Op6** can stabilize positively charge molecules using chloride anion in [MMIM]Cl by around 14 kcal mol^{-1} obtaining complex **Op4'** and **Op6'**. The rate-determining step in [MMIM]Cl is the protonation step of **Op5** with $32.4 \text{ kcal mol}^{-1}$ activation free energy.

For overall reaction of glucose-fructose isomerization (**Glu**→**Fruc**), the barrier of isomerization in [MMIM]Cl via open chain mechanism are $4.5 \text{ kcal mol}^{-1}$ lower than the cyclic mechanism. On the other hand, the cyclic mechanism is favorable by $8.7 \text{ kcal mol}^{-1}$ in water lower than those in open chain mechanism. Therefore, open chain mechanism is preferable mechanism for glucose-fructose transformation in [MMIM]Cl, whereas cyclic mechanism is the more favorable pathway in acidic aqueous solutions.

4.2.2 Fructose dehydration into HMF

The fructose transformation to HMF in water has been proposed by Antal *et al.*, which could take place via a cyclic mechanism.^[78] Furthermore, this mechanism has been theoretically studied at G4MP2-B3LYP/6-31G(d,p) levels of theory and SMD solvation model by Assary *et al.*^[80] Likewise, Yang *et al.* at have also examined using similar level of theory (G4MP2-B3LYP/6-311+G(d,p)) but employed PCM and COSMO solvation model.^[85] Nevertheless, it is still interesting and challenging to elucidate the mechanism for fructose to HMF transformation. Since the essential TSs among intermediates during this mechanism have not yet been considered, in this section, the vital TSs of dehydration step in [MMIM]Cl are investigated.

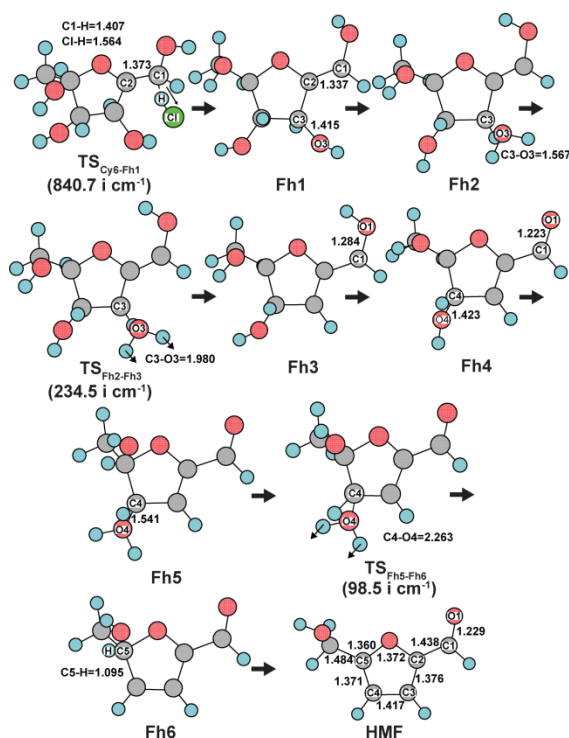


Figure 4.13 Geometry changes during the fructose transformation into HMF via cyclic mechanism in [MMIM]Cl at 1 atm, 353.15 K. It is started from **TS_{Cy6-Fh1}**. The selected bond lengths are given in unit of Angstrom.

The sequential progression of protonation, dehydration, and deprotonation reactions is supposed for the fructose dehydration to HMF (**Fruc**→**HMF**). Firstly, the reaction takes place in the reverse direction of glucose isomerization into fructose starting from **Fruc** to **Cy6** following the cyclic mechanism, followed by the deprotonation of C1 of **Cy6** to form **Fh1**. **Figure 4.13** demonstrated the optimized structures starting from **TS_{Cy6-Fh1}** and important transition states in [MMIM]Cl. Then, **Fh2** is created by the protonation at C3-OH, so that the leaving OH₂ group can be formed. This result is in the longer bond distance of C3-O3 by 0.1 Å. For the transition state of the dehydration reaction **Fh2**→**Fh3**+H₂O (**TS_{Fh2-Fh3}**), the distance of C3-O3 is 1.980 Å. **Fh3** is deprotonated at C1-OH to form **Fh4** which was detected as a stable intermediate from experiments.[207, 208] Then, **Fh4** is protonated at the C4-OH and water leaves. The dehydration of **Fh5** takes place through **TS_{Fh5-Fh6}**, which makes the bond distance between C3 and C4 become smaller (1.1 Å). Finally, the

final product, namely **HMF**, is formed by the deprotonation at C5 site of **Fh6**. Additionally; optimized structures of fructose dehydration in water were obtained and given in Appendix.

The energy profile of the fructose dehydration to HMF in [MMIM]Cl and water were displayed in **Figure 4.14**. The dehydration step **Cy7**→**TS_{Cy6-Cy7}** only demands 4.9 kcal mol⁻¹ in water, while **Fruc**→**TS_{Cy6-Cy7}** desires 18.4 kcal mol⁻¹ in [MMIM]Cl

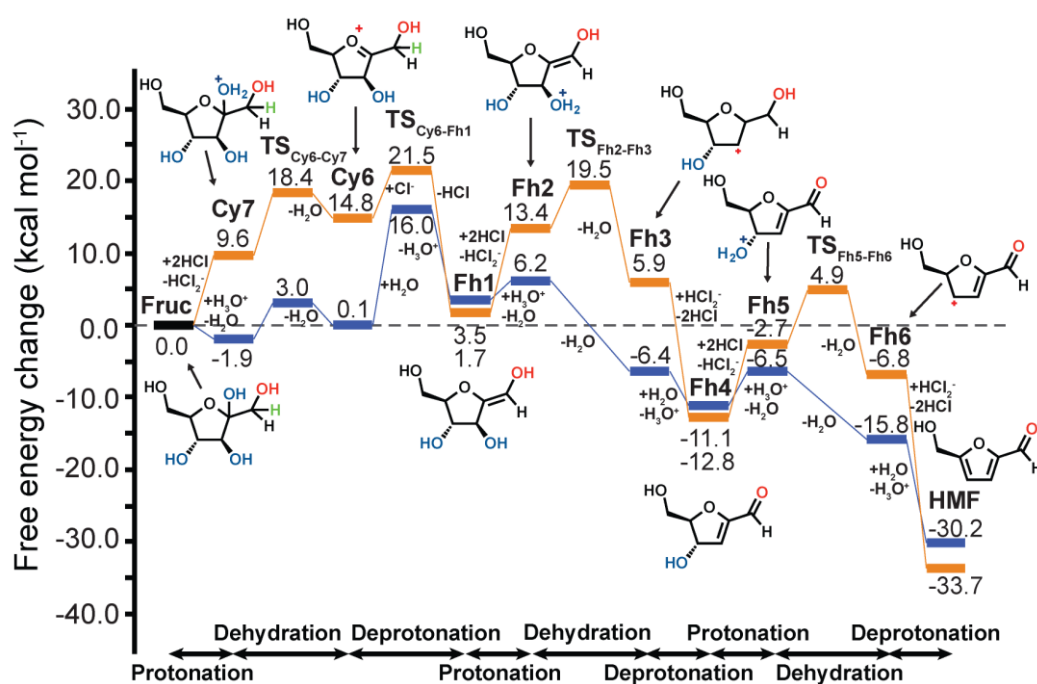


Figure 4.14 Free energy profile of fructose transformation into HMF. Orange line shows the free energy changes in [MMIM]Cl at (1 atm, 353.15 K) condition. Blue line shows the free energy changes in water at (10 MPa, 473.15 K) condition. All values are reported in kcal mol⁻¹.

Hence, other dehydration steps in water were not calculated. The 6.7 and 15.9 kcal mol⁻¹ have been required for deprotonation reactions of C1 from **Cy6** in [MMIM]Cl and water, respectively. The activation barrier of the second and the third dehydration process in [MMIM]Cl are 19.5 and 4.9 kcal mol⁻¹, respectively. Thus, the RDS for the conversion of fructose to HMF is **TS_{Cy6-Fh1}** for both [MMIM]Cl and water, which required 21.5 and 17.9 kcal mol⁻¹ activation barrier, respectively. As the results, the isomerization to fructose becomes the RDS of overall pathway starting from glucose and leading to HMF eventually.

4.2.3 Energy decomposition analysis

In the following section, the RDS for whole reaction pathways of **Glu** leading to HMF in ILs, **TS_{Op5-Op6'}**, was finely examined. The free energy changes ($\Delta\Delta G$) can be decomposed as follows:

$$\Delta\Delta G = \Delta E_u + \Delta G_{\text{coor}} + \Delta\Delta\mu \quad (\text{Eq. 4.1})$$

where ΔE_u is related to the electronic energy changes of solute, ΔG_{coor} is the difference of thermal correction to the free energy, and $\Delta\Delta\mu$ is the change on the solvation free energy. For the **Glu**→**TS_{Op5-Op6'}** reaction, we found that ΔE_u , ΔG_{coor} , and $\Delta\Delta\mu$ are 33.0, 7.2, and -7.8 kcal mol⁻¹ respectively. Hence, it is suggested that the solvation effect is essentially to decrease the free energy barrier in ILs.

For RISM calculation, the sum of the value from each atomic site α was computed for solvation free energy of the solute molecules.^[152, 182, 183]

$$\Delta\Delta\mu = \sum_{\alpha}^{\text{atom}} \Delta\Delta\mu_{\alpha} \quad (\text{Eq. 4.2})$$

Table 4.2 The change of solvation free energy on each site.

Atomic label ^[a]	$\Delta\Delta\mu_\alpha$
Main	-6.9
H	7.3
Cl	-8.2

[a] The definition of labels is given in **Figure 4.15**.

*Energies are given in kcal mol⁻¹.

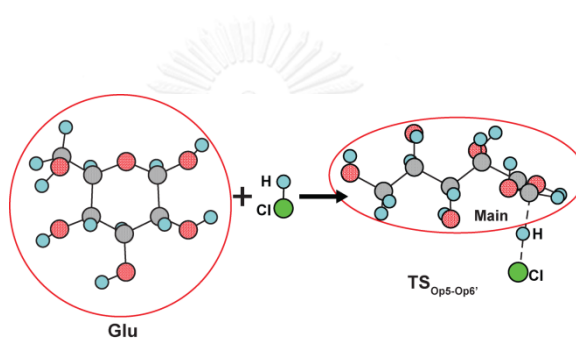


Figure 4.15 Definition of atomic labels (Main, H, Cl) for the contribution to the solvation free energy. The regions surrounded by the red line are represented as 'Main'.

Table 4.2 demonstrates the contribution of each site to the change of solvation free energy $\Delta\Delta\mu$. The analysis obviously shows that the chain form of **Glu** is greatly stabilized by [MMIM]Cl, in contrast to the cyclic form, by 6.9 kcal mol⁻¹. As well, it is noteworthy that the Cl sites is the main stabilization of **TS_{Op5-Op6'}**.

The solvent effect is clarified by the microscopic interaction between solute and solvents demonstrated in the RDFs. **Figure 4.16** (a) displays the RDFs for the interactions between Cl and solvent sites. There are two peaks of RDFs located at 3.7 Å for the Cl site in free HCl located at 3.7 Å with the largely positive site of [MMIM]⁺ (CR_v site), followed by less intense peak at 5.7 Å. The peaks profile of free HCl are not so much different with CR_v-Cl in **TS_{Op5-Op6'}**. However, the RDFs of the free HCl

and $\text{TS}_{\text{Op5-Op6}'}$ is totally different for the Cl with the Cl_v^- anion of solvent (Cl_v). The first peak of $\text{Cl}_{\text{HCl}}-\text{Cl}_v$ at 4.0 Å shows that it is very intense, which corresponding to the first solvation peak of H_{HCl} with Cl_v . Nevertheless, the peak of Cl site in $\text{TS}_{\text{Op5-Op6}'}$ (at 4.0 Å) is very low compare to free HCl. This suggests the lower repulsive interactions between hydrogen site of solute and the chloride anions in solvent, as this peak shows the direct contact. In addition, cations and anions around free HCl and $\text{TS}_{\text{Op5-Op6}'}$ can be proposed in **Figure 4.16** (b). The hydrogen sites of hydroxyl groups in $\text{TS}_{\text{Op5-Op6}'}$ were distributed by chloride anions. This make the peak was rosen up at larger distances. To sum up, the Cl site in $\text{TS}_{\text{Op5-Op6}'}$ was stabilized by the chloride anions as weaker repulsive interactions.

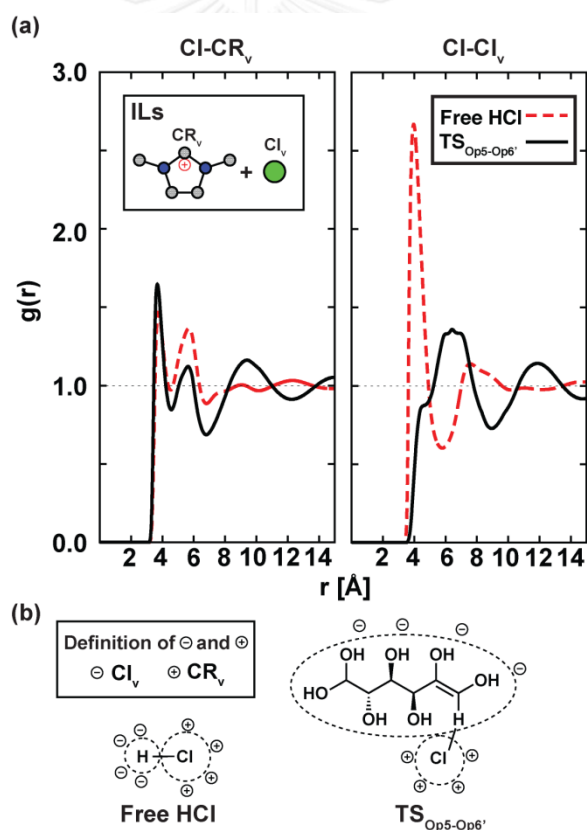


Figure 4.16 (a) RDFs between Cl sites in HCl and $\text{TS}_{\text{Op5-Op6}'}$. Inset on shows the interactions of the solute sites with Cl_v and CR_v sites. (b) Schematic figure of cations and anions around free HCl and $\text{TS}_{\text{Op5-Op6}'}$.

CHAPTER V CONCLUSION

Theoretical investigation by means of DFT calculation was utilized to clarify the reaction mechanisms of the organic reactions. In this thesis, the two of essential organic reactions have been focused: 1) the Biginelli reaction and 2) the glucose transformation to 5-HMF.

Three possible routes of Biginelli reaction, iminium route (route A), enamime route (route B), and Knoevenagel route (route C) of benzaldehyde, urea and ethyl acetoacetate were searched by means of AFIR. The route A was found to be the lowest energy pathways. The rate-determining step for this route is the C-N bond formations during the cyclization step with a $21.5 \text{ kcal mol}^{-1}$ activation barrier, in contrary to the common knowledge.^[64] For the route B, the rate-determining step is still the cyclization step. However, the barrier for its RDS was found to be almost 10 kcal mol^{-1} higher in energy than that in Route A. The C-O bond breaking in the dehydration step was predicted as the RDS for route C. With the barrier of almost $6.5 \text{ kcal mol}^{-1}$ higher in energy than that of route A. Thus, the route A was found to be the lowest energy pathway for the Biginelli reaction.

It is noteworthy to observe that all steps are catalyzed by the presence of an extra urea. Surprisingly, an extra urea is directly involved in this reaction by reserving proton and stabilizing Lewis acid. Also, it insures all proton transfer during the dehydration steps. This suggests that an extra urea acts as organocatalyst in the Biginelli reaction. This results explains why similar yields were obtained experimentally when a protic polar solvent, such as ethanol, or an aprotic and non-polar solvent such as toluene is used. This is consistent with the experimental fact that an excess of urea is often used experimentally.^[14, 15, 60, 61, 173-175]

Regarding to small variance in the reaction barrier, It is possible that the most favorable pathway might be changed with very bulky substituents due to the close contact among reactants. Therefore, to determine Biginelli reactions with different catalysts and substituents would be advertent and challenging topics.

For the glucose transformation to 5-HMF, the combination of RISM and quantum mechanical calculation, the so-called RISM-SCF-SEDD, have been applied in acidic aqueous and ILs solutions. In water, by the cyclic mechanism is the most favourable pathway for glucose isomerization, with a $23.8 \text{ kcal mol}^{-1}$ activation free energy ($\text{Glu} \rightarrow \text{TS}_{\text{Cy1-Cy2}}$) as compared to the barrier of $32.5 \text{ kcal mol}^{-1}$ for the open chain mechanism. On the other hand, the open chain mechanism becomes more favourable in IL with a $32.4 \text{ kcal mol}^{-1}$ activation barrier ($\text{Glu} \rightarrow \text{TS}_{\text{Op5-Op6}}$) whereas the barrier of the cyclic mechanism is $36.9 \text{ kcal mol}^{-1}$. For the fructose conversion to HMF, the rate-determining step is the deprotonation at C1 ($\text{TS}_{\text{Cy6-FH1}}$). The activation barriers were found to be $21.5 \text{ kcal mol}^{-1}$ and $17.9 \text{ kcal mol}^{-1}$, in ILs and water, respectively. Although, the free energies for the reactions in IL are higher than in acidic aqueous solvent, the various side reactions often occur in the reaction in water. This is the major disadvantage which rises up the cost of product purification.^[78, 184] Thus, it is necessary to determine these reactions in near future.

In addition, the detail of solvent effect carried out by RISM-SCF-SEDD can suggest both short-range and long-range solvent-solute interaction, the information that cannot be earned from the continuum model. The decomposition of free energy was utilized to analyse the solvent effect. Moreover, we could assign the contribution to solvation free energy of each site or group by RDFs with RISM-SCF-SEDD. The contribution of solvation free energy change in IL was elucidated and found that it gives large contribution to reduce the free energy barrier. The solvation structures demonstrate that the weak repulsive interactions by the chloride anions in ILs bring about the stabilization of Cl site in $\text{TS}_{\text{Op5-Op6}}$. Albeit, the reaction mechanism in other solvents and even the use of metal catalyst have not been discussed. We hope that the results of this research would provide a deeper insight and notions on reactions of glucose transformation to 5-hydroxymethylfurfural in the acidic condition.

REFERENCES

- [1] Cioc, R.C., Ruijter, E., and Orru, R.V.A. Multicomponent reactions: advanced tools for sustainable organic synthesis. Green Chemistry 16(6) (2014): 2958-2975.
- [2] Kappe, C.O. Biologically active dihydropyrimidones of the Biginelli-type — a literature survey. European Journal of Medicinal Chemistry 35(12) (2000): 1043-1052.
- [3] Kappe, C.O. 100 years of the biginelli dihydropyrimidine synthesis. Tetrahedron 49(32) (1993): 6937-6963.
- [4] Tron, G.C., Minassi, A., and Appendino, G. Pietro Biginelli: The Man Behind the Reaction. European Journal of Organic Chemistry 2011(28) (2011): 5541-5550.
- [5] Rubin, E.M. Genomics of cellulosic biofuels. Nature 454(7206) (2008): 841-845.
- [6] Dömling, A. Recent Developments in Isocyanide Based Multicomponent Reactions in Applied Chemistry. Chemical Reviews 106(1) (2006): 17-89.
- [7] Dömling, A. and Ugi, I. Multicomponent Reactions with Isocyanides. Angewandte Chemie International Edition 39(18) (2000): 3168-3210.
- [8] Alvim, H.G.O., da Silva Junior, E.N., and Neto, B.A.D. What do we know about multicomponent reactions? Mechanisms and trends for the Biginelli, Hantzsch, Mannich, Passerini and Ugi MCRs. RSC Advances 4(97) (2014): 54282-54299.
- [9] Bienaymé, H., Hulme, C., Oddon, G., and Schmitt, P. Maximizing Synthetic Efficiency: Multi-Component Transformations Lead the Way. Chemistry – A European Journal 6(18) (2000): 3321-3329.
- [10] Ugi, I., Werner, B., and Dömling, A. The Chemistry of Isocyanides, their MultiComponent Reactions and their Libraries. Molecules 8(1) (2003): 53-56.
- [11] Dömling, A., Wang, W., and Wang, K. Chemistry and Biology Of Multicomponent Reactions. Chemical Reviews 112(6) (2012): 3083-3135.
- [12] Santos, V.G., et al. The Multicomponent Hantzsch Reaction: Comprehensive Mass Spectrometry Monitoring Using Charge-Tagged Reagents. Chemistry – A European Journal 20(40) (2014): 12808-12816.

- [13] Sweet, F. and Fissekis, J.D. Synthesis of 3,4-dihydro-2(1H)-pyrimidinones and the mechanism of the Biginelli reaction. Journal of the American Chemical Society 95(26) (1973): 8741-8749.
- [14] Folkers, K. and Johnson, T.B. Researches on Pyrimidines. CXXXVI. The Mechanism of Formation of Tetrahydropyrimidines by the Biginelli Reaction1. Journal of the American Chemical Society 55(9) (1933): 3784-3791.
- [15] Cepanec, I., Litvić, M., Filipan-Litvić, M., and Grüngold, I. Antimony(III) chloride-catalysed Biginelli reaction: a versatile method for the synthesis of dihydropyrimidinones through a different reaction mechanism. Tetrahedron 63(48) (2007): 11822-11827.
- [16] Passerini, M. and Simone, L. Sopra gli isonitrili (I). Composto del p-isonitrilazobenzolo con acetone ed acido acetico. Gazz Chim Ital 51(II) (1921): 126-129.
- [17] Passerini, M. and Ragni, G. Sopra gli isonitrili Gazz Chim Ital 61 (1931): 964-969.
- [18] Maeda, S., Komagawa, S., Uchiyama, M., and Morokuma, K. Finding Reaction Pathways for Multicomponent Reactions: The Passerini Reaction is a Four-Component Reaction. Angewandte Chemie 123(3) (2011): 670-675.
- [19] Ramozzi, R. and Morokuma, K. Revisiting the Passerini Reaction Mechanism: Existence of the Nitrilium, Organocatalysis of Its Formation, and Solvent Effect. The Journal of Organic Chemistry 80(11) (2015): 5652-5657.
- [20] Ugi, I., Meyr, R., Fetzer, U., and Steinbrückner, C. Versuche mit Isonitrilen. Angewandte Chemie 71(Ugi I, Meyr R, Fetzer U, Steinbrückner C.) (1959): 386-388.
- [21] Ugi, I. and Steinbrückner, C. Über ein neues Kondensations-Prinzip. Angewandte Chemie 72(7-8) (1960): 267-268.
- [22] Chéron, N., Ramozzi, R., Kaïm, L.E., Grimaud, L., and Fleurat-Lessard, P. Challenging 50 Years of Established Views on Ugi Reaction: A Theoretical Approach. The Journal of Organic Chemistry 77(3) (2012): 1361-1366.
- [23] Biginelli, P. Aldehyde-urea derivatives of aceto-and oxaloacetic acids. Gazz. Chim. Ital 23(1) (1893): 360-413.
- [24] Biginelli, P. Ber. Dtsch. Chem. Ges. 26 (1893): 447.

- [25] Hantzsch, A. Condensationsprodukte aus Aldehydammoniak und ketonartigen Verbindungen. Berichte der deutschen chemischen Gesellschaft 14(2) (1881): 1637-1638.
- [26] Hantzsch, A. Ueber die Synthese pyridinartiger Verbindungen aus Acetessigäther und Aldehydammoniak. Justus Liebigs Annalen der Chemie 215(1) (1882): 1-82.
- [27] Sandhu, J.S. and Sandhu, S. Past, present and future of the Biginelli reaction: a critical perspective. ARKIVOC i (2012): 66-133.
- [28] Biginelli, P. Ueber Aldehyduramide des Acetessigäthers. Berichte der deutschen chemischen Gesellschaft 24(1) (1891): 1317-1319.
- [29] Alam, O., Khan, S.A., Siddiqui, N., Ahsan, W., Verma, S.P., and Gilani, S.J. Antihypertensive activity of newer 1,4-dihydro-5-pyrimidine carboxamides: Synthesis and pharmacological evaluation. European Journal of Medicinal Chemistry 45(11) (2010): 5113-5119.
- [30] Lloyd, J., et al. Dihydropyrazolopyrimidines containing benzimidazoles as KV1.5 potassium channel antagonists. Bioorganic & Medicinal Chemistry Letters 19(18) (2009): 5469-5473.
- [31] Patil, A.D., et al. Novel Alkaloids from the Sponge *Batzella* sp.: Inhibitors of HIV gp120-Human CD4 Binding. The Journal of Organic Chemistry 60(5) (1995): 1182-1188.
- [32] China Raju, B., et al. Synthesis, structure–activity relationship of novel substituted 4H-chromen-1,2,3,4-tetrahydropyrimidine-5-carboxylates as potential anti-mycobacterial and anticancer agents. Bioorganic & Medicinal Chemistry Letters 21(10) (2011): 2855-2859.
- [33] Chiang, A.N., et al. Select pyrimidinones inhibit the propagation of the malarial parasite, *Plasmodium falciparum*. Bioorganic & Medicinal Chemistry 17(4) (2009): 1527-1533.
- [34] Agbaje, O.C., Fadeyi, O.O., Fadeyi, S.A., Myles, L.E., and Okoro, C.O. Synthesis and in vitro cytotoxicity evaluation of some fluorinated hexahydropyrimidine derivatives. Bioorganic & Medicinal Chemistry Letters 21(3) (2011): 989-992.

- [35] Lewis, R.W., Mabry, J., Polisar, J.G., Eagen, K.P., Ganem, B., and Hess, G.P. Dihydropyrimidinone Positive Modulation of δ -Subunit-Containing γ -Aminobutyric Acid Type A Receptors, Including an Epilepsy-Linked Mutant Variant. Biochemistry 49(23) (2010): 4841-4851.
- [36] Rajanarendar, E., et al. Synthesis, antimicrobial, and mosquito larvicidal activity of 1-aryl-4-methyl-3,6-bis-(5-methylisoxazol-3-yl)-2-thioxo-2,3,6,10b-tetrahydro-1H-pyrimido[5,4-c]quinolin-5-ones. Bioorganic & Medicinal Chemistry Letters 20(20) (2010): 6052-6055.
- [37] Mokale, S.N., Shinde, S.S., Elgire, R.D., Sangshetti, J.N., and Shinde, D.B. Synthesis and anti-inflammatory activity of some 3-(4,6-disubstituted-2-thioxo-1,2,3,4-tetrahydropyrimidin-5-yl) propanoic acid derivatives. Bioorganic & Medicinal Chemistry Letters 20(15) (2010): 4424-4426.
- [38] Trivedi, A.R., Bhuva, V.R., Dholariya, B.H., Dodiya, D.K., Kataria, V.B., and Shah, V.H. Novel dihydropyrimidines as a potential new class of antitubercular agents. Bioorganic & Medicinal Chemistry Letters 20(20) (2010): 6100-6102.
- [39] Chitra, S., Devanathan, D., and Pandiarajan, K. Synthesis and in vitro microbiological evaluation of novel 4-aryl-5-isopropoxycarbonyl-6-methyl-3,4-dihydropyrimidinones. European Journal of Medicinal Chemistry 45(1) (2010): 367-371.
- [40] Rajesh, S.M., Kumar, R.S., Libertsen, L.A., Perumal, S., Yogeeswari, P., and Sriram, D. A green expedient synthesis of pyridopyrimidine-2-thiones and their antitubercular activity. Bioorganic & Medicinal Chemistry Letters 21(10) (2011): 3012-3016.
- [41] Puripat, M., Ramozzi, R., Hatanaka, M., Parasuk, W., Parasuk, V., and Morokuma, K. The Biginelli Reaction Is a Urea-Catalyzed Organocatalytic Multicomponent Reaction. The Journal of Organic Chemistry 80(14) (2015): 6959-6967.
- [42] Gorobets, N.Y., et al. Unexpected alternative direction of a Biginelli-like multicomponent reaction with 3-amino-1,2,4-triazole as the urea component. Tetrahedron Letters 51(16) (2010): 2095-2098.

- [43] Světlík, J. and Kettmann, V. The chameleon-like behaviour of 3-amino-1,2,4-triazole in the Biginelli reaction: unexpected formation of a novel spiroheterocyclic system. Tetrahedron Letters 52(10) (2011): 1062-1066.
- [44] Cho, H., et al. Synthesis of 4-unsubstituted dihydropyrimidines. Nucleophilic substitution at position-2 of dihydropyrimidines. Tetrahedron 67(14) (2011): 2661-2669.
- [45] Hassani, Z., Islami, M.R., and Kalantari, M. An efficient one-pot synthesis of octahydroquinazolinone derivatives using catalytic amount of H₂SO₄ in water. Bioorganic & Medicinal Chemistry Letters 16(17) (2006): 4479-4482.
- [46] Tu, S.-J., et al. One-pot Synthesis of Bis(dihydropyrimidinone-4-yl)benzene Using Boric Acid as a Catalyst. Chinese Journal of Chemistry 23(5) (2005): 596-598.
- [47] Ramos, L.M., et al. Mechanistic Studies on Lewis Acid Catalyzed Biginelli Reactions in Ionic Liquids: Evidence for the Reactive Intermediates and the Role of the Reagents. The Journal of Organic Chemistry 77(22) (2012): 10184-10193.
- [48] Singh, O.M. and Devi, N.S. Application of β -Oxodithioesters in Domino and Multicomponent Reactions: Facile Route to Dihydropyrimidines and Coumarins. The Journal of Organic Chemistry 74(8) (2009): 3141-3144.
- [49] Hu, E.H., Sidler, D.R., and Dolling, U.-H. Unprecedented Catalytic Three Component One-Pot Condensation Reaction: An Efficient Synthesis of 5-Alkoxy-carbonyl-4-aryl-3,4-dihydropyrimidin-2(1H)-ones. The Journal of Organic Chemistry 63(10) (1998): 3454-3457.
- [50] Maiti, G., Kundu, P., and Guin, C. One-pot synthesis of dihydropyrimidinones catalysed by lithium bromide: an improved procedure for the Biginelli reaction. Tetrahedron Letters 44(13) (2003): 2757-2758.
- [51] Alvim, H.G.O., et al. Ionic Liquid Effect over the Biginelli Reaction under Homogeneous and Heterogeneous Catalysis. ACS Catalysis 3(7) (2013): 1420-1430.

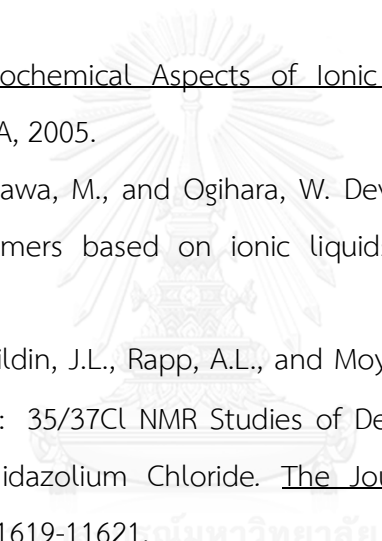
- [52] Ramos, L.M., et al. The Biginelli Reaction with an Imidazolium-Tagged Recyclable Iron Catalyst: Kinetics, Mechanism, and Antitumoral Activity. Chemistry – A European Journal 19(13) (2013): 4156-4168.
- [53] Kore, R. and Srivastava, R. Synthesis and applications of novel imidazole and benzimidazole based sulfonic acid group functionalized Brønsted acidic ionic liquid catalysts. Journal of Molecular Catalysis A: Chemical 345(1-2) (2011): 117-126.
- [54] Joseph, J.K., Jain, S.L., Singhal, S., and Sain, B. Efficient Synthesis of 3,4-Dihydropyrimidinones in 1-n-Butyl-3-methylimidazolium Tetrachloroindate (BMI-InCl₄). Industrial & Engineering Chemistry Research 50(20) (2011): 11463-11466.
- [55] Chen, X. and Peng, Y. Chloroferrate(III) Ionic Liquid: Efficient and Recyclable Catalyst for Solvent-free Synthesis of 3,4-Dihydropyrimidin-2(1H)-ones. Catalysis Letters 122(3) (2008): 310-313.
- [56] Li, M., Guo, W.-S., Wen, L.-R., Li, Y.-F., and Yang, H.-Z. One-pot synthesis of Biginelli and Hantzsch products catalyzed by non-toxic ionic liquid (BMImSac) and structural determination of two products. Journal of Molecular Catalysis A: Chemical 258(1-2) (2006): 133-138.
- [57] Kappe, C.O. A Reexamination of the Mechanism of the Biginelli Dihydropyrimidine Synthesis. Support for an N-Acyliminium Ion Intermediate¹. The Journal of Organic Chemistry 62(21) (1997): 7201-7204.
- [58] Xu, D.-Z., Li, H., and Wang, Y. Highly enantioselective Biginelli reaction catalyzed by a simple chiral primary amine catalyst: asymmetric synthesis of dihydropyrimidines. Tetrahedron 68(38) (2012): 7867-7872.
- [59] Alvim, H.G.O., et al. Facts, Presumptions, and Myths on the Solvent-Free and Catalyst-Free Biginelli Reaction. What is Catalysis for? The Journal of Organic Chemistry 79(8) (2014): 3383-3397.
- [60] Shen, Z.-L., Xu, X.-P., and Ji, S.-J. Brønsted Base-Catalyzed One-Pot Three-Component Biginelli-Type Reaction: An Efficient Synthesis of 4,5,6-Triaryl-3,4-dihydropyrimidin-2(1H)-one and Mechanistic Study. The Journal of Organic Chemistry 75(4) (2010): 1162-1167.

- [61] Litvić, M., Večenaj, I., Ladišić, Z.M., Lovrić, M., Vinković, V., and Filipan-Litvić, M. First application of hexaaquaaluminium(III) tetrafluoroborate as a mild, recyclable, non-hygroscopic acid catalyst in organic synthesis: a simple and efficient protocol for the multigram scale synthesis of 3,4-dihydropyrimidinones by Biginelli reaction. Tetrahedron 66(19) (2010): 3463-3471.
- [62] Kamal Raj, M., et al. A mechanistic investigation of Biginelli reaction under base catalysis. Tetrahedron Letters 52(28) (2011): 3605-3609.
- [63] Atwal, K.S., Rovnyak, G.C., O'Reilly, B.C., and Schwartz, J. Substituted 1,4-dihydropyrimidines. 3. Synthesis of selectively functionalized 2-hetero-1,4-dihydropyrimidines. The Journal of Organic Chemistry 54(25) (1989): 5898-5907.
- [64] De Souza, R.O.M.A., et al. The Three-Component Biginelli Reaction: A Combined Experimental and Theoretical Mechanistic Investigation. Chemistry – A European Journal 15(38) (2009): 9799-9804.
- [65] Clark, J.H., Macquarrie, D.J., and Sherwood, J. The Combined Role of Catalysis and Solvent Effects on the Biginelli Reaction: Improving Efficiency and Sustainability. Chemistry – A European Journal 19(16) (2013): 5174-5182.
- [66] Tong, X., Ma, Y., and Li, Y. Biomass into chemicals: Conversion of sugars to furan derivatives by catalytic processes. Applied Catalysis A: General 385(1–2) (2010): 1-13.
- [67] Carlmark, A., Larsson, E., and Malmström, E. Grafting of cellulose by ring-opening polymerisation – A review. European Polymer Journal 48(10) (2012): 1646-1659.
- [68] Swatloski, R.P., Spear, S.K., Holbrey, J.D., and Rogers, R.D. Dissolution of Cellulose with Ionic Liquids. Journal of the American Chemical Society 124(18) (2002): 4974-4975.
- [69] Wei, X., Lu, Q., Sui, X., Wang, Z., and Zhang, Y. Characterization of the water-insoluble pyrolytic cellulose from cellulose pyrolysis oil. Journal of Analytical and Applied Pyrolysis 97 (2012): 49-54.

- [70] Medronho, B. and Lindman, B. Competing forces during cellulose dissolution: From solvents to mechanisms. Current Opinion in Colloid & Interface Science 19(1) (2014): 32-40.
- [71] loelovich, M. Study of Cellulose Interaction with Concentrated Solutions of Sulfuric Acid. ISRN Chemical Engineering 2012 (2012): 1-7.
- [72] Ma, X.J., et al. Hydrothermal pretreatment of bamboo and cellulose degradation. Bioresource Technology 148 (2013): 408-413.
- [73] Binder, J.B. and Raines, R.T. Simple Chemical Transformation of Lignocellulosic Biomass into Furans for Fuels and Chemicals. Journal of the American Chemical Society 131(5) (2009): 1979-1985.
- [74] Peng, L., Lin, L., Zhang, J., Zhuang, J., Zhang, B., and Gong, Y. Catalytic Conversion of Cellulose to Levulinic Acid by Metal Chlorides. Molecules 15(8) (2010): 5258-5272.
- [75] Girisuta, B., Janssen, L.P.B.M., and Heeres, H.J. Kinetic Study on the Acid-Catalyzed Hydrolysis of Cellulose to Levulinic Acid. Industrial & Engineering Chemistry Research 46(6) (2007): 1696-1708.
- [76] Arifin, Puripat, M., Yokogawa, D., Parasuk, V., and Irle, S. Glucose transformation to 5-hydroxymethylfurfural in acidic ionic liquid: A quantum mechanical study. Journal of Computational Chemistry 37(3) (2016): 327-335.
- [77] Rasmussen, H., Sørensen, H.R., and Meyer, A.S. Formation of degradation compounds from lignocellulosic biomass in the biorefinery: sugar reaction mechanisms. Carbohydrate Research 385 (2014): 45-57.
- [78] Antal Jr, M.J., Mok, W.S.L., and Richards, G.N. Mechanism of formation of 5-(hydroxymethyl)-2-furaldehyde from d-fructose and sucrose. Carbohydrate Research 199(1) (1990): 91-109.
- [79] Antal Jr, M.J., Leesomboon, T., Mok, W.S., and Richards, G.N. Mechanism of formation of 2-furaldehyde from d-xylose. Carbohydrate Research 217 (1991): 71-85.
- [80] Assary, R.S., Kim, T., Low, J.J., Greeley, J., and Curtiss, L.A. Glucose and fructose to platform chemicals: understanding the thermodynamic

- landscapes of acid-catalysed reactions using high-level ab initio methods. Physical Chemistry Chemical Physics 14(48) (2012): 16603-16611.
- [81] Assary, R.S., Redfern, P.C., Hammond, J.R., Greeley, J., and Curtiss, L.A. Computational Studies of the Thermochemistry for Conversion of Glucose to Levulinic Acid. The Journal of Physical Chemistry B 114(27) (2010): 9002-9009.
- [82] Caratzoulas, S. and Vlachos, D.G. Converting fructose to 5-hydroxymethylfurfural: a quantum mechanics/molecular mechanics study of the mechanism and energetics. Carbohydrate Research 346(5) (2011): 664-672.
- [83] Qian, X. Mechanisms and Energetics for Acid Catalyzed β -d-Glucose Conversion to 5-Hydroxymethylfurfural. The Journal of Physical Chemistry A 115(42) (2011): 11740-11748.
- [84] Qian, X. Mechanisms and energetics for Bronsted acid-catalyzed glucose condensation, dehydration and isomerization reactions. Topics in Catalysis 55(3-4) (2012): 218-226.
- [85] Yang, G., Pidko, E.A., and Hensen, E.J.M. Mechanism of Brønsted acid-catalyzed conversion of carbohydrates. Journal of Catalysis 295 (2012): 122-132.
- [86] Kimura, H., Nakahara, M., and Matubayasi, N. In Situ Kinetic Study on Hydrothermal Transformation of d-Glucose into 5-Hydroxymethylfurfural through d-Fructose with ^{13}C NMR. The Journal of Physical Chemistry A 115(48) (2011): 14013-14021.
- [87] Daorattanachai, P., Namuangruk, S., Viriya-empikul, N., Laosiripojana, N., and Faungnawakij, K. 5-Hydroxymethylfurfural production from sugars and cellulose in acid- and base-catalyzed conditions under hot compressed water. Journal of Industrial and Engineering Chemistry 18(6) (2012): 1893-1901.
- [88] Feather, M.S., Harris, D.W., and Nichols, S.B. Routes of conversion of D-xylose, hexuronic acids, and L-ascorbic acid to 2-furaldehyde. The Journal of Organic Chemistry 37(10) (1972): 1606-1608.
- [89] Feather, M.S. and Harris, J.F. On the mechanism of conversion of hexoses into 5-(hydroxymethyl)-2-furaldehyde and metasaccharinic acid. Carbohydrate Research 15(2) (1970): 304-309.

- [90] Harris, D.W. and Feather, M.S. Evidence for a C-2→C-1 intramolecular hydrogen-transfer during the acid-catalyzed isomerization of D-glucose to D-fructose ag]. Carbohydrate Research 30(2) (1973): 359-365.
- [91] Kabyemela, B.M., Adschiri, T., Malaluan, R.M., and Arai, K. Kinetics of Glucose Epimerization and Decomposition in Subcritical and Supercritical Water. Industrial & Engineering Chemistry Research 36(5) (1997): 1552-1558.
- [92] Graenacher, C. Cellulose solution. 1934, Chem, Ind Basel: United States.
- [93] Heinze, T., Schwikal, K., and Barthel, S. Ionic Liquids as Reaction Medium in Cellulose Functionalization. Macromolecular Bioscience 5(6) (2005): 520-525.
- [94] Xu, A., Zhang, Y., Zhao, Y., and Wang, J. Cellulose dissolution at ambient temperature: Role of preferential solvation of cations of ionic liquids by a cosolvent. Carbohydrate Polymers 92(1) (2013): 540-544.
- [95] Zavrel, M., Bross, D., Funke, M., Büchs, J., and Spiess, A.C. High-throughput screening for ionic liquids dissolving (ligno-)cellulose. Bioresource Technology 100(9) (2009): 2580-2587.
- [96] Wang, X., Li, H., Cao, Y., and Tang, Q. Cellulose extraction from wood chip in an ionic liquid 1-allyl-3-methylimidazolium chloride (AmimCl). Bioresource Technology 102(17) (2011): 7959-7965.
- [97] Zhao, D., et al. Dissolution of cellulose in phosphate-based ionic liquids. Carbohydrate Polymers 87(2) (2012): 1490-1494.
- [98] Xu, J.-K., Sun, Y.-C., and Sun, R.-C. Synergistic effects of ionic liquid plus alkaline pretreatments on eucalyptus: Lignin structure and cellulose hydrolysis. Process Biochemistry 50(6) (2015): 955-965.
- [99] Auxenfans, T., Buchoux, S., Djellab, K., Avondo, C., Husson, E., and Sarazin, C. Mild pretreatment and enzymatic saccharification of cellulose with recycled ionic liquids towards one-batch process. Carbohydrate Polymers 90(2) (2012): 805-813.
- [100] Kim, M.H., An, S., Won, K., Kim, H.J., and Lee, S.H. Entrapment of enzymes into cellulose–biopolymer composite hydrogel beads using biocompatible ionic liquid. Journal of Molecular Catalysis B: Enzymatic 75 (2012): 68-72.

- [101] Lee, H.-Y., Won, J.-E., Shin, U.S., and Kim, H.-W. Using hydrophilic ionic liquids as a facile route to prepare porous-structured biopolymer scaffolds. Materials Letters 65(14) (2011): 2114-2117.
- [102] Jing-Xian, C., et al. Catalytic fixation of CO₂ to cyclic carbonates over biopolymer chitosan-grafted quarternary phosphonium ionic liquid as a recyclable catalyst. Applied Catalysis A: General 484 (2014): 26-32.
- [103] Chaumont, A. and Wipff, G. Solvation of “big” spherical solutes in room temperature ionic liquids and at their aqueous interface: A molecular dynamics simulation study. Journal of Molecular Liquids 131–132 (2007): 36-47.
- [104] Ohno, H. Electrochemical Aspects of Ionic Liquids. John Wiley & Sons, Hoboken, NJ, USA, 2005.
- [105] Ohno, H., Yoshizawa, M., and Ogihara, W. Development of new class of ion conductive polymers based on ionic liquids. Electrochimica Acta 50(2–3) (2004): 255-261.
- [106] Rensing, R.C., Wildin, J.L., Rapp, A.L., and Moyna, G. Hydrogen Bonds in Ionic Liquids Revisited: ³⁵/³⁷Cl NMR Studies of Deuterium Isotope Effects in 1-n-Butyl-3-Methylimidazolium Chloride. The Journal of Physical Chemistry B 111(40) (2007): 11619-11621. 
- [107] Pinkert, A., Marsh, K.N., Pang, S., and Staiger, M.P. Ionic Liquids and Their Interaction with Cellulose. Chemical Reviews 109(12) (2009): 6712-6728.
- [108] Welton, T. Room-Temperature Ionic Liquids. Solvents for Synthesis and Catalysis. Chemical Reviews 99(8) (1999): 2071-2084.
- [109] Nishimura, Y., Yokogawa, D., and Irle, S. Theoretical study of cellobiose hydrolysis to glucose in ionic liquids. Chemical Physics Letters 603 (2014): 7-12.
- [110] Zhao, H., Holladay, J.E., Brown, H., and Zhang, Z.C. Metal Chlorides in Ionic Liquid Solvents Convert Sugars to 5-Hydroxymethylfurfural. Science 316(5831) (2007): 1597-1600.

- [111] Qian, X. and Wei, X. Glucose Isomerization to Fructose from ab Initio Molecular Dynamics Simulations. The Journal of Physical Chemistry B 116(35) (2012): 10898-10904.
- [112] Assary, R.S., Redfern, P.C., Greeley, J., and Curtiss, L.A. Mechanistic Insights into the Decomposition of Fructose to Hydroxy Methyl Furfural in Neutral and Acidic Environments Using High-Level Quantum Chemical Methods. The Journal of Physical Chemistry B 115(15) (2011): 4341-4349.
- [113] Liu, H., Sale, K.L., Holmes, B.M., Simmons, B.A., and Singh, S. Understanding the Interactions of Cellulose with Ionic Liquids: A Molecular Dynamics Study. The Journal of Physical Chemistry B 114(12) (2010): 4293-4301.
- [114] Remsing, R.C., Swatloski, R.P., Rogers, R.D., and Moyna, G. Mechanism of cellulose dissolution in the ionic liquid 1-n-butyl-3-methylimidazolium chloride: a ^{13}C and $^{35/37}\text{Cl}$ NMR relaxation study on model systems. Chemical Communications (12) (2006): 1271-1273.
- [115] Remsing, R.C., Liu, Z., Sergeyev, I., and Moyna, G. Solvation and Aggregation of N,N'-Dialkylimidazolium Ionic Liquids: A Multinuclear NMR Spectroscopy and Molecular Dynamics Simulation Study. The Journal of Physical Chemistry B 112(25) (2008): 7363-7369.
- [116] Ståhlberg, T., Rodriguez-Rodriguez, S., Fristrup, P., and Riisager, A. Metal-Free Dehydration of Glucose to 5-(Hydroxymethyl)furfural in Ionic Liquids with Boric Acid as a Promoter. Chemistry – A European Journal 17(5) (2011): 1456-1464.
- [117] Qian, X. Free Energy Surface for Brønsted Acid-Catalyzed Glucose Ring-Opening in Aqueous Solution. The Journal of Physical Chemistry B 117(39) (2013): 11460-11465.
- [118] Qian, X., Nimlos, M.R., Davis, M., Johnson, D.K., and Himmel, M.E. Ab initio molecular dynamics simulations of β -d-glucose and β -d-xylose degradation mechanisms in acidic aqueous solution. Carbohydrate Research 340(14) (2005): 2319-2327.
- [119] Parasuk, V. Quantum Mechanical Calculations and Applications in Chemistry. Bangkok, Thailand: Ideol Digital Printing Ltd., 2016.

- [120] Nisbet, H.B. J Inst Pet. 32 (1946): 162–166.
- [121] Roman-Leshkov, Y., Barrett, C.J., Liu, Z.Y., and Dumesic, J.A. Production of dimethylfuran for liquid fuels from biomass-derived carbohydrates. Nature 447(7147) (2007): 982-985.
- [122] Truhlar, D.G., Garrett, B.C., and Klippenstein, S.J. Current Status of Transition-State Theory. The Journal of Physical Chemistry 100(31) (1996): 12771-12800.
- [123] Koga, N. and Morokuma, K. Ab initio molecular orbital studies of catalytic elementary reactions and catalytic cycles of transition-metal complexes. Chemical Reviews 91(5) (1991): 823-842.
- [124] Niu, S. and Hall, M.B. Theoretical Studies on Reactions of Transition-Metal Complexes. Chemical Reviews 100(2) (2000): 353-406.
- [125] Torrent, M., Solà, M., and Frenking, G. Theoretical Studies of Some Transition-Metal-Mediated Reactions of Industrial and Synthetic Importance. Chemical Reviews 100(2) (2000): 439-494.
- [126] Ziegler, T. and Autschbach, J. Theoretical Methods of Potential Use for Studies of Inorganic Reaction Mechanisms. Chemical Reviews 105(6) (2005): 2695-2722.
- [127] Houk, K.N. and Cheong, P.H.-Y. Computational prediction of small-molecule catalysts. Nature 455(7211) (2008): 309-313.
- [128] Tanaka, A., Maekawa, K., and Suzuki, K. Theoretical Calculations in Reaction Mechanism Studies. 2013, Organic Synthesis Research Laboratory, Sumitomo Chemical Co., Ltd.: Japan. 43-52.
- [129] Jensen, F. Introduction to Computational Chemistry. 2 ed. England: John Wiley & Sons Ltd, 2007.
- [130] Mark, A.R. and Geoge, C.S. Quantum Mechanics. in Introduction to Quantum Mechanics in Chemistry New Jersey: Prentice, 2000.
- [131] Poompub, U. Structure and Acidities of HZSM-5 with Si/Al Ratio of 47 and 95. Master Degree, Petrochemistry and Polymer Science, Faculty of Science Chulalongkorn University, 2004.

- [132] Szabo, A. and Ostlund, N.S. The Born-Oppenheimer Approximation. in Modern Quantum Chemistry: Introduction to Advanced Electronic Structure Theory. New York: MacMillan Publishing Co., 1982.
- [133] Atkins, P. and Friedman, R. Molecular Quantum Mechanics. 4 ed. New York: Oxford University Press, 2005.
- [134] Bartlett, R.J. Coupled-cluster approach to molecular structure and spectra: a step toward predictive quantum chemistry. The Journal of Physical Chemistry 93(5) (1989): 1697-1708.
- [135] Jankunas, J., et al. Is the simplest chemical reaction really so simple? Proceedings of the National Academy of Sciences of the United States of America 111(1) (2014): 15-20.
- [136] Hayes, D.M. and Morokuma, K. Theoretical studies of carbonyl photochemistry. I. ab initio potential energy surfaces for the photodissociation $\text{H}_2\text{CO}^* \rightarrow \text{H} + \text{HCO}$. Chemical Physics Letters 12(4) (1972): 539-543.
- [137] Jaffe, R.L., Hayes, D.M., and Morokuma, K. Photodissociation of formaldehyde: Potential energy surfaces for $\text{H}_2\text{CO} \rightarrow \text{H}_2 + \text{CO}$. The Journal of Chemical Physics 60(12) (1974): 5108-5109.
- [138] Černohorský, M., Kettou, S., and Koča, J. VADER: New Software for Exploring Interconversions on Potential Energy Surfaces. Journal of Chemical Information and Computer Sciences 39(4) (1999): 705-712.
- [139] Laio, A. and Parrinello, M. Escaping free-energy minima. Proceedings of the National Academy of Sciences of the United States of America 99(20) (2002): 12562-12566.
- [140] Ensing, B., De Vivo, M., Liu, Z., Moore, P., and Klein, M.L. Metadynamics as a Tool for Exploring Free Energy Landscapes of Chemical Reactions. Accounts of Chemical Research 39(2) (2006): 73-81.
- [141] Burger, S.K. and Ayers, P.W. Dual Grid Methods for Finding the Reaction Path on Reduced Potential Energy Surfaces. Journal of Chemical Theory and Computation 6(5) (2010): 1490-1497.

- [142] Maeda, S. and Morokuma, K. Communications: A systematic method for locating transition structures of $A+B\rightarrow X$ type reactions. The Journal of Chemical Physics 132(24) (2010): 241102.
- [143] Maeda, S. and Morokuma, K. Finding Reaction Pathways of Type $A + B \rightarrow X$: Toward Systematic Prediction of Reaction Mechanisms. Journal of Chemical Theory and Computation 7(8) (2011): 2335-2345.
- [144] Collins, A.M. Molecular potential-energy surfaces for chemical reaction dynamics. Theoretical Chemistry Accounts 108(6) (2002): 313-324.
- [145] Maeda, S., Komagawa, S., Uchiyama, M., and Morokuma, K. Finding Reaction Pathways for Multicomponent Reactions: The Passerini Reaction is a Four-Component Reaction. Angewandte Chemie International Edition 50(3) (2011): 644-649.
- [146] Tomasi, J., Mennucci, B., and Cammi, R. Quantum Mechanical Continuum Solvation Models. Chemical Reviews 105(8) (2005): 2999-3094.
- [147] Chandler, D. and Andersen, H.C. Optimized Cluster Expansions for Classical Fluids. II. Theory of Molecular Liquids. The Journal of Chemical Physics 57(5) (1972): 1930-1937.
- [148] Hirata, F. and Rossky, P.J. An extended rism equation for molecular polar fluids. Chemical Physics Letters 83(2) (1981): 329-334.
- [149] Maw, S.A., Bryce, R.A., Hall, R.J., Masters, A.J., and Hillier, I.H. Integral Equation and ab Initio Study of the Effect of Solvation on Anomeric Equilibria in Aqueous Solution: Application to 4,6-Dimethyl-2-methoxytetrahydropyran. The Journal of Physical Chemistry B 102(21) (1998): 4089-4095.
- [150] Miyata, T. Reference interaction site model study on the anomeric equilibrium of D-glucose in aqueous solution Condensed Matter Physics 1 (2007): 433-440.
- [151] Hayaki, S., Kido, K., Yokogawa, D., Sato, H., and Sakaki, S. A Theoretical Analysis of a Diels–Alder Reaction in Ionic Liquids. The Journal of Physical Chemistry B 113(24) (2009): 8227-8230.

- [152] Hayaki, S., Kido, K., Sato, H., and Sakaki, S. Ab initio study on SN2 reaction of methyl p-nitrobenzenesulfonate and chloride anion in [mmim][PF6]. Physical Chemistry Chemical Physics 12(8) (2010): 1822-1826.
- [153] Iida, K., Yokogawa, D., Ikeda, A., Sato, H., and Sakaki, S. Carbon dioxide capture at the molecular level. Physical Chemistry Chemical Physics 11(38) (2009): 8556-8559.
- [154] Yokogawa, D., Sato, H., and Sakaki, S. New generation of the reference interaction site model self-consistent field method: Introduction of spatial electron density distribution to the solvation theory. The Journal of Chemical Physics 126(24) (2007): 244504.
- [155] Ten-no, S., Hirata, F., and Kato, S. Reference interaction site model self-consistent field study for solvation effect on carbonyl compounds in aqueous solution. The Journal of Chemical Physics 100(10) (1994): 7443-7453.
- [156] Sato, H., Hirata, F., and Kato, S. Analytical energy gradient for the reference interaction site model multiconfigurational self-consistent-field method: Application to 1,2-difluoroethylene in aqueous solution. The Journal of Chemical Physics 105(4) (1996): 1546-1551.
- [157] Kovalenko, A. and Hirata, F. Self-consistent description of a metal-water interface by the Kohn-Sham density functional theory and the three-dimensional reference interaction site model. The Journal of Chemical Physics 110(20) (1999): 10095-10112.
- [158] Maeda, S., Ohno, K., and Morokuma, K. Systematic exploration of the mechanism of chemical reactions: the global reaction route mapping (GRRM) strategy using the ADDF and AFIR methods. Physical Chemistry Chemical Physics 15(11) (2013): 3683-3701.
- [159] Cossi, M., Barone, V., Mennucci, B., and Tomasi, J. Ab initio study of ionic solutions by a polarizable continuum dielectric model. Chemical Physics Letters 286(3-4) (1998): 253-260.

- [160] Cossi, M., Barone, V., Cammi, R., and Tomasi, J. Ab initio study of solvated molecules: a new implementation of the polarizable continuum model. Chemical Physics Letters 255(4-6) (1996): 327-335.
- [161] Fukui, K. Formulation of the reaction coordinate. The Journal of Physical Chemistry 74(23) (1970): 4161-4163.
- [162] Ishida, K., Morokuma, K., and Komornicki, A. The intrinsic reaction coordinate. An abinitio calculation for $\text{HNC} \rightarrow \text{HCN}$ and $\text{H}^- + \text{CH}_4 \rightarrow \text{CH}_4 + \text{H}^-$. The Journal of Chemical Physics 66(5) (1977): 2153-2156.
- [163] Ohno, K. and Maeda, S. Automated exploration of reaction channels. Physica Scripta 78(5) (2008): 058122.
- [164] Ohno, K. and Maeda, S. A scaled hypersphere search method for the topography of reaction pathways on the potential energy surface. Chemical Physics Letters 384(4-6) (2004): 277-282.
- [165] Frisch, M.J., et al. Gaussian 09. in revision D.01. 2009, Gaussian Inc.: Wallingford, CT.
- [166] Xiang, Q., Lee, Y.Y., and Torget, R.W. Kinetics of glucose decomposition during dilute-acid hydrolysis of lignocellulosic biomass. Appl. Biochem. Biotechnol. 113-116 (2004): 1127-1138.
- [167] Qi, J. and Xiuyang, L. Kinetics of Non-catalyzed Decomposition of Glucose in High-temperature Liquid Water. Chin.J.Chem.Eng. 16(6) (2008): 890-894.
- [168] Li, Y., Lu, X., Yuan, L., and Liu, X. Fructose decomposition kinetics in organic acids-enriched high temperature liquid water. Biomass and Bioenergy 33(9) (2009): 1182-1187.
- [169] Damm, W., Frontera, A., Tirado-Rives, J., and Jorgensen, W.L. OPLS all-atom force field for carbohydrates. Journal of Computational Chemistry 18(16) (1997): 1955-1970.
- [170] Berendsen, H.J.C., Postma, J.P.M., Gunsteren, W.F., and Hermans, J. Interaction Models for Water in Relation to Protein Hydration. in Pullman, B. (ed.) Intermolecular Forces: Proceedings of the Fourteenth Jerusalem Symposium on Quantum Chemistry and Biochemistry Held in Jerusalem, Israel, April 13-16, 1981, pp. 331-342. Dordrecht: Springer Netherlands, 1981.

- [171] Yokogawa, D., Sato, H., and Sakaki, S. Analytical energy gradient for reference interaction site model self-consistent field explicitly including spatial electron density distribution. The Journal of Chemical Physics 131(21) (2009): 214504.
- [172] Schmidt, M.W., et al. General atomic and molecular electronic structure system. Journal of Computational Chemistry 14(11) (1993): 1347-1363.
- [173] Holden, M.S. and Crouch, R.D. The Biginelli Reaction. Journal of Chemical Education 78(8) (2001): 1104.
- [174] Damkaci, F. and Szymaniak, A. Multicomponent Heterocyclic Chemistry for Undergraduate Organic Laboratory: Biginelli Reaction with Multiple Unknowns. Journal of Chemical Education 91(6) (2014): 943-945.
- [175] Li, N., Chen, X.-H., Song, J., Luo, S.-W., Fan, W., and Gong, L.-Z. Highly Enantioselective Organocatalytic Biginelli and Biginelli-Like Condensations: Reversal of the Stereochemistry by Tuning the 3,3'-Disubstituents of Phosphoric Acids. Journal of the American Chemical Society 131(42) (2009): 15301-15310.
- [176] Campbell, J.L. and Johnson, K.E. The Ternary HCl : ImCl : AlCl₃ Ambient-Temperature Molten Salt System: Expansion of the Electrochemical Window on Proton Addition to a Weakly Basic Ionic Liquid. Journal of The Electrochemical Society 141(3) (1994): L19-L21.
- [177] Aldous, L., Silvester, D.S., Pitner, W.R., Compton, R.G., Lagunas, M.C., and Hardacre, C. Voltammetric Studies of Gold, Protons, and [HCl₂]⁻ in Ionic Liquids. The Journal of Physical Chemistry C 111(24) (2007): 8496-8503.
- [178] Trulove, P.C. and Osteryoung, R.A. Proton speciation in ambient-temperature chloroaluminate ionic liquids. Inorganic Chemistry 31(19) (1992): 3980-3985.
- [179] Pópolo, M.G.D., Kohanoff, J., and Lynden-Bell, R.M. Solvation Structure and Transport of Acidic Protons in Ionic Liquids: A First-principles Simulation Study. The Journal of Physical Chemistry B 110(17) (2006): 8798-8803.
- [180] Silvester, D.S., Aldous, L., Hardacre, C., and Compton, R.G. An Electrochemical Study of the Oxidation of Hydrogen at Platinum Electrodes in Several Room

- Temperature Ionic Liquids. The Journal of Physical Chemistry B 111(18) (2007): 5000-5007.
- [181] Olivier-Bourbigou, H., Magna, L., and Morvan, D. Ionic liquids and catalysis: Recent progress from knowledge to applications. Applied Catalysis A: General 373(1–2) (2010): 1-56.
- [182] Sato, H. and Hirata, F. The syn-/anti-conformational equilibrium of acetic acid in water studied by the RISM-SCF/MCSCF method1. Journal of Molecular Structure: THEOCHEM 461–462 (1999): 113-120.
- [183] Hayaki, S., Yokogawa, D., Sato, H., and Sakaki, S. Solvation effects in oxidative addition reaction of Methyl iodide to Pt(II) complex: A theoretical study with RISM–SCF method. Chemical Physics Letters 458(4–6) (2008): 329-332.
- [184] van Putten, R.-J., van der Waal, J.C., de Jong, E., Rasrendra, C.B., Heeres, H.J., and de Vries, J.G. Hydroxymethylfurfural, A Versatile Platform Chemical Made from Renewable Resources. Chemical Reviews 113(3) (2013): 1499-1597.
- [185] Bruzzzone, S., Malvaldi, M., and Chiappe, C. Solvation thermodynamics of alkali and halide ions in ionic liquids through integral equations. The Journal of Chemical Physics 129(7) (2008): 074509.
- [186] Chandrasekhar, J., Spellmeyer, D.C., and Jorgensen, W.L. Energy component analysis for dilute aqueous solutions of lithium(1+), sodium(1+), fluoride(1-), and chloride(1-) ions. Journal of the American Chemical Society 106(4) (1984): 903-910.



APPENDIX

จุฬาลงกรณ์มหาวิทยาลัย
CHULALONGKORN UNIVERSITY

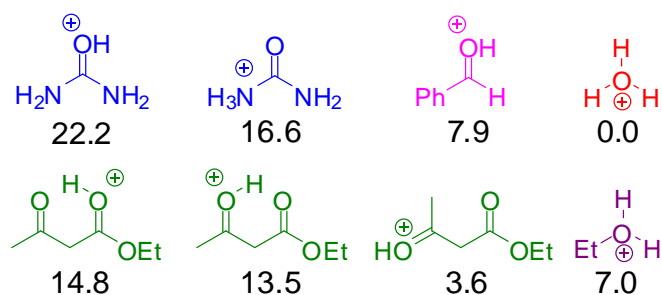


Figure S1 Proton Affinity (Gibbs free energy in kcal mol⁻¹) in PCM ethanol with respect to H₃O⁺ at the M06-2X/6-31+G(d) level.

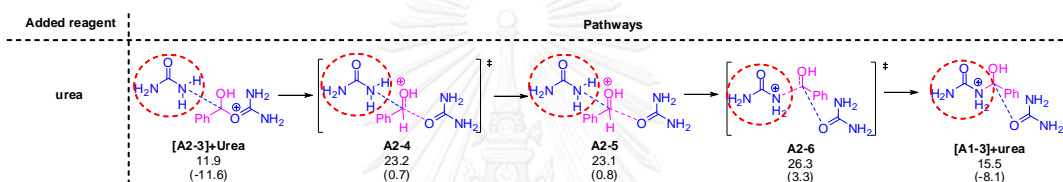


Figure S2 Detailed mechanism with a second urea (in red circle) to the intermediate **A2-3** and leading to product **A1-3**. Gibbs free energies (P=1 atm, T=298.15 K) (energies with ZPE correction in parentheses), in kcal mol⁻¹ relative to individual reactants, were obtained at the M06-2X/6-31+G(d) level in PCM (ethanol).

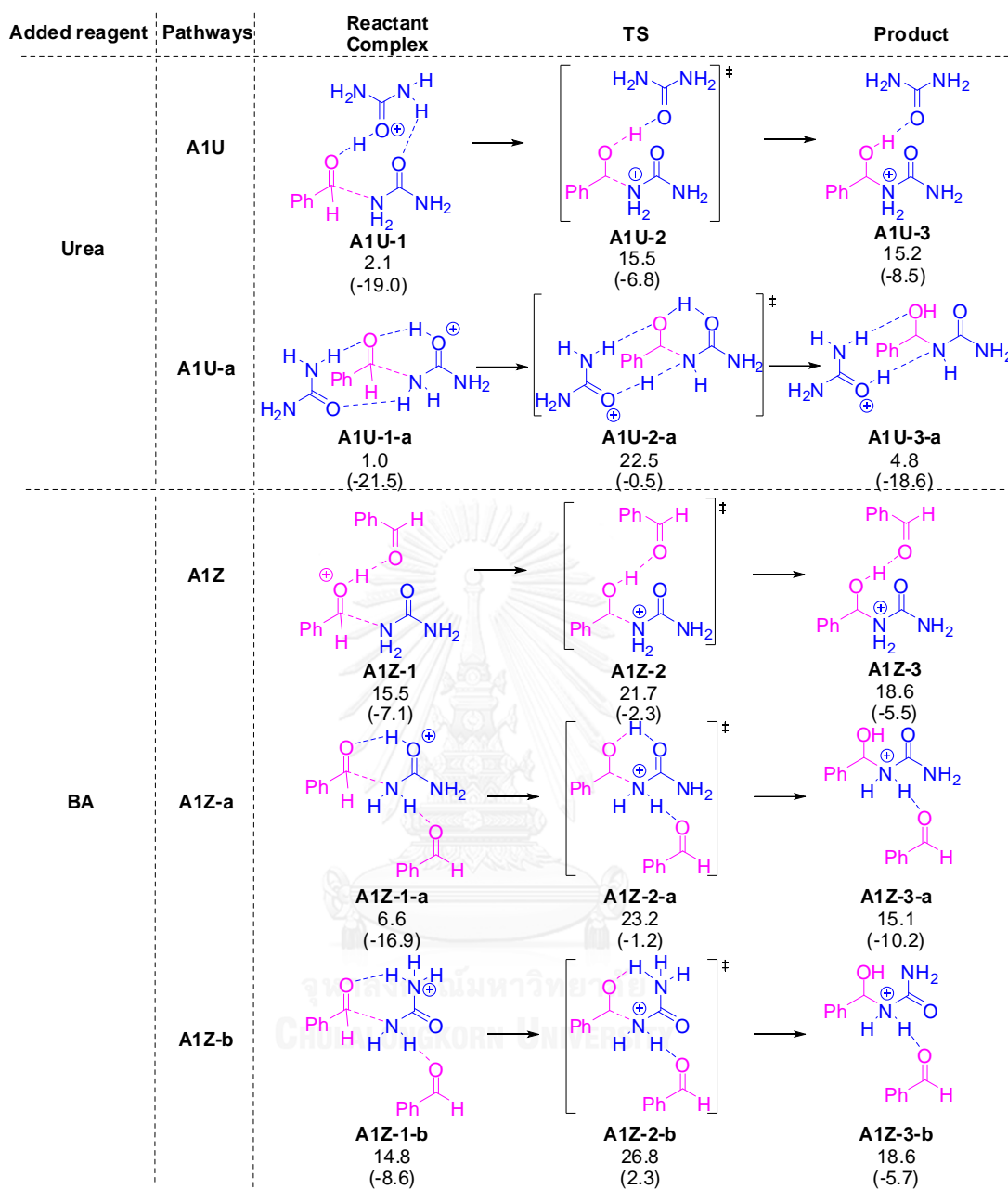


Figure S3 The obtained three-component pathways for Step I (C-N bond formation) with an extra urea and benzaldehyde for Route A. See Figure S2 for computational details.

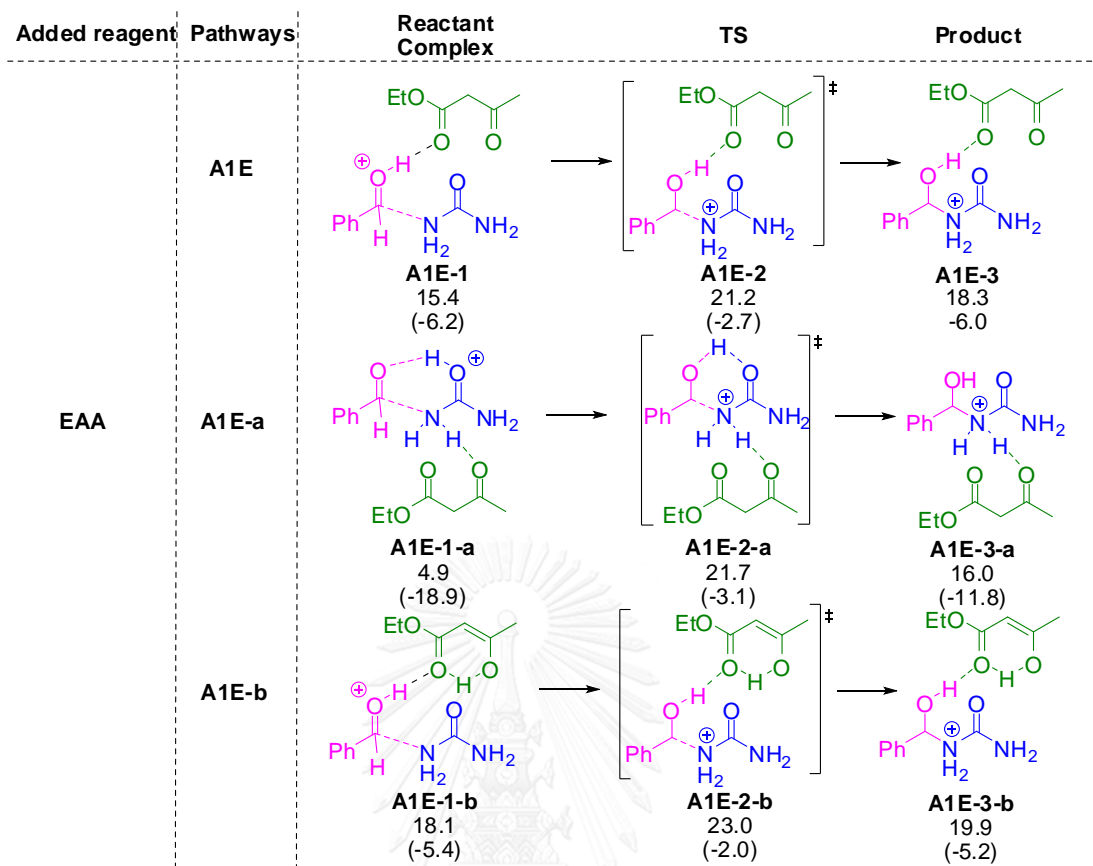


Figure S4 The obtained three-component pathways for Step I (C-N bond formation) with an extra ethyl acetoacetate for Route A. See Figure S2 for computational details.

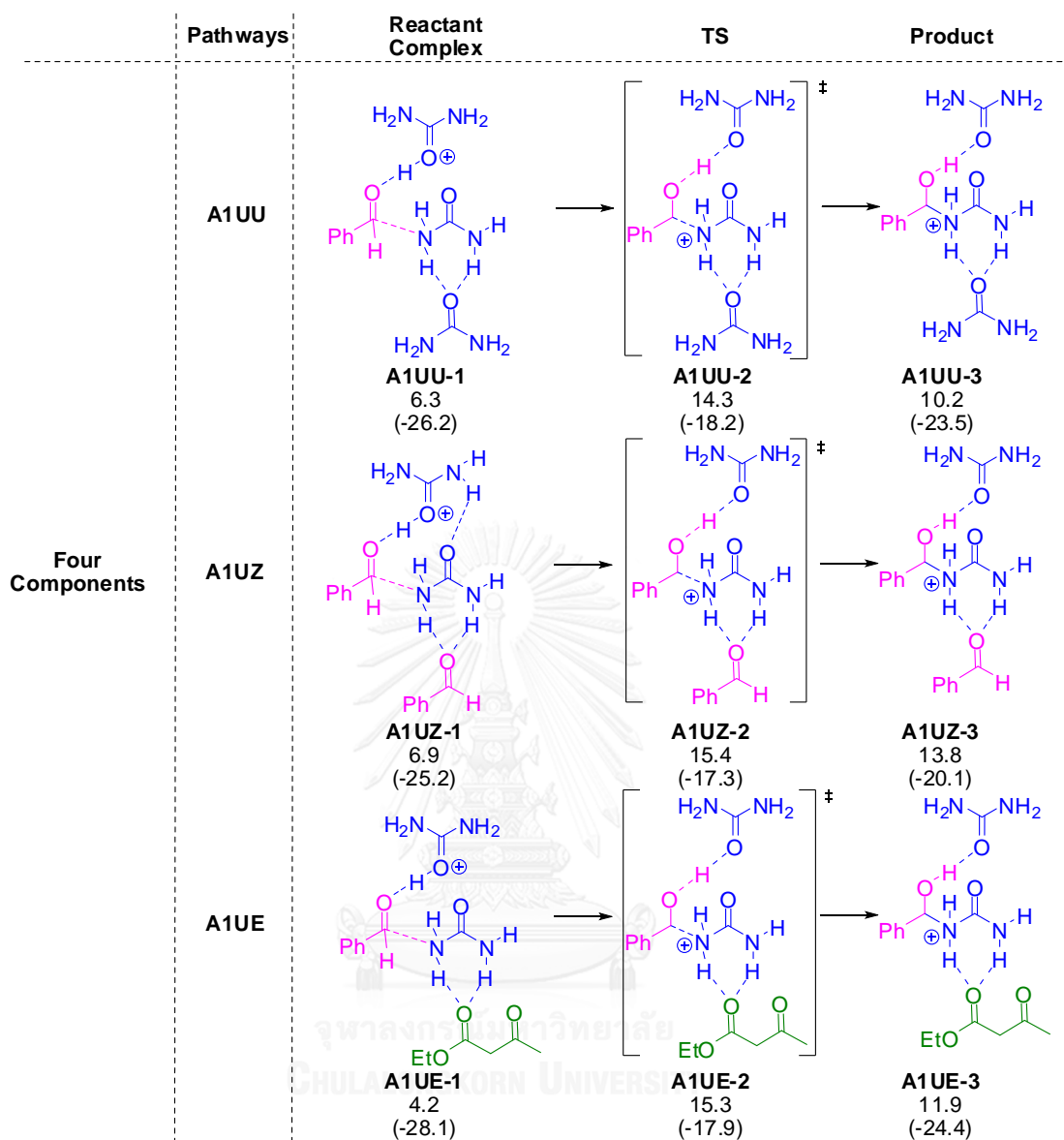


Figure S5 Pathways for Step I (C-N bond formation) with four components for Route A. See Figure S2 for computational details.

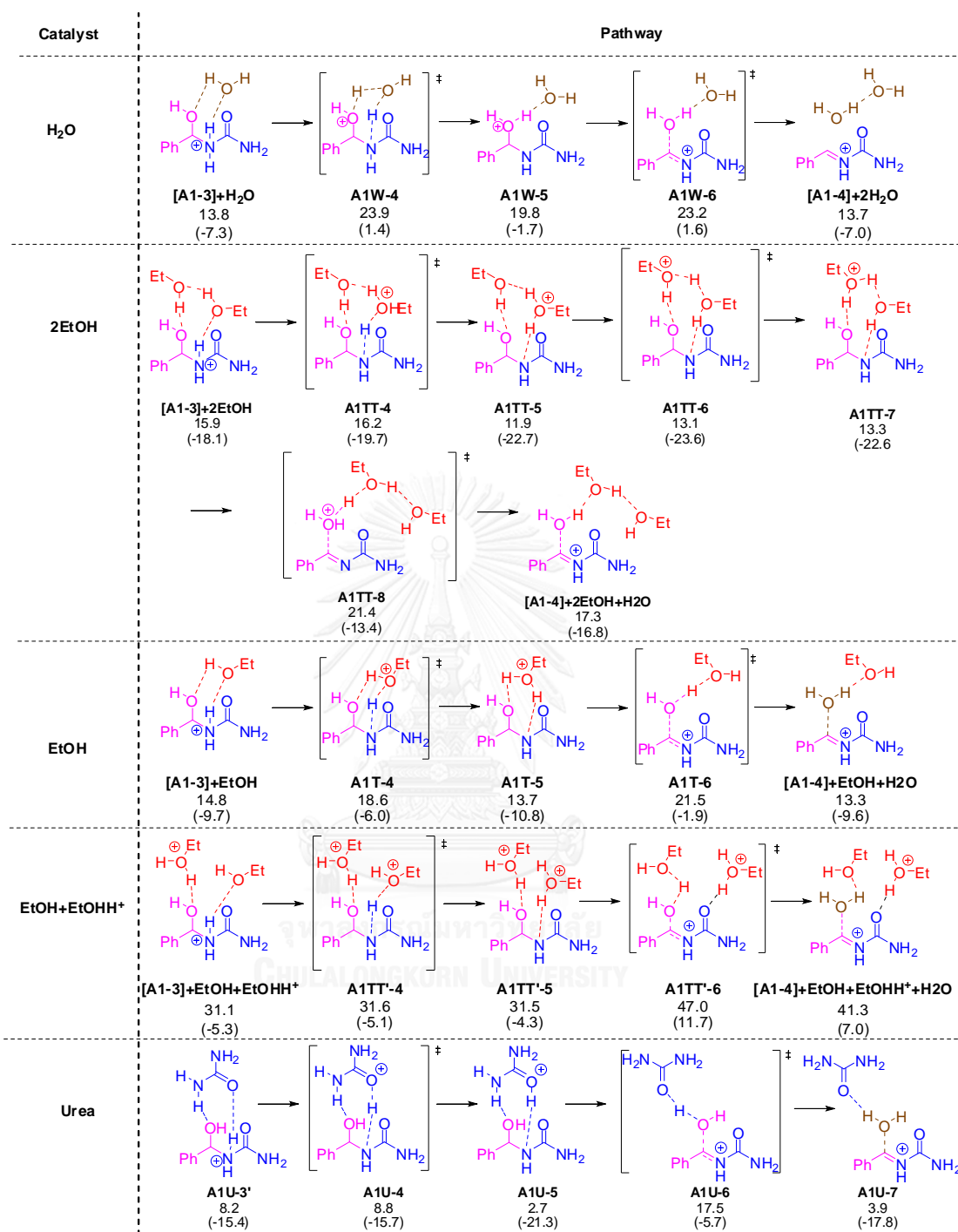


Figure S6 Detailed mechanism of Step II (Dehydration) of Route A with different catalysts. See Figure S2 for computational details.

Table S1 Activation energy difference of Step II (Dehydration) of Route **A** with different catalysts at the M06-2X/6-31+G(d) level. All energies are relative to the activation energy of reaction using urea+ ethyl acetoacetate (EAA) as catalysts.

Catalyst	$\Delta\Delta G$ (kcal mol ⁻¹)	$\Delta\Delta(E+ZPE)$ (kcal mol ⁻¹)
H ₂ O	7.3	20.2
EtOH	4.9	16.9
2EtOH	4.7	5.5
EtOH+EtOHH ⁺	30.4	30.5
urea	0.8	13.2
urea+EAA	0.0	0.0

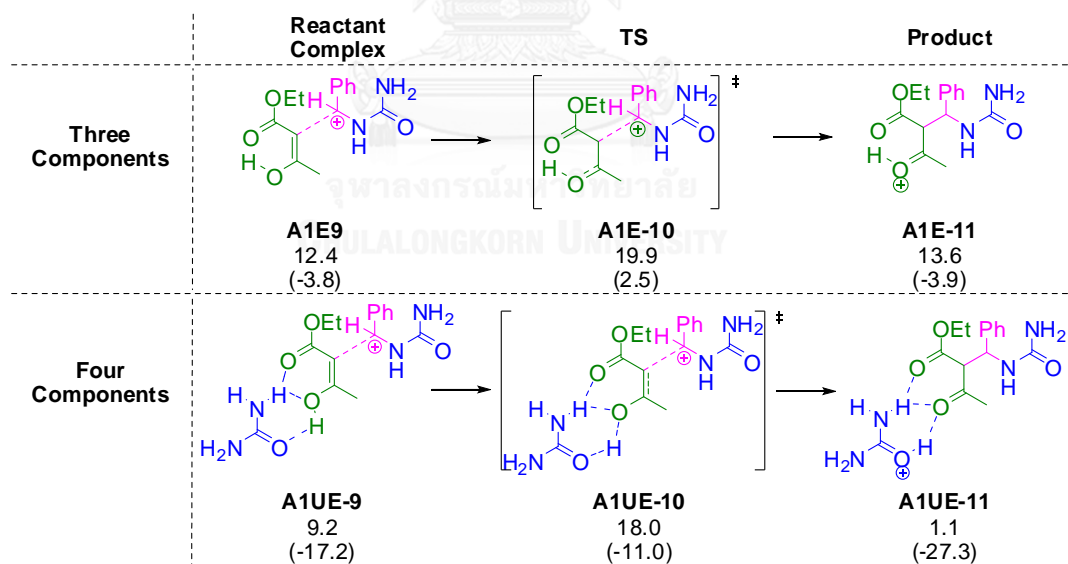


Figure S7 Pathways for Step III (Bond formation with ethyl acetoacetate) with three and four components for Route **A**. See Figure S2 for computational details.

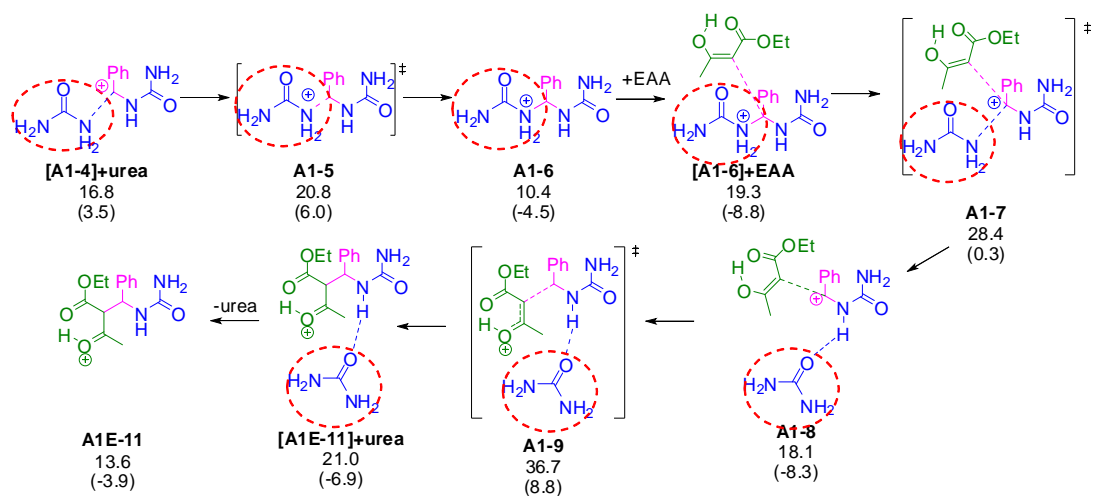


Figure S8 Detailed mechanism for Step III (C-C bond formation) passing through a diurea derivative (**A1-6**) leading to product **A1E-11**. See Figure S2 for computational details.

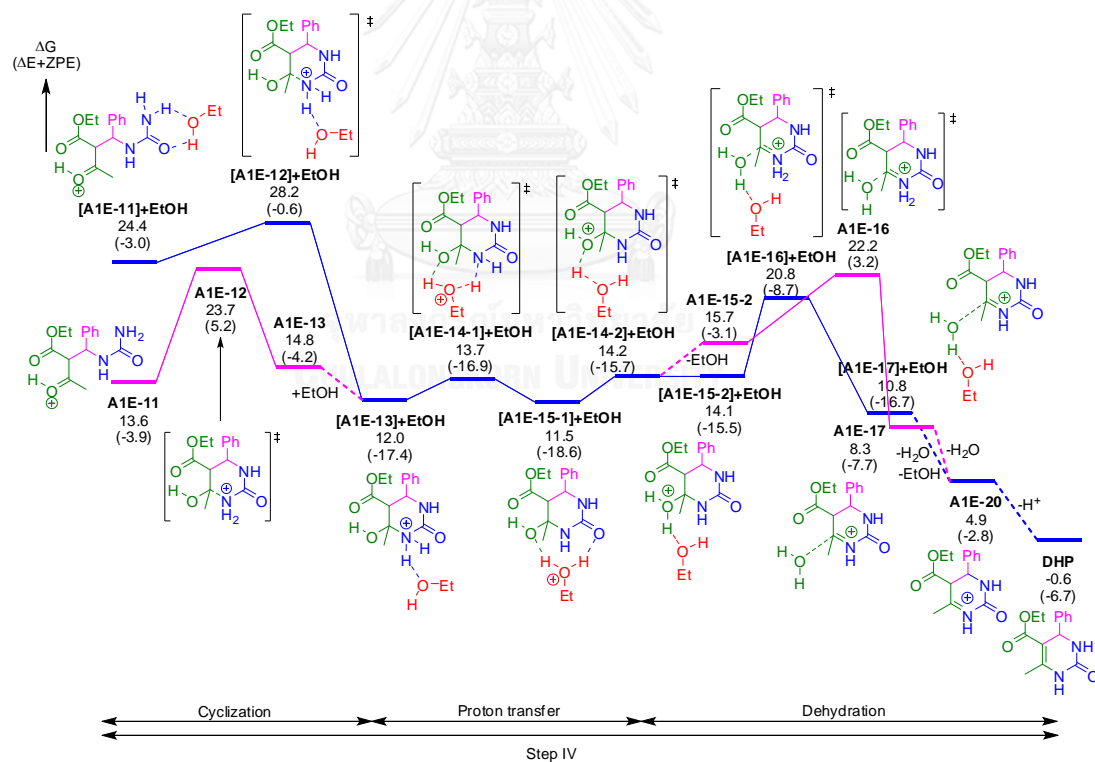


Figure S9 Gibbs Free energy profiles for Step IV (Route A) in ethanol. See Figure S2 for computational details.

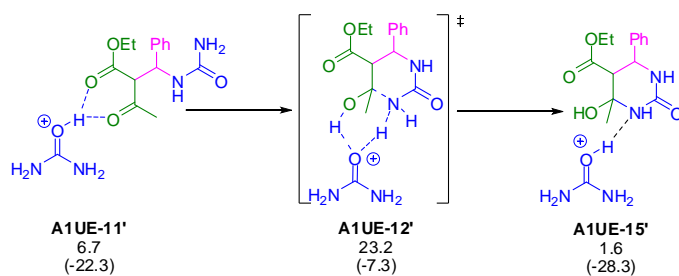


Figure S10 Additional concerted pathway of cyclization step for Route **A** from **A1UE-11'** to **A1UE-15'** which does not go through **A1UE-13**. See Figure S2 for computational details.

Table S2 The energies (in kcal mol⁻¹) of the transition states of the rate-determining step for the different routes with para-substitution on aryl ring of benzaldehyde, were obtained at the M06-2X/6-31+G(d) level in PCM ethanol.

Route: Rate-Determining Step	Para-substitution on aryl ring	ΔG^\ddagger
Route A : Cyclization/C-N bond formation (A1UE-12)	W/O	21.5
	NO ₂	23.0
	OMe	23.1
Route B : Cyclization/C-N bond formation (B1UZ-17)	W/O	31.2
	NO ₂	33.7
	OMe	29.2
Route C : C-N bond formation (C1UU-6)	W/O	28.0
	NO ₂	28.3
	OMe	29.0

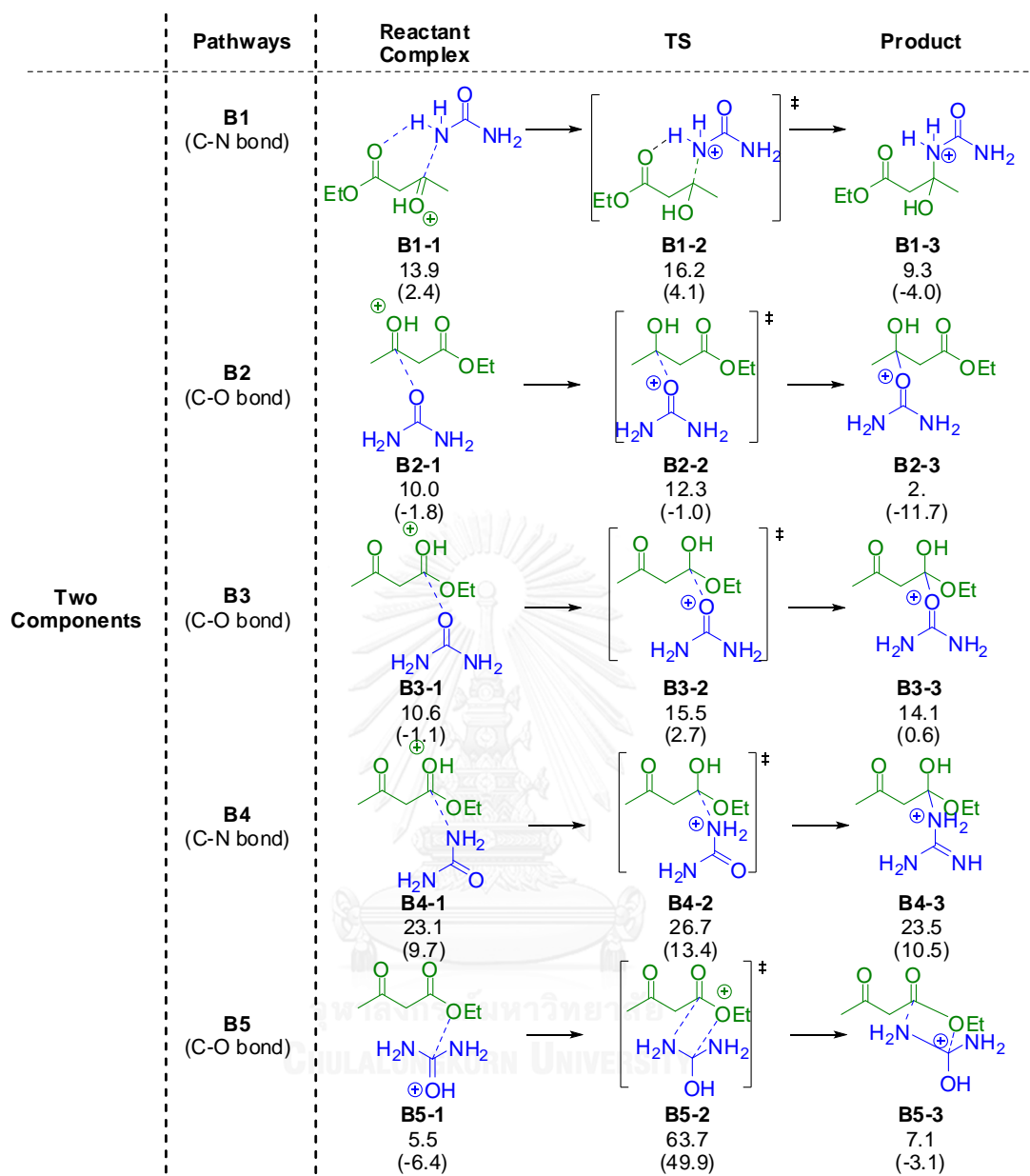


Figure S11 All obtained initial association pathways for Route **B**. See Figure S2 for computational details.

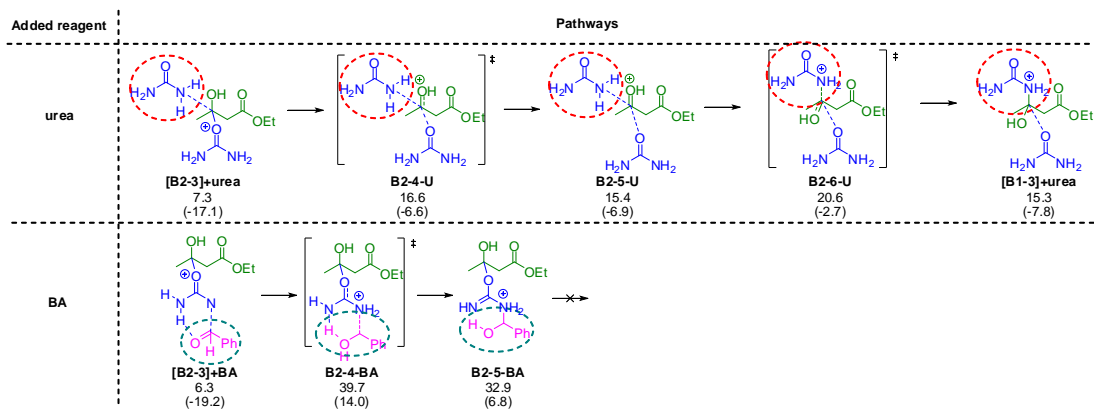


Figure S12 Detailed mechanism with an additional urea (in red circle) and benzaldehyde (BA) (in blue circle) to the intermediate **B2-3** and leading to product **B1-3**. See Figure S2 for computational details.

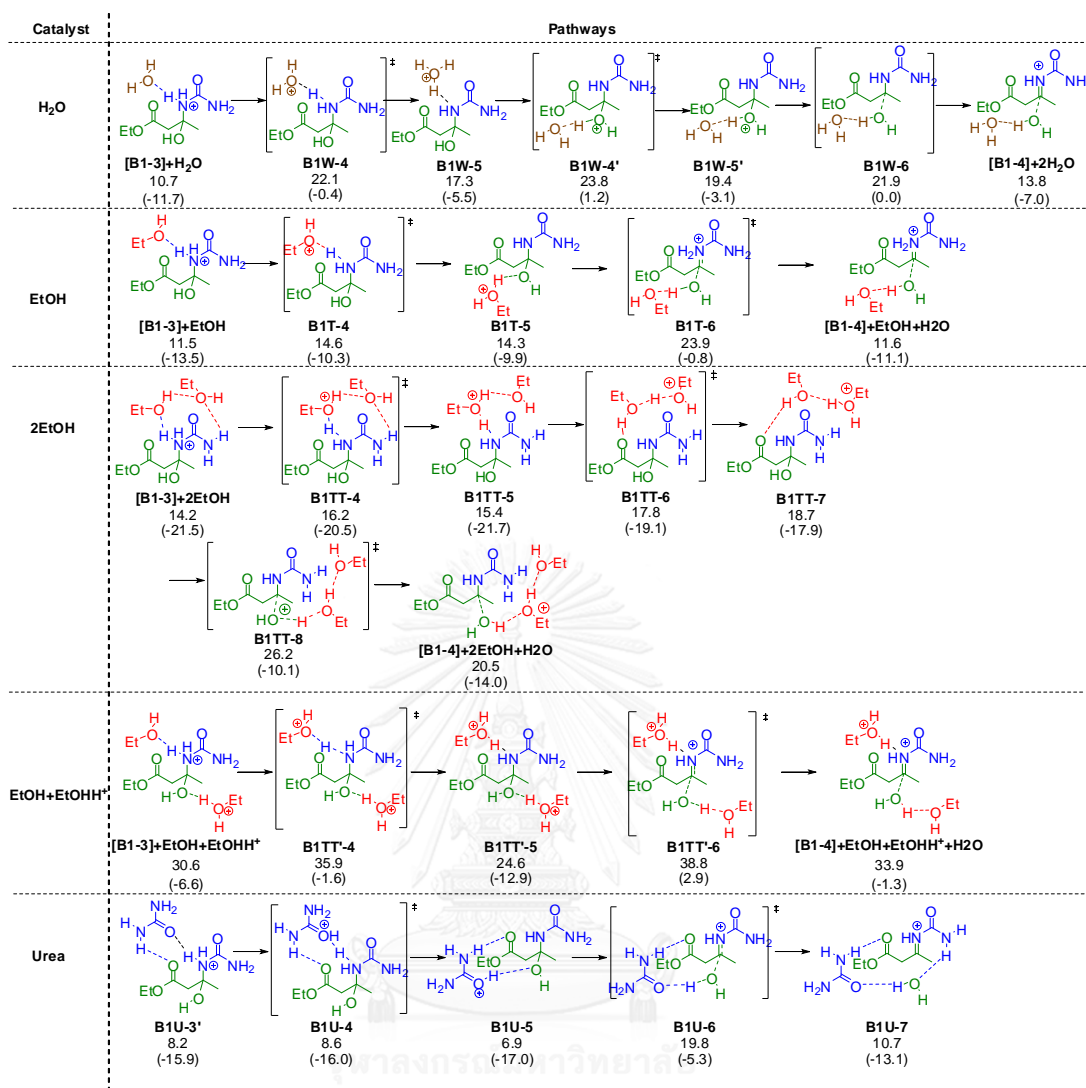


Figure S13 Detailed mechanism for Step II (Dehydration) of Route B with different catalysts. See Figure S2 for computational details.

Table S3 Activation energy difference for Step II (Dehydration) of Route **B** with different catalysts at the M06-2X/6-31+G(d) level. All energies are relative to the activation energy of reaction using urea as a catalyst.

Catalyst	$\Delta\Delta G$ (kcal mol ⁻¹)	$\Delta\Delta$ (E+ZPE) (kcal mol ⁻¹)
H ₂ O	4.1	6.5
EtOH	4.1	4.5
2EtOH	6.4	4.8
EtOH+EtOHH ⁺	19.0	8.2
urea	0.0	0.0
urea+BA	1.7	-7.6

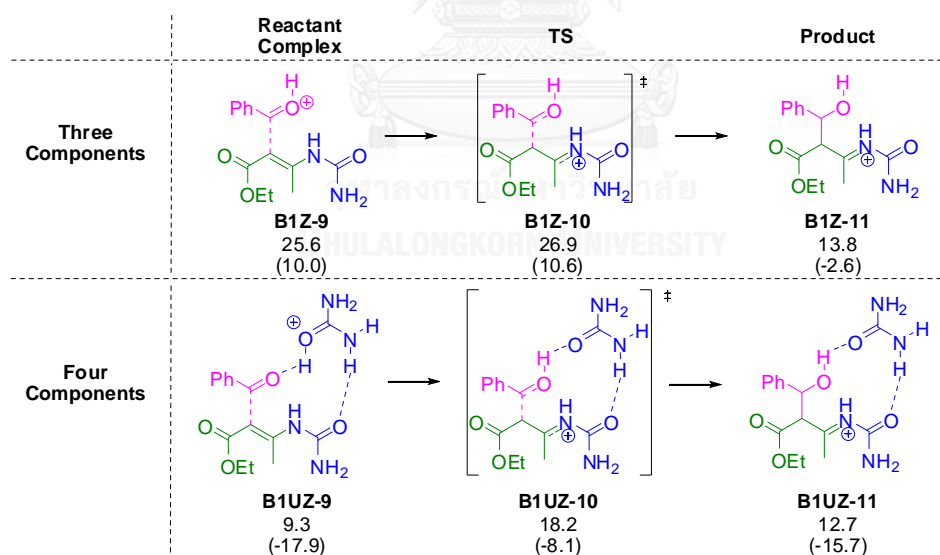


Figure S14 Pathways for Step III (Bond formation with benzaldehyde) with three and four components for Route **B**. See Figure S2 for computational details.

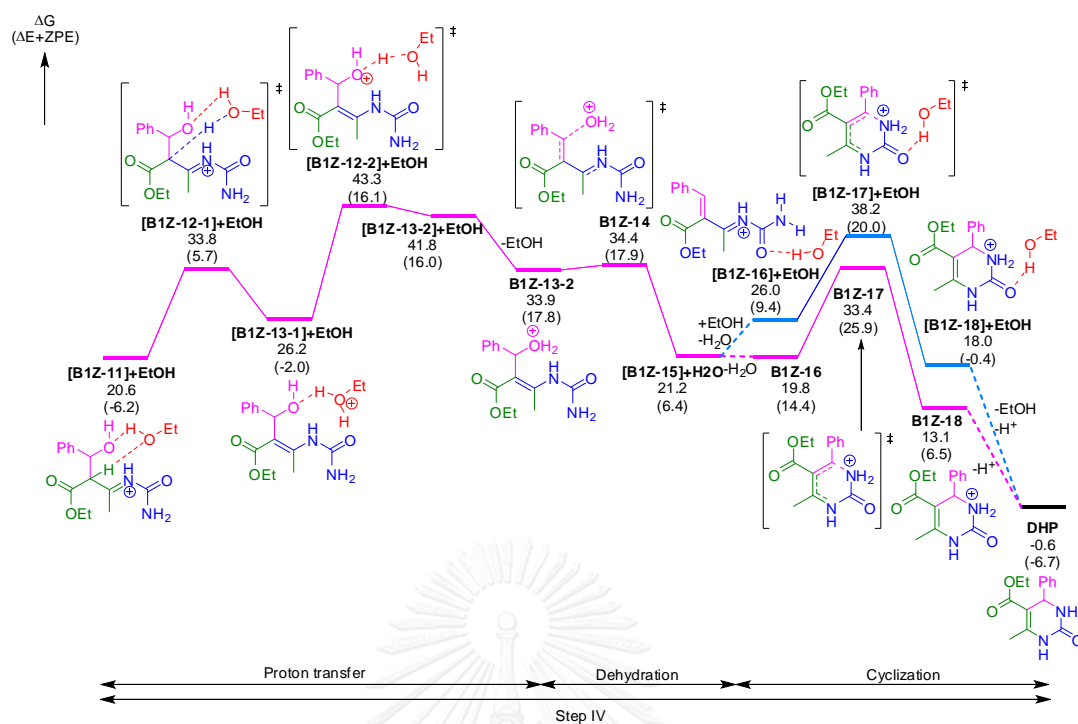


Figure S15 Gibbs Free energy profiles for Step IV (Route B) in ethanol. See Figure S2 for computational details.

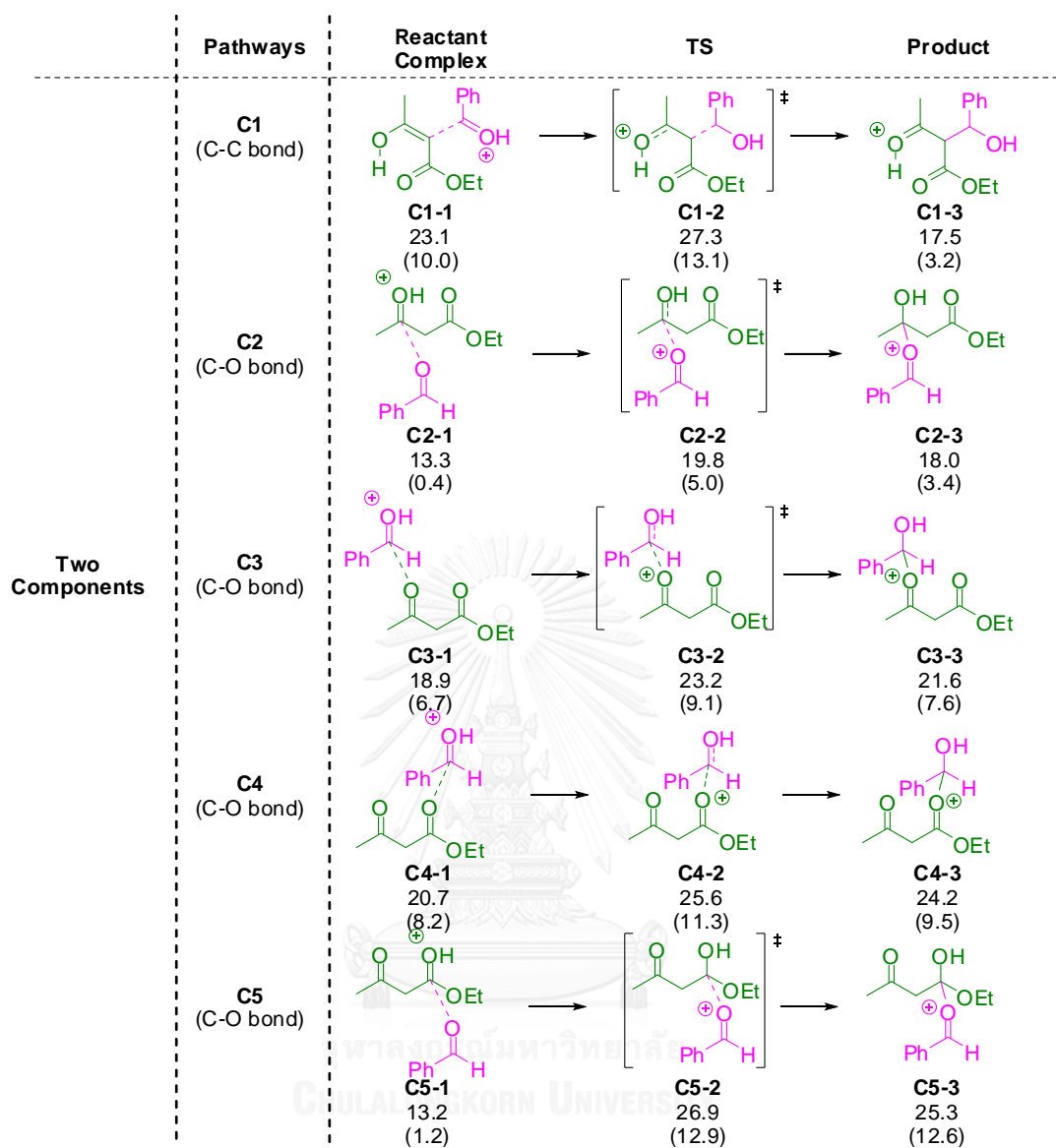


Figure S16 All obtained initial association pathways for Route C. See Figure S2 for computational details

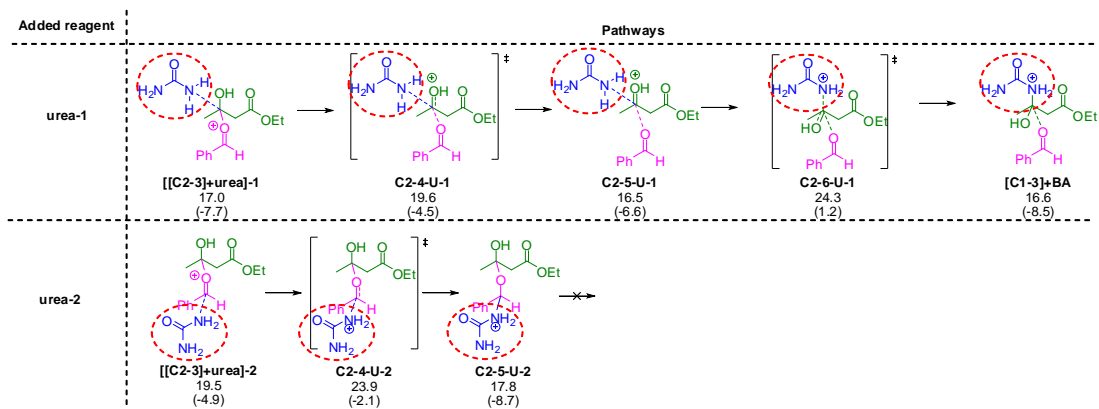


Figure S17 Detailed mechanism of adding a second urea (in red circle) to the intermediate **C2-3** leading to product **C1-3**. See Figure S2 for computational details.



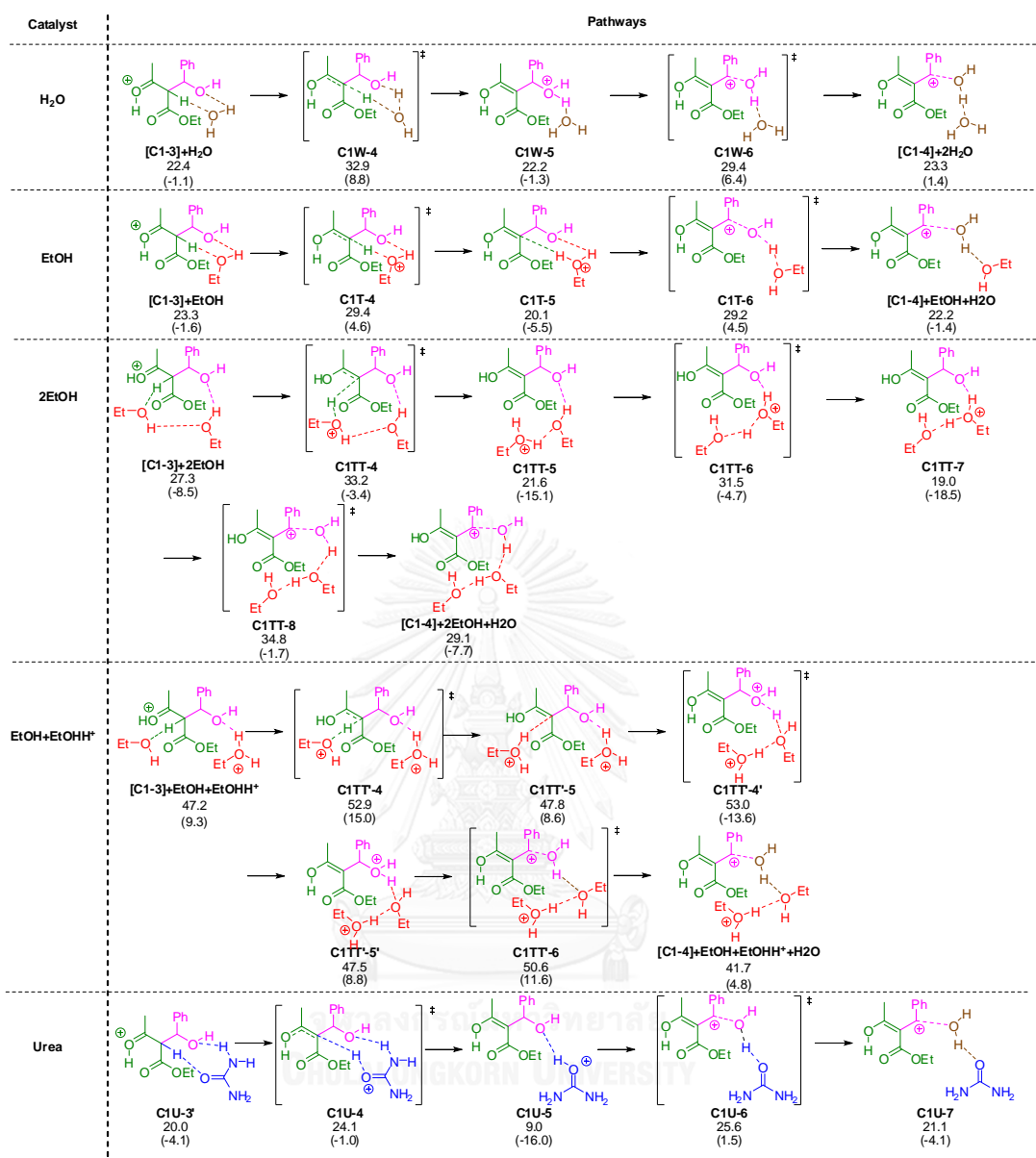


Figure S18 Detailed mechanism of Step II (Dehydration) of Route C with different catalysts. See Figure S2 for computational details.

Table S4 Activation energy difference of Step II (Dehydration) of Route **C** with different catalysts at M06-2X/6-31+G(d) level. All energies are relative to the activation energy of reaction using urea as a catalyst.

Catalyst	$\Delta\Delta G$ (kcal mol ⁻¹)	$\Delta\Delta(E+ZPE)$ (kcal mol ⁻¹)
H ₂ O	7.3	7.3
EtOH	3.8	3.1
2EtOH	9.2	3.2
EtOH+EtOHH ⁺	27.4	12.1
urea	0.0	0.0
2urea	2.4	-10.8

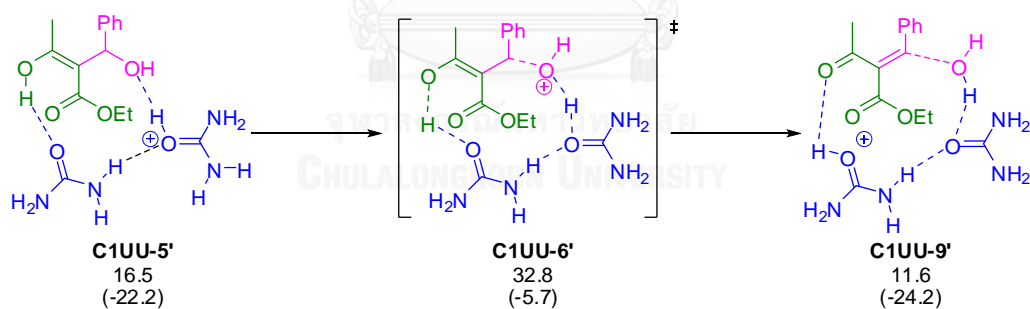


Figure S19 Additional concerted pathway of dehydration step for Route **C** from **C1UU-5'** to **C1UU-9'** which does not go through **C1UU-7**. See Figure S2 for computational details.

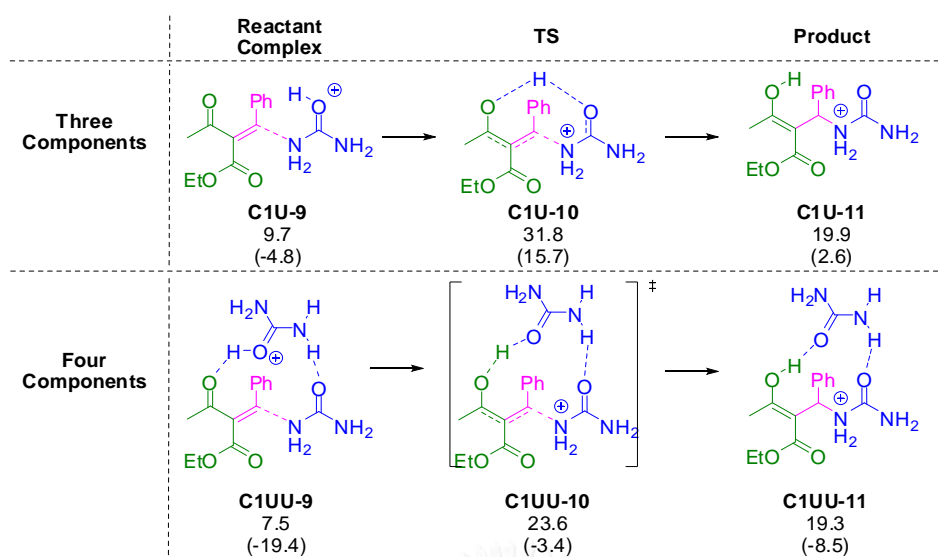


Figure S20 Pathways for Step III (Bond formation with urea) with three and four components for Route C. See Figure S2 for computational details.

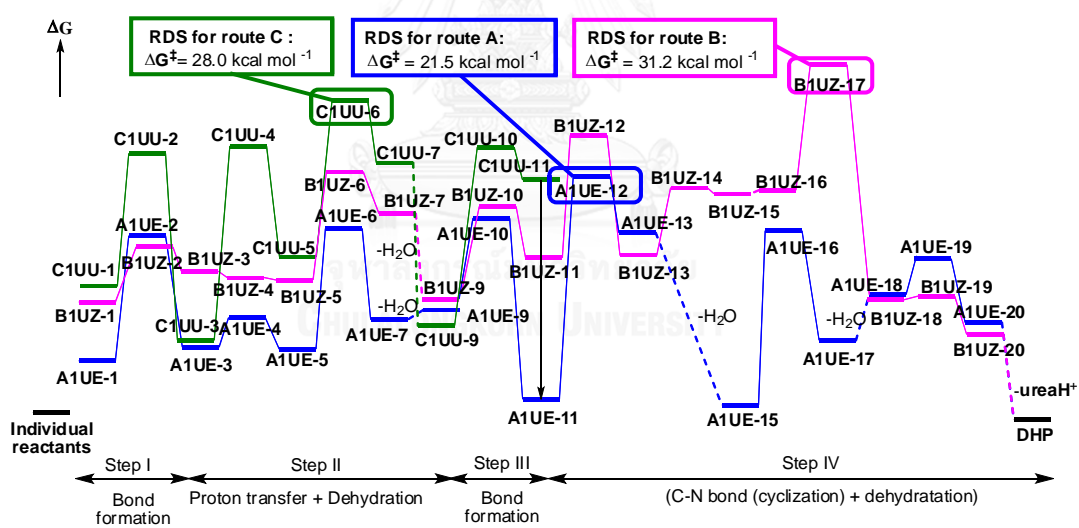


Figure S21 Free energy profiles of three main routes: Route A in blue, Route B in pink and Route C in green See Figure S2 for computational details.

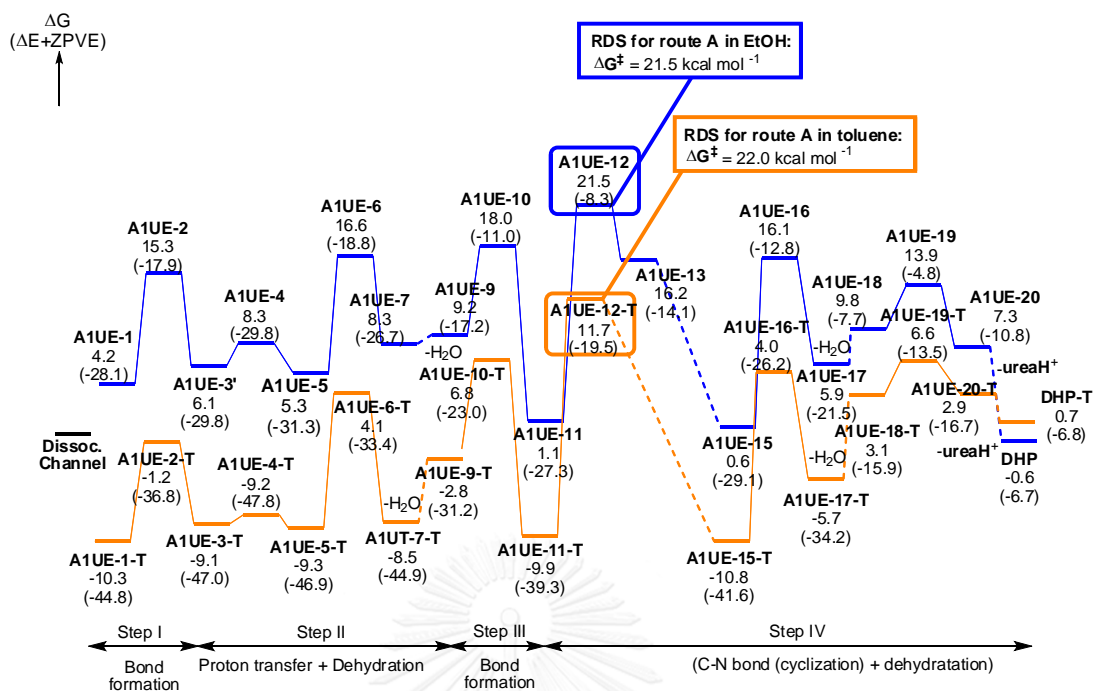


Figure S22 Free energy profiles of overall reaction for route A with four components at the M06-2x/6-31+G(d) level. Reactions in EtOH and toluene were demonstrated in blue line and orange line, respectively.

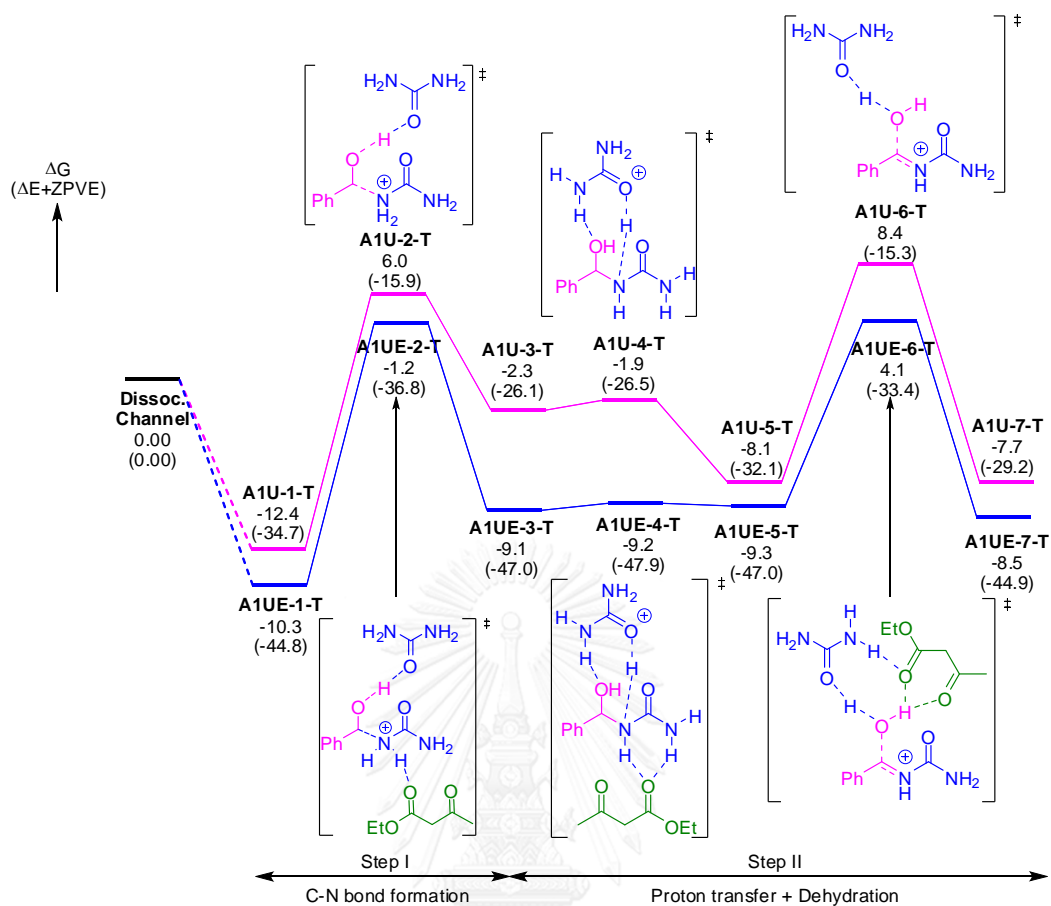


Figure S23 Free energy profiles of the most favorable pathways of step I-II (Route A) in toluene. Three- and four-components step were demonstrated in pink line and blue line, respectively. See Figure S2 for computational details.

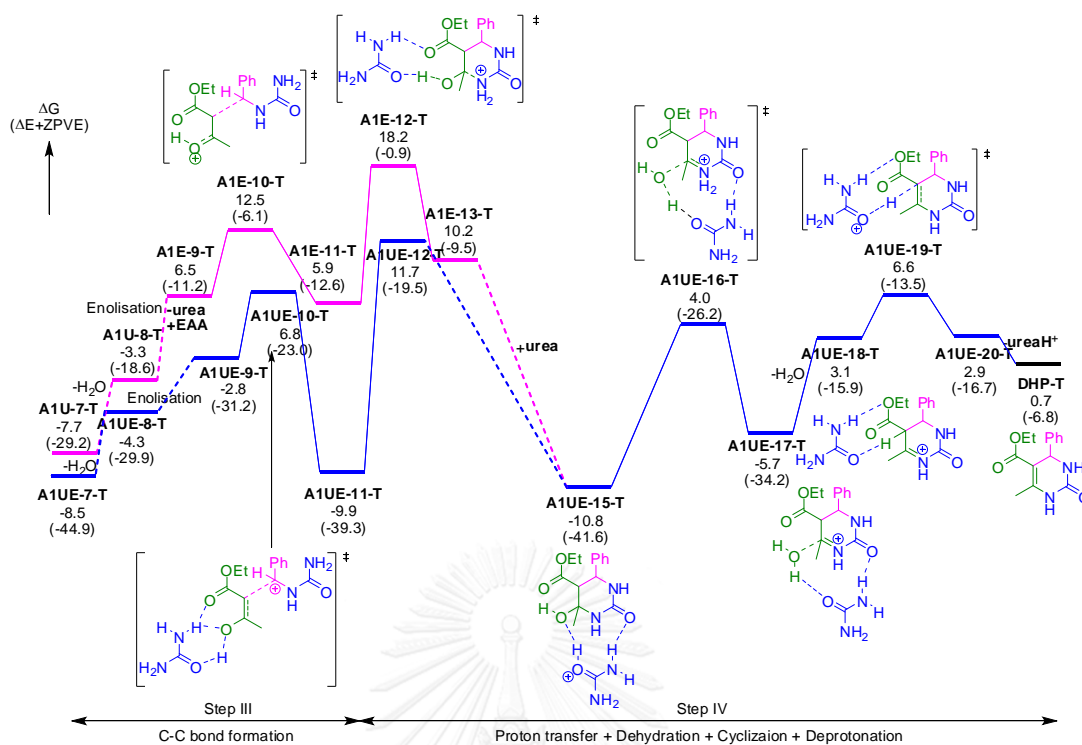


Figure S24 Free energy profiles of the most favorable pathways of step III-IV (Route A) in toluene. Three- and four components step were demonstrated in pink line and blue line, respectively. See Figure S2 for computational details.

Table S5 The energies (in kcal mol⁻¹) of the transition states of the rate-determining step for the different routes, were obtained at the M06-2X/6-31+G(d) level in PCM toluene.

Route: Rate-Determining Step	ΔG^\ddagger
Route A : Cyclization/C-N bond formation (A1UE-12-T)	22.0
Route B : Cyclization/C-N bond formation (B1UZ-17-T)	31.6
Route C : C-N bond formation (C1UU-10-T)	23.8

Table S6 Lennard-Jones parameters of solvents

Species	Site	$\sigma/\text{\AA}$	$\epsilon/\text{kcal mol}^{-1}$	Ref.
[MMIM] ⁺	C _R	3.88000	0.10414	[185]
	C _W	3.88000	0.10414	
	N	3.25000	0.16692	
	Me	3.77500	0.20350	
Cl ⁻	Cl	4.41724	0.11800	[186]
Water	H	1.00000	0.05600	[155]
	O	3.16600	0.15500	[155]

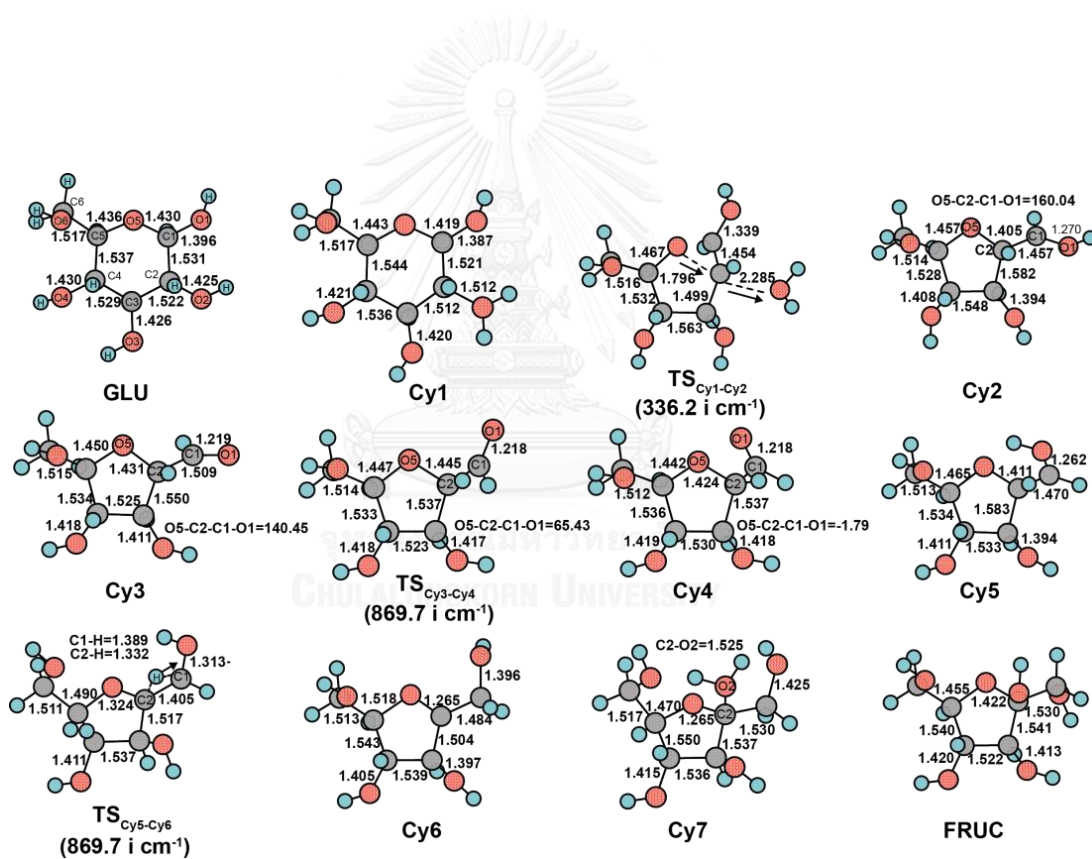


Figure S25 Geometry changes during the glucose-fructose isomerization via cyclic mechanism in water at 10 MPa, 473.15 K. The selected bond lengths are given in unit of Angstrom.

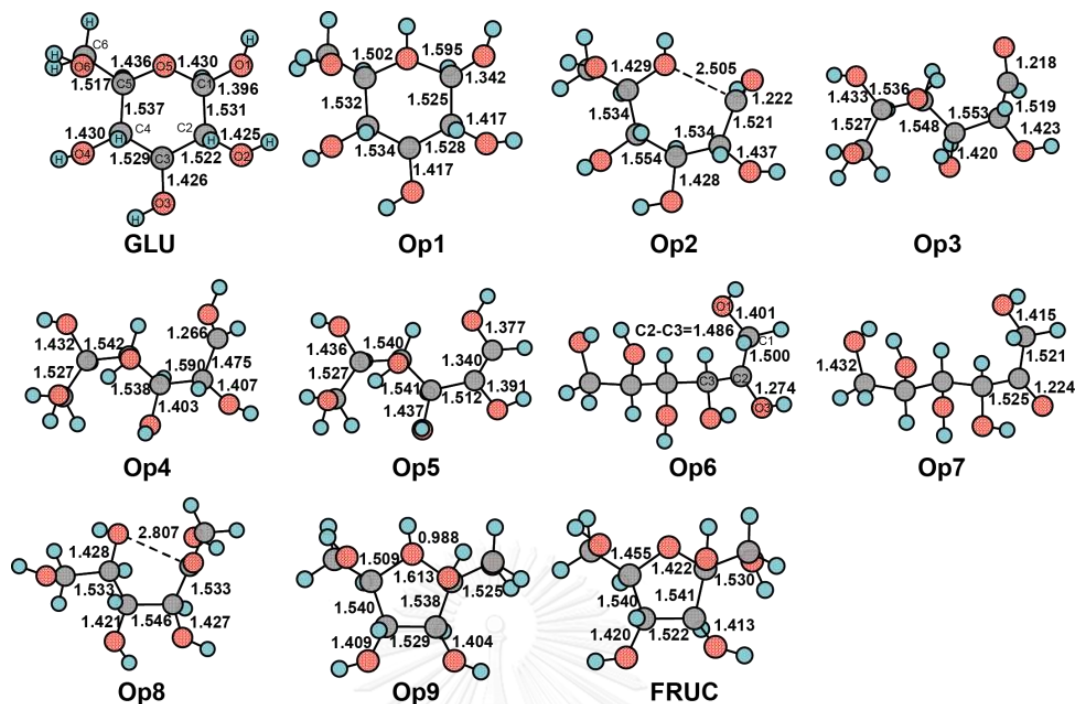


Figure S26 Geometry changes during the glucose-fructose isomerization via open chain mechanism in water at 10 MPa, 473.15 K. The selected bond lengths are given in unit of Angstrom.

Table S7 Energy difference of **Op4'** and **Op6'** stabilized by chloride anion in [MMIM]Cl

Intermediate	$\Delta\Delta G$ (kcal mol ⁻¹)	$\Delta\Delta\Delta G$ (kcal mol ⁻¹)
Op4	25.81	14.50
Op4'	11.31	
Op6	29.83	14.40
Op6'	15.43	

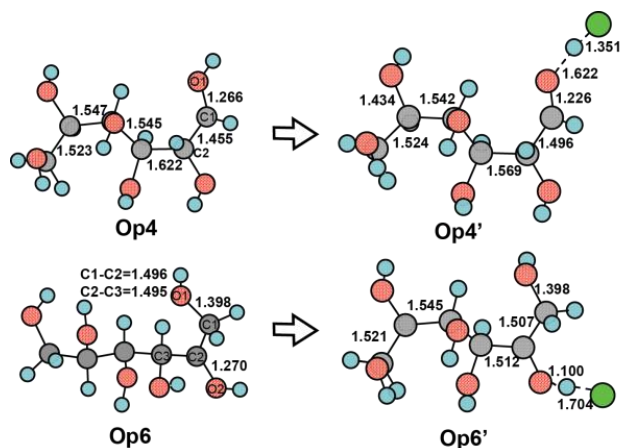


Figure S27 Geometry changes **Op4** and **Op6** stabilized by Cl^- ion (**Op4'** and **Op6'**, respectively) in open mechanism in $[\text{MMIM}]\text{Cl}$ at 1 atm, 373.15 K. The selected bond lengths are given in unit of Angstrom.

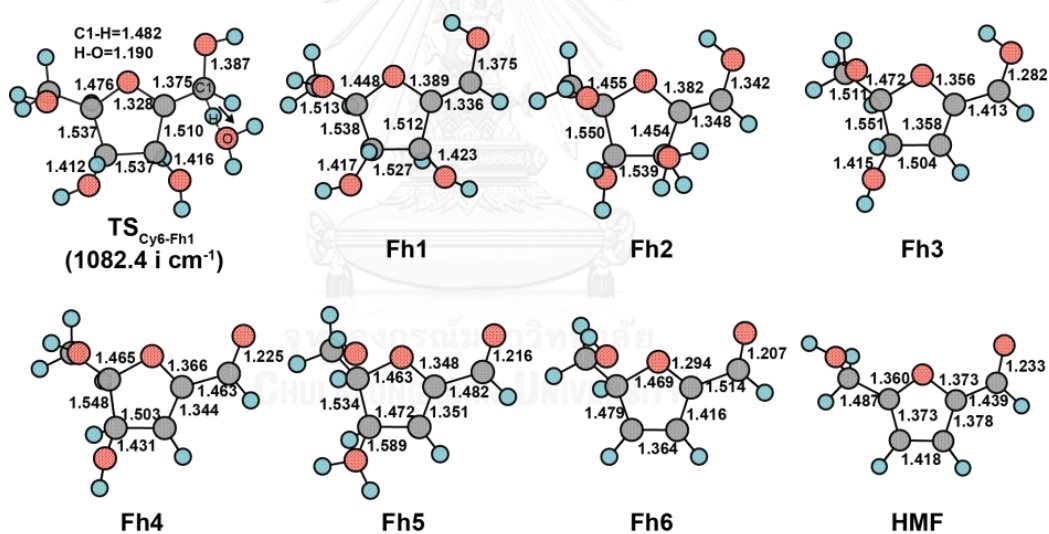


Figure S28 Geometry changes during the fructose transformation into HMF via cyclic mechanism in water at 10 MPa, 473.15 K. The selected bond lengths are given in unit of Angstrom.

A. Scholarship

2004-present The Development and Promotion of Science and Technology Talents Project (DPST) (Royal Government of Thailand scholarship) of Thailand

B. Research Visiting

June 2011- Present Computational Chemistry Unit Cell (CCUC) Laboratory, Department of Chemistry, Faculty of Science, Chulalongkorn University, Bangkok, Thailand, with Assoc. Prof. Vudhichai Parasuk

February 2014- February 2015 Fukui Institute for Fundamental Chemistry (FIFC), Kyoto University, Kyoto, Japan with Prof. Keiji Morokuma

February 2014- February 2015 Quantum Chemistry (QC) Group, Institute for Advanced Research, Department of Chemistry, Graduate School of Science, Nagoya University, Nagoya, Japan, with Prof. Stephan Irle

January 1st-31st 2014 Department of Chemistry, Faculty of Science, Chiang Mai University, Chiang Mai, Thailand, with Assist. Prof. Dr. Narin Lawan

February 18th-22nd 2013 JAIST International Winter School 2013 in topic "Quantum Monte Carlo Electronic Structure Calculation" at Japan Advanced Institute of Science And Technology (JAIST), Ishikawa Campus, Japan

October 27th-31st 2005 Nanyang Technological University, Singapore

C. Awards

- 2016 *Best Poster Presentation* of **Pure and Applied Chemistry International Conference (PACCON 2016)** ‘Thailand: One Hundread Years of Advancement in Chemistry, in titled “The Biginelli Reaction Is a Urea-Catalyzed Organocatalytic Multicomponent Reaction”, which took place in Bangkok, Thailand, during 9th-11th February 2016.
- 2016 *Excellent Student Oral Award* in **the plenary students oral contest of the Seventh Asia-Pacific Conference of Theoretical and Computational Chemistry (APCTCC-7)**, in titled "The Biginelli Reaction Is a Urea-Catalyzed Organocatalytic Multicomponent Reaction", which took place in Kaohsiung, Taiwan, during 25th-28th January 2016.
- 2016 *The 1st Runner Up Prize* of **Thailand Computational Chemistry Challenge by UBE** in titled “Prediction of Mechanical Properties of Natural Rubbers Investigated by Computational Chemistry”, which took place in Department of Chemistry, Chulalongkorn University on 22nd January 2016. 
- 2011 *Consolation prize (Poster presentation)* of **The 6th Congress on Science and Technology of Thailand (Youth)** in titled “Analysis of Mimicried Speech in Talking Bird”, which took place in Bangkok, Thailand, during 18th-19th March 2011.
- 2011 *Consolation prize (Oral presentation)* of **Hitachi Trophy on Science Forum 2011 (SF2011)** in titled “Analysis of Mimicried Speech in Talking Bird”, which took place in Faculty of Science, Chulalongkorn University, Bangkok, Thailand, during 10th-11th March 2011.

E. Conferences (Oral and Poster presentation) and activities

1. The Pure and Applied Chemistry International Conference (PACCON 2016) 'Thailand: One Hundred Years of Advancement in Chemistry, which took place in Bangkok, Thailand, during 9th -11th February 2016.
2. The Seventh Asia-Pacific Conference of Theoretical and Computational Chemistry (APCTCC-7), which took place in Kaohsiung, Taiwan, from 25th January to 28th January 2016
3. Workshop on The Vienna Ab initio Simulation Package (VASP): VASP Tutorial Workshop for Beginner by National Electronics and Computer Technology Center (NECTEC), which took place in Department of Chemistry, Faculty of Science, Kasetsart University, Bangkok, Thailand, on 21st October 2015
4. The 16th International Conference on Density Functional Theory and its Applications (DFT 2015), which took place in Debrecen, Hungary, August 31st - September 4th, 2015
5. The 12th Fukui Institute for Fundamental Chemistry Kyoto University (FIFC) Symposium, which took place in Kyoto, Japan on 23rd January 2015.
6. The Conference on C–C Bond Cleavage (CCCC), which was held in Kyoto, Japan on October 24th – 26th, 2014.
7. The 10th Thai Summer School of Computational Chemistry workshop (10th TS2C2) on "Computational Modeling of protein-ligand Interaction" on October 14th-17th, 2013 at Department of Chemistry, Faculty of Science, Kasetsart University Si Racha District Campus, Chonburi, Thailand.
8. The Sixth Asia-Pacific Conference of Theoretical and Computational Chemistry (APCTCC 6), in Gyeongju, Korea, from 10th to 13th July 2013.
9. Workshop on Computer-aided Molecular Design on Small molecule sketching using SYBYL-X program, Ligand based drug designed (LBDD): 3D-QSAR and Structure based drug designed (LBDD): Molecular Docking, from 9th to 10th May 2013 at Department of Chemistry, Faculty of Science, Chulalongkorn University , Bangkok, Thailand.
10. The 9th Thai Summer School of Computational Chemistry workshop (9th TS2C2) on "Current Computational Methods in Drug Design" on October 22nd –

25th, 2012 at Department of Chemistry, Faculty of Science, Thaksin University, Phatthalung Province, Thailand.

11. The Science Forum 2011 (SF2011), which took place in Faculty of Science, Chulalongkorn University, Bangkok, Thailand, during 10th-11th March 2011.



VITA

Name Maneeporn Puripat
Nationality Thai
Date of birth August 25th, 1988
E-mail Address puripat.ma@gmail.com

Education

2011 Bachelor of Science (B.Sc.) in Physics (2nd class honor),
Chulalongkorn University, Bangkok 10330, Thailand
2011 Bachelor of Laws (B.L.),
Sukhothai Thammathirat Open University, Nonthaburi 11120,
Thailand
2016 Doctor of Philosophy (Ph.D.) in Nanoscience Technology,
International Program of Nanoscience and Technology,
Chulalongkorn University, Bangkok 10330, Thailand

Publications (*Corresponding Author)

1. Puripat M.; Ramozzi R.; Hatanaka M.; Parasuk W.; Parasuk V.;
and Morokuma K*, J. Org. Chem., 2015, 80 (14),
pp. 6959-6967. (IF = 4.721)
2. Arifin‡; Puripat M.‡; Yokogawa D.*; Parasuk V.*; and Irle S.,
J. Comput. Chem., 2016, 37 (3), pp. 327-335 (‡These authors
equally contributed to the work), including the cover image,
2016, 37 (3), pp. i. (IF = 3.589)